The

PHILOSOPHICAL MAGAZINE

FIRST PUBLISHED IN 1798

L. 41 SEVENTH SERIES No. 319 AUGUST, 1950

A Journal of Theoretical Experimental and Applied Physics

PRICE 10s.

Annual Subscription £5 2s. 6d. payable in advance.

TED AND PUBLISHED BY TAYLOR & FRANCIS LTD., RED LION COURT, FLEET ST., LONDON, E.C.4

CONTENTS OF No. 319.

*** All communications for the Philosophical Magazine should be addressed, post-paid, to the Editors, c/o Messrs. Taylor and Francis, Ltd., Red Lion Court, Fleet Street, London, England.

LXVI. *On the Inhomogeneous Deformation of a Plastic Lamina in a Compression Test.*

By R. Hill, M.A.Ph.D.,
Metal Flow Research Laboratory, Sheffield*.

[Received April 14, 1950.]

Summary.

A theory is formulated for the calculation of stresses and displacements in a thin sheet of arbitrary shape which is being plastically compressed between parallel plates. Account is taken of inhomogeneous distortion caused by friction or edge constraints. By a transformation the solution is made to depend on that for a certain elastic problem of plane strain. Experimental data in support of the theory is provided by compression tests on long rectangular strips with both fluid and solid lubricants. A new method is suggested for estimating coefficients of friction relevant for cold-working processes.

§1. Introduction.

The paper is concerned with the behaviour of a metal lamina compressed plastically between parallel rigid platens†. The term lamina is to be understood as referring to a uniform plane sheet of arbitrary shape, having a thickness small compared with other dimensions. This restriction is made for the sake of simplicity, since the variations of stress and strain through the thickness can then be disregarded provided that the friction on the platens is not too great.

So long as the platens overlap the specimen all parts of the latter are compressed equally and, if there were no friction, the deformation would be uniform and the lateral expansion equal in all directions. The slightest trace of friction, however, causes pronounced inhomogeneous deformation if some dimension of the lamina is very large compared with the thickness. For example, in a long rectangular lamina the compressive stress in the plane needed to overcome the frictional resistance to longitudinal expansion is of order $2\mu Yb/h$, where h is the thickness, $2b$ the length, Y the compressive yield stress, and μ the coefficient of friction. Thus, even when the lubricant is so good that μ is 0·05, the compressive stress in the plane is of order Y/2 at the centre of a specimen whose length is ten times the thickness. In a plastically deforming metal this implies that local expansion in the length direction is almost or totally inhibited (the third principal stress being small). In general, a lamina changes its shape appreciably

* Communicated by the Author.

† Platen is the technical term for a compression plate in a press.

during compression unless it is initially circular (the friction being isotropic). Moreover, the distribution of pressure over the platens is non-uniform, so that the test cannot give a direct measure of the uniaxial stress–strain curve. It is necessary to know the relation between the applied mean pressure $\bar{p}$ and the current yield stress Y in compression. An estimate of $\bar{p}$ for a circular disk, due to Siebel (1923), is

$$\bar{p}=\left(1+\frac{2\mu a}{3h}\right)\mathrm{Y},$$

where a and h are respectively the current radius and thickness. This formula should be a good approximation for a lamina when $\mu a/h$ is not too large, say less than $\frac{1}{2}$. No similar formula has been suggested for a lamina of arbitrary shape, and it is the purpose of the present paper to show how one may be obtained. The change of shape of a non-circular lamina can be regarded as a sensitive indication of the presence of friction. It is certainly a more delicate indication than the barrelling of a solid cylinder, which is not known invariably to accompany friction. Furthermore, by the help of the theory to be described, the coefficient of friction can be deduced from measurements of the dimensional changes during compression.

When, on the other hand, the lamina overlaps the platens, the material outside the platens is not compressed, although a part of it will usually be deformed plastically by the stresses in its plane. A constraint is thereby exerted on the material between the platens, tending to produce an inhomogeneous distortion which may overshadow that caused by friction. In a test suggested by Orowan and described by Ford (1948), advantage is taken of this constraint to secure compression under approximate conditions of plane strain. A rectangular strip is indented by platens completely spanning its width. The material outside the platens is almost entirely rigid and, except near the edges, prevents all strain in the width direction when the compressed area is sufficiently long and narrow. The falling-off in pressure towards the ends of the platens is investigated here. The situation resembles that in the roll-gap in strip-rolling, and the results of the investigation should furnish a method for estimating the state of stress near the edges of the strip.

§2. Frictionless Platens with Edge Constraint.

We suppose, to begin with, that the platens are perfectly smooth, the non-homogeneous distortion being due solely to constraints applied to the edge of the material between the platens. Although the constraints would in general produce a varia ion in stress and strain through the thickness, this is confined to the part of the lamina lying within a distance of order h from the edges of the platens*. It can therefore be neglected since we are assuming the width to be large compared with the thickness.

* See, for instance, the solution by Hill and Lee (1946) to the problem of the plane indentation of a block by perfectly rough dies.

Let Cartesian axes of reference (x, y, z) be taken, with z normal to the lamina. The components of the mean stress (averaged through the thickness) satisfy the equations of equilibrium :

$$\frac{\partial \sigma_x}{\partial x} + \frac{\partial \tau_{xy}}{\partial y} = 0, \qquad \frac{\partial \sigma_y}{\partial y} + \frac{\partial \tau_{xy}}{\partial x} = 0. \quad . \quad . \quad . \quad . \quad . \quad (1)$$

Let S denote the speed of approach of the plates at any moment ; the corresponding rate of compression is S/h. The Lévy-Mises plastic stress–strain relations are then

$$\left.\begin{aligned} -\frac{h}{S}\frac{\partial U}{\partial x} &= \frac{\sigma_x - \frac{1}{2}(\sigma_y + \sigma_z)}{\sigma_z - \frac{1}{2}(\sigma_x + \sigma_y)}, \\ -\frac{h}{S}\frac{\partial V}{\partial y} &= \frac{\sigma_y - \frac{1}{2}(\sigma_z + \sigma_x)}{\sigma_z - \frac{1}{2}(\sigma_x + \sigma_y)}, \\ -\frac{h}{S}\left(\frac{\partial U}{\partial y} + \frac{\partial V}{\partial x}\right) &= \frac{3\tau_{xy}}{\sigma_z - \frac{1}{2}(\sigma_x + \sigma_y)}, \end{aligned}\right\} \quad . \quad . \quad . \quad . \quad (2)$$

where (U, V) are the (x, y) components of velocity averaged through the thickness. We have, finally, the criterion of plastic yielding :

$$\sigma_z = f(\sigma_1, \sigma_2), \quad . \quad . \quad . \quad . \quad . \quad . \quad . \quad . \quad . \quad (3)$$

where σ_1 and σ_2 are the principal stresses in the plane of the lamina.

Since the lateral strain is non-homogeneous, different elements receive different amounts of work-hardening. However, when the variation in the lateral component of strain is not too great (as we shall assume), all elements are in virtually the same state of work-hardening at any moment. Let Y be the current value of the uniaxial yield stress corresponding to this state. We now take advantage of the fact that the stress in any element will normally not be far from uniaxial compression in the z direction. Then, the hydrostatic component of stress being without influence on yielding, the criterion (3) can be approximated by the linear expression

$$\sigma_z - \tfrac{1}{2}(\sigma_x + \sigma_y) = -mY, \qquad (|\sigma_1 - \sigma_2| \leqslant \tfrac{2}{3}mY), \quad . \quad . \quad . \quad (4)$$

where m is a constant which is to be chosen to give the best overall approximation, and we have used the fact that $\sigma_x + \sigma_y \equiv \sigma_1 + \sigma_2$. When the values of the principal stresses are plotted along rectangular axes, the equation (4) represents one face of a regular hexagonal prism whose axis is in the direction (1, 1, 1). When $m = 1$, the prism encloses the circular cylinder representing von Mises' criterion and touches it along the generators corresponding to uniaxial tension or compression. By suitably choosing m, equation (4) can therefore be made to approximate von Mises', or indeed any, criterion for states of stress which do not depart far from uniaxial compression*. If m is assigned the value $\sqrt{3}/2$, (4) agrees with

* Similarly, the maximum shear-stress criterion (represented by a hexagonal prism inscribed in the Mises' cylinder) can sometimes be used as a convenient linearizing approximation to any actual criterion for states of stress near a pure shear.

von Mises' criterion in a state of pure shear. Hence by choosing m between $\sqrt{3}/2$ and 1, we ensure that (4) is never in error by more than about 8 per cent for any stress in the range $|\sigma_1-\sigma_2| \leqslant 2m\mathrm{Y}/3$. If the shear stress in the plane exceeds $m\mathrm{Y}/3$, the error can only be kept below 8 per cent by replacing (4) by another face of the hexagonal prism. This would not be analytically convenient and we shall therefore take (4) as an approximation for *all* stress states. However, since (4) is introduced mainly to simplify the stress–strain relations (2), the accurate criterion (3) can still be used for an improved estimate of σ_z when approximate values of σ_x and σ_y have been calculated.

On inserting (4) and (2), we find that

$$\left.\begin{aligned} \frac{h}{\mathrm{S}}\frac{\partial \mathrm{U}}{\partial x} &= \tfrac{1}{2}+\frac{3(\sigma_x-\sigma_y)}{4m\mathrm{Y}}, \\ \frac{h}{\mathrm{S}}\frac{\partial \mathrm{V}}{\partial y} &= \tfrac{1}{2}-\frac{3(\sigma_x-\sigma_y)}{4m\mathrm{Y}}, \\ \frac{h}{\mathrm{S}}\left(\frac{\partial \mathrm{U}}{\partial y}+\frac{\partial \mathrm{V}}{\partial x}\right) &= \frac{3\tau_{xy}}{m\mathrm{Y}}. \end{aligned}\right\} \quad . \ . \ . \ . \quad (5)$$

We now substitute

$$u=\frac{m\mathrm{Y}}{\mathrm{E}}\left(\frac{h\mathrm{U}}{\mathrm{S}}-\tfrac{1}{2}x\right), \qquad v=\frac{m\mathrm{Y}}{\mathrm{E}}\left(\frac{h\mathrm{V}}{\mathrm{S}}-\tfrac{1}{2}y\right), \quad . \ . \ . \quad (6)$$

where E denotes Young's modulus, and the new variables (u, v) have the dimensions of length. We obtain

$$\mathrm{E}\frac{\partial u}{\partial x}=\tfrac{3}{4}(\sigma_x-\sigma_y)=-\mathrm{E}\frac{\partial v}{\partial y}, \qquad \mathrm{E}\left(\frac{\partial u}{\partial y}+\frac{\partial v}{\partial x}\right)=3\tau_{xy}. \quad . \ . \quad (7)$$

These will be recognized as the *elastic* equations for a material which has a Young's modulus E and Poisson's ratio $\frac{1}{2}$, and which is deformed in *plane strain*. The distribution of stress and strain in the plastic lamina can therefore be derived from that in a geometrically similar lamina of incompressible material deformed elastically in plane strain. The (x, y) stresses are indentical in both, while according to (6), the elastic displacement is proportional to the plastic velocity representing the non-homogeneous part of the strain (*i. e.* over and above uniform compression and expansion). The z component of stress needed to maintain plane elastic strain in an incompressible material is $\frac{1}{2}(\sigma_x+\sigma_y)$; thus, from (4), the pressure exerted by the platens on the plastic lamina is equal to $m\mathrm{Y}$ plus the pressure on the elastic lamina.

Consider, for example, a long rectangular lamina which is being compressed between smooth platens completely spanning its width (fig. 1). Let the width of the lamina be $2b$ and the width of the platens $2a$. Let the x and y axes be taken parallel to the sides of the lamina, with the origin at the geometric centre of the area under compression. If the material lying outside the platens is assumed to be rigid, the conditions along the boundary of the rectangular compressed area are

$$\mathrm{U}=\text{constant}=\pm\lambda \mathrm{S}a/h, \text{ say}; \qquad \mathrm{V}=0; \qquad \text{on } x=\pm a;$$

together with zero applied stress on the surfaces $y=\pm b$. The unknown constant λ must lie between $\frac{1}{2}$ (corresponding to free expansion) and 1 (corresponding to complete prevention of lateral strain). The precise value is determined by the condition that the resultant force over a lateral section, acting in the x direction, is zero (the ends of the lamina being unconstrained). The boundary-conditions in the associated elastic problem for a rectangular lamina (with sides $2a$ and $2b$) are

$$u=\text{constant}=\pm(\lambda-\tfrac{1}{2})m\mathrm{Y}a/\mathrm{E}, \qquad v=-m\mathrm{Y}y/2\mathrm{E}, \qquad \text{on } x=\pm a\ ;$$

Fig. 1.

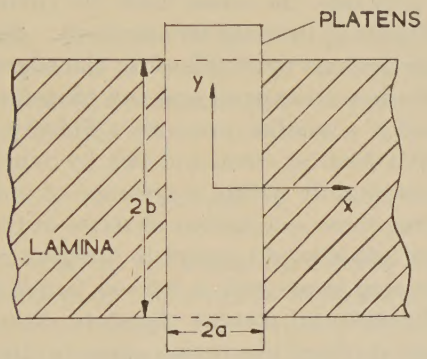

Lamina compressed between platens which overlap across the width only.

Fig. 2.

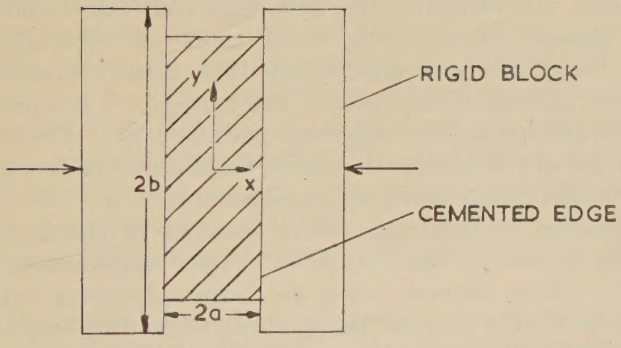

Associated elastic problem.

together with zero applied stress along $y=\pm b$ and zero resultant force on the surfaces $x=\pm a$. These conditions are satisfied by superposing a uniform tensile stress $2m\mathrm{Y}/3$ in the x direction on the stress distribution due to a compressive load $4m\mathrm{Y}b/3$ applied through inextensible *rigid* bars *cemented* along $x=\pm a$ (fig. 2). According to (7) the tensile stress produces displacements

$$\pm m\mathrm{Y}a/2\mathrm{E}, \qquad -m\mathrm{Y}y/2\mathrm{E}, \qquad \text{on } x=\pm a.$$

The compressive load balances this tension (so satisfying the condition for zero resultant force), and produces along $x = \pm a$ a zero displacement in the y direction (since the bars are cemented and inextensible) and a certain uniform displacement in the x direction (since the bars are rigid). The magnitude of the latter has to equal $(1-\lambda)\, mYa/E$, and this determines the value of λ.

The problem of compressing a rectangular elastic block between massive cemented bars does not appear to have been solved*. A photo-elastic investigation is projected, though the achievement of plane strain presents difficulties. We may, however, safely make certain generalizations about the distribution of stress, without a detailed solution. In the first place, by Saint-Venant's principle, the stress must be virtually uniform except within a distance of order $2a$ from the free surfaces. Secondly, the pressure transmitted through the bars must fall off at the edges, since the material there has greater freedom to expand and can therefore be compressed by a given amount under a smaller pressure. Thirdly, since the bars are cemented, they exert a shearing stress and this, by Saint-Venant's principle, must be concentrated mainly within a distance of order $2a$ from the free surfaces. Translating these conclusions in terms of the plastic lamina, we can expect a state of plane strain except in a region near the edge, where there is both a shearing stress and a *tension* parallel to the edge. The pressure applied through the platens therefore diminishes towards the edge, the fall-off being confined to a region whose width is roughly equal to that of the platens.

§3. Rough Platens Without Edge Constraint.

We consider, now, a lamina free from edge constraints and compressed by rough platens which overlap it all round its circumference. The coefficient of friction μ is assumed so small that terms containing second or higher powers of μ can be neglected. For example, σ_z is a principal stress to first-order, and so the yield criterion is still (3) or (4). The theory is only a valid account of a first-order departure from pure uniform compression. This is the reason for excluding edge constraints.

It is necessary to determine which element of the lamina remains momentarily at rest at each stage of a slow compression. In a fast compression, where inertial forces are large compared with frictional forces, it is clearly the element momentarily coinciding with the centroid, since there are no other lateral external forces. The situation is different, however, when the compression is so slow that inertial forces are negligible compared with frictional forces. For a first-order calculation of the distribution of the frictional shear stress over the faces of the lamina, the deformation may be taken to be uniform expansion. We must also allow for the possibility of a small rotation of the lamina in its plane. Then,

* An approximate method, yielding limited information and applied only to a square block, has been described by H. J. Greenberg and R. Truell (1948).

to first order, the relative velocity of an element distant r from the momentarily fixed point is compounded of a radial velocity proportional to r (due to the uniform expansion) and a velocity which is perpendicular to this and also proportional to r (due to the rigid-body rotation). The resultant velocity is therefore proportional to r and inclined at a fixed angle θ to the radius. Hence the frictional stress, opposing the relative motion, is directed at the same constant angle θ to the radius. To first order, the magnitude of the frictional stresses is μY, and they therefore exert no resultant torque on the lamina if

$$\mu Y \sin\theta \iint r\, dx\, dy = 0,$$

taken over the lamina. Since the integral is essentially positive, it follows that $\theta=0$, or that there is no rotation of the lamina as a whole. The friction is therefore directed toward the point at rest, and the condition for zero resultant frictional force is

$$\iint \mathbf{t}\, dx\, dy = 0, \qquad (8)$$

where $\mathbf{t}$ is the unit vector in the radial direction. This is the equation determining the position of the element momentarily at rest. If the lamina has two axes of symmetry, the centroidal element always remains at rest. For a lamina of arbitrary shape, however, the point defined by (8) is not the centroid.

Let (x, y) axes be taken with the origin coinciding with the point at rest. The frictional stress contributes to the equations (1) additional terms which are equivalent to a body stress with potential $2\mu Yr/h$. Such a body stress can be balanced by a variable hydrostatic tension whose value is equal to the potential. The remaining part of the actual stress then satisfies the equations (1) of equilibrium. Furthermore, the remaining part of the actual stress still satisfies the plastic stress–strain relations and yield criterion, since these are unaffected by the addition of a hydrostatic stress. The corresponding external stress on the edge of the lamina must be equal to a normal pressure of amount $2\mu Yr/h$ at each point in order to produce, when combined with the hydrostatic tension, zero resultant stress on the edge.

Thus, to obtain the distribution of stress in a lamina compressed by rough platens, we combine a varying hydrostatic tension $2\mu Yr/h$ with the distribution of stress in a similar lamina compressed along its faces by smooth platens and along its edge by a varying normal pressure $2\mu Yr/h$. The deformation is identical in the two laminæ. Since the edge pressure is proportional to the distance from the point at rest, it offers the least resistance to lateral expansion of the parts of the edge nearest to this point. In other words, as one would naturally expect, friction on the platens causes the lamina to expand most in the direction of its least dimension.

The elastic analogy described in §2 is, of course, still applicable. Let us, for example, apply it to determine the stress in a circular lamina of radius a. The corresponding edge pressure produces a uniform hydrostatic pressure $2\mu Ya/h$ in the plane of the elastic lamina and hence also in the plastic lamina between smooth platens. Combining this with the varying hydrostatic tension $2\mu Yr/h$, we obtain equal radial and circumferential compressive stresses $2\mu Y\ (a-r)/h$ in the plane of the lamina between rough platens. From (4), taking $m=1$, the pressure exerted by the platens is

$$Y+2\mu Y(a-r)/h$$

and the mean pressure is $Y\ (1+2\mu a/3h)$, in agreement with Siebel's formula.

§4. Experimental Determination of the Coefficient of Friction.

The preceding theory provides a means of estimating the coefficient of friction in a compression test from observations of the change in shape of a rectangular lamina.

The coefficient of friction, so determined, corresponds to the conditions in a compression test, viz : where one of the sliding bodies is distorted elastically in bulk and the other has yielded plastically. Such coefficients of friction are relevant for all processes for cold-working metals .

The method is obviously more sensitive when the change of shape is large, but then the first-order approximation of the theory is less accurate. However, when the lamina is long and narrow, a more exact calculation can be made. If the length $2b$ is greater than about 10 times the width $2a$, and if a/h is of order unity, it is probably legitimate to neglect the variation in stress across the width in comparison with the variations along the length. The only stress components are then the longitudinal compressive stress q, the pressure p, and the friction μp. To the same order of approximation we may disregard the change of *shape* when setting up the equation of equilibrium. This then reduces to

$$h\frac{dq}{dy}=2\mu p, \quad . \quad . \quad . \quad . \quad . \quad . \quad . \quad . \quad . \quad (9)$$

where y is measured along the lamina from its shorter side $2a$. For any yield criterion near that of von Mises, it is sufficiently accurate to use equation (4) :

$$p-\tfrac{1}{2}q=mY. \quad . \quad . \quad . \quad . \quad . \quad . \quad . \quad . \quad . \quad (10)$$

Eliminating q from (9), and integrating, we obtain

$$p=mY \exp(\mu y/h), \quad . \quad . \quad . \quad . \quad . \quad . \quad . \quad . \quad (11)$$

after using the boundary-condition $p=mY$ on $y=0$.

The longitudinal strain-increment vanishes at a section distant y' from the shorter side, such that $q=\frac{1}{2}p$ or

$$\mu y'/h=\ln(4/3)\simeq 0{\cdot}288. \quad . \quad . \quad . \quad . \quad . \quad . \quad (12)$$

Hence, if $\mu b/h < 0{\cdot}288$, all parts of the specimen continue to elongate. It follows from equations (2), (10) and (11), that the increase in b during a further small *decrease* dh in thickness is

$$db = \frac{dh}{h}\int_0^b (2-\tfrac{3}{2}e^{\mu x/h})\,dx = dh\left[\frac{2b}{h} - \frac{3}{2\mu}(e^{\mu b/h}-1)\right].$$

This may be written to the present order of approximation as

$$\frac{db}{b} \simeq \left(1-\frac{3\mu b}{2h}\right)\frac{dh}{2h}.$$

Integration gives

$$\frac{b}{b_0} = \left(\frac{1-\dfrac{\mu b}{2h}}{1-\dfrac{\mu b_0}{2h_0}}\right)\sqrt{\left(\frac{h_0}{h}\right)}; \quad \frac{\mu b}{h} \leqslant 0{\cdot}288\,; \quad . \quad . \quad . \quad . \quad (13)$$

where b_0 and h_0 are initial values. The first factor in this equation becomes increasingly less than unity as the compression proceeds, and represents the effect of friction in hindering changes of length. The corresponding formula for the mean pressure is, with $m \sim 1$,

$$\bar{p} \simeq \left(1+\frac{\mu b}{2h}\right)\mathrm{Y}\,; \quad \frac{\mu b}{h} \leqslant 0{\cdot}288. \quad . \quad . \quad . \quad . \quad . \quad (14)$$

On the other hand, when $\mu b/h > 0{\cdot}288$, a central region of the lamina, of length $2(b-y')$, momentarily undergoes no extension. Since there is no relative longitudinal slip in this region, p has the uniform value $4m\mathrm{Y}/3$ and q is equal to $2m\mathrm{Y}/3$ (m should be taken nearer to $\sqrt{3}/2$ as y'/b becomes progressively less). The mean pressure is easily found to be

$$\bar{p} \simeq \left(\frac{4}{3} - 0{\cdot}051\frac{h}{\mu b}\right)m\mathrm{Y}\,; \quad \frac{\mu b}{h} \geqslant 0{\cdot}288. \quad . \quad . \quad . \quad . \quad (15)$$

The increase in length during a small decrease dh in thickness is given by

$$\frac{db}{y'} = \left(4-\frac{h}{\mu y'}\right)\frac{dh}{2h},$$

or

$$\frac{db}{dh} \simeq \frac{0{\cdot}076}{\mu}; \quad \frac{\mu b}{h} \geqslant 0{\cdot}288. \quad . \quad . \quad . \quad . \quad . \quad . \quad (16)$$

In the present experiments the nominal specimen dimensions were $1{\cdot}0 \times 0{\cdot}1 \times 0{\cdot}05$ in., so that $b_0/h_0 = 10$. Fig. 3 shows the corresponding theoretical relation between the fractional change in length $(b/b_0 - 1)$ and the fractional reduction in height $(1 - h/h_0)$ for various values of μ. At the critical value of b/h, for which the centre of the lamina undergoes no extension, the curve (13) is replaced by a line of slope $0{\cdot}076\,h_0/\mu b_0$, according to (16). When μ is greater than 0·0288 the relation is linear from the start when $b_0/h_0 = 10$.

Also shown in fig. 3 are experimental points for two lubricants: powdered calcium oleate and vacuum solvac. Copper specimens were used, the respective dimensions being

$1{\cdot}000 \times 0{\cdot}100 \times 0{\cdot}050$ in. and $1{\cdot}002 \times 0{\cdot}103 \times 0{\cdot}049$ in.

The copper was rendered isotropic by suitable rolling and heat treatment; this was confirmed by compression tests on circular disks, which remained effectively circular The lubrication was renewed whenever the test was interrupted to take measurements of length and thickness. The experimental points follow the trend of the calculated curves, thus affording indirect evidence that the theory is sound. The deduced

Fig. 3.

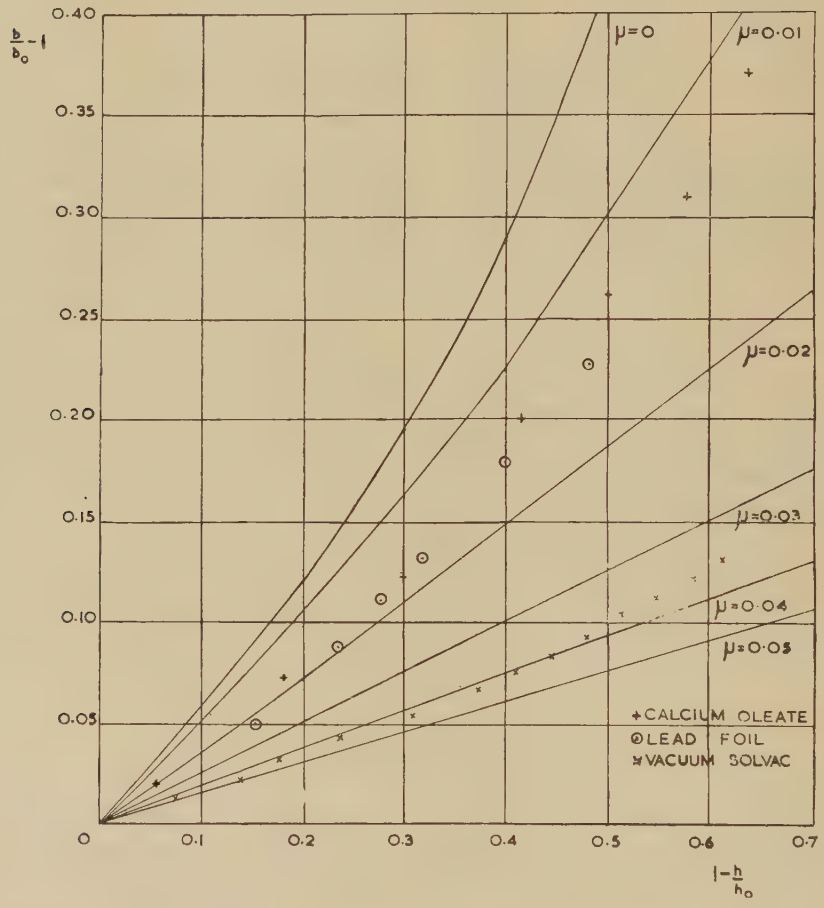

Comparison of calculated and observed values of the extension of laminæ of dimensions $1{\cdot}0\times0{\cdot}1\times0{\cdot}05$ ins.

coefficients of friction are 0·015 and 0·045, respectively. The latter is comparable with values inferred from measurements of roll-force when rolling *short* lengths of copper strip with vacuum solvac as a flood lubricant *.

* Private communication from Mr. R. B. Sims, Head of the Rolling Section, British Iron and Steel Research Association.

The low coefficient of friction obtained with calcium oleate indicates that true boundary-lubrication was not operative, and this was confirmed by the appearance of the copper after compression. The surface was still mainly in the ' orange-peel ' condition, in marked contrast to the smoothed and burnished surface of the specimen lubricated with vacuum solvac.

For a direct check of the theory it is necessary to use a lubricant whose frictional properties are known independently.

A *sufficiently thin* foil of some softer metal acts as an efficient lubricating agent, the frictional stress being equal to the limiting yield stress s in shear of the foil at large strains. The foil must not be too thick, or it will extrude in the width direction before (or while) the specimen itself is compressed, and so exert a *negative* frictional drag in that direction. A rough criterion, ensuring non-extrusion, is that Y/s should be less than w/t, where t is the foil thickness and w is the specimen width. This follows from the condition that the hydrostatic component of the stress at the middle of the foil, necessary to cause extrusion in the width direction, should be greater than Y. For lead foil on copper, Y/s is less than about $25/0{\cdot}5$ (units of tn./in^2.) at all strains, and so t/w should be less than $1/50$. In the present experiment t was not more than 0·002 in., while w was initially 0·1 in. The foil was removed and replaced by a new piece each time measurements were taken. The results are shown in fig. 3 and correspond to an apparent coefficient of friction of about 0·017 (the changes needed in the theory when the frictional stress is constant are insignificant here). By comparison s/Y is about $0{\cdot}4/20$ or 0·02 for large strains. The agreement is excellent in view of the various uncertainties. Similar confirmation was obtained with pure lead foil on aluminium where the apparent coefficient of friction was found to be 0·042 ($s/Y \sim 0{\cdot}4/10 = 0{\cdot}04$), and with indium foil on a lead alloy where the coefficient of friction was 0·033 ($s/Y \sim 0{\cdot}1/3 = 0{\cdot}033$). The limiting values of Y at large strains (greater than 20 per cent compression) were obtained from measurements of the load and thickness during the test (the current area being calculated as initial volume divided by current thickness). The limiting shear stress of the indium foil was inferred from hardness tests on the bulk metal. An $\frac{1}{8}$ in. diameter ball under a 4 lb. load of 20 seconds duration gave an impression diameter of 0·066 in. (average of three tests). This corresponds to a Meyer hardness of 0·52 tn./in^2. and hence to a mean uniaxial yield stress of about 0·17 tn./in^2. over the range of strains produced around a ball indentation.

For indium foil on copper and aluminium, or lead foil on steel, extrusion must have occurred since the change in length was much smaller than would be expected if the foil had behaved as a true lubricant ; extrusion would, indeed, be expected by the criterion mentioned previously. In agreement with this hypothesis, a solid cylinder of copper showed barrelling when lubricated with lead, but a concavity when lubricated with indium.

A further check on the theory is provided by a comparison of the observed and calculated values of the length of that part of the specimen

which is deformed *throughout* in plane strain. Theoretically this is, from (12),

$$2(b_0-y_0') = 2b_0\left(1-\frac{0{\cdot}288\,h_0}{\mu b_0}\right), \text{ when } \mu b_0/h_0 \geqslant 0{\cdot}288.$$

For the copper lubricated with vacuum solvac, where $b_0=0{\cdot}501$, $h_0=0{\cdot}049$, $\mu=0{\cdot}045$, this unextended central region is calculated to be of length 0·37 in. This is indicated on fig. 4, which shows the measured profile of the lamina after a reduction in thickness of 60 per cent. The agreement is excellent. The final maximum width is 0·248 in., while the width calculated on the assumption of plane strain is 0·26 in. When calcium oleate was the lubricant the profile was completely rounded, again in agreement with theory since $\mu b_0/h_0=0{\cdot}15<0{\cdot}288$.

It should be carefully noted that the theory becomes less accurate as the lamina is progressively compressed, since the length/width ratio decreases from the initial value of 10 to about 5 after a 50 per cent reduction. Tests on laminæ with an initial length/width ratio of 4 showed that the theory significantly underestimated the increase in length : this was to be expected

Fig. 4.

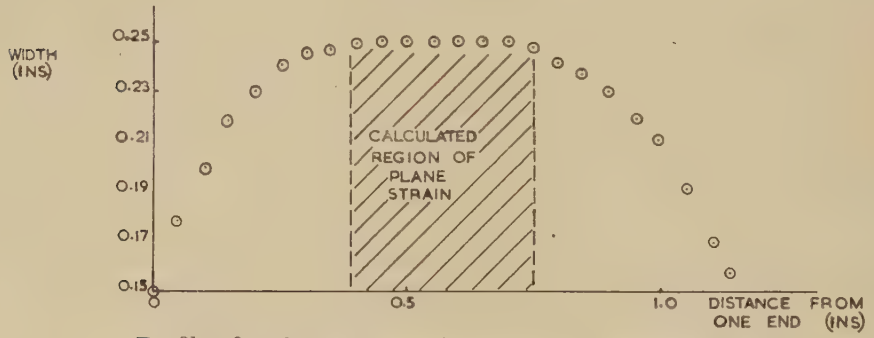

Profile after 60 per cent reduction with vacuum solvac.

from the neglect of the component of the frictional forces restraining the expansion in the width direction. This effect can be recognized in fig. 3, where the upward trend of the experimental results at large reductions is more pronounced than the theory predicts. For this reason the coefficients of friction were deduced from the experimental results below about 40 per cent, where the length/width ratio is greater than 7.

Acknowledgments.

I am grateful to the Director of the British Iron and Steel Research Association for permission to publish this paper; to Mr. N. Haslam of the Metzllurgy Section at the Metal Flow Research Laboratory, Sheffield, for carrying out the experiments ; and to Dr. D. Tabor for helpful discussions.

References.

Ford, H., 1948, *Proc. Inst. Mech. Eng.*, **159,** 115.
Greenberg, H. J., and Truell, R., 1948, *Quart. App. Maths.*, **6,** 53.
Hill, R., and Lee, E. H., 1946, *Proc. 6th Int. Cong. App. Mech.* (Paris).
Siebel, E., 1923, *Stahl und Eisen*, **43,** 1295.

LXVII. *A Theoretical Investigation of the Effect of Specimen Size in the Measurement of Hardness.*

By R. Hill, M.A., Ph.D.,
Metal Flow Research Laboratory, Sheffield*.

[Received April 25, 1950.]

Summary.

The theory of plane plastic strain due to Hencky and Geiringer is applied to calculating the minimum dimensions that a specimen should have for a valid hardness test. Critical widths and thicknesses are determined for rectangular specimens indented by flat dies and wedges of any angle. The manner in which the specimen deforms during the indentation is considered in detail.

§1. Introduction.

The definition of indentation hardness adopted in the present paper is the ratio of the applied load to the projected area of the impression. It is equal to the work done per additional unit volume of indentation, or, when the frictional resistance is negligible, to the mean normal pressure between indenter and medium. It is well known that the hardness is not observably dependent on the size of the specimen provided this is greater than a certain minimum (other things being equal). The minimum size depends mainly on the properties of the material under test and on the shape of the indenter. If the specimen is too thin or too narrow, the plastic zone penetrates either to the rear or lateral surfaces ; this is accompanied by a change in the apparent hardness (usually a reduction).

The minimum width and thickness of a rectangular specimen are calculated here for indentation by a wedge. At present, this is the only indenter for which a reasonably accurate calculation of the surface distortion and stress distribution is feasible. The problem is treated as two-dimensional, the strain being zero in the direction made by the intersecting faces of the wedge. The material is supposed to be rigid up to the yield point, after which the maximum shear stress retains a constant value in plane strain.

§2. Criterion for the Critical Thickness.

The slip-line field† ABCDE in the region of plastically-deforming material around a wedge indenting the plane surface of a semi-infinite mass is shown in fig. 1 (Hill, Lee, and Tupper 1947). The wedge angle is

* Communicated by the Author.

† For an account of the theory of plane plastic strain, see the writer's *The Mathematical Theory of Plasticity*, Chap. VI. (Oxford : Clarendon Press. 1950).

denoted by 2θ, the depth of penetration by c, and the length of the line of contact by h. The displaced surface is straight, and, when the wedge is smooth (as assumed here), the coronet is of length h. The inclination of the displaced surface to the horizontal is denoted by $\theta-\psi$; such a raised coronet is characteristic of a cold-worked metal (Heyer 1937). Fig. 2 shows the relations between $h\cos\theta/c$, ψ and θ. When the specimen is semi-infinite and homogeneous the configuration remains geometrically similar and the hardness is independent of load. This may be realized in practice, for example in a Vickers pyramid hardness test, provided the impression is large compared with the grain-size of the specimen and the radius of curvature of the tip of the indenter (Field Foster 1948).

Fig. 1.

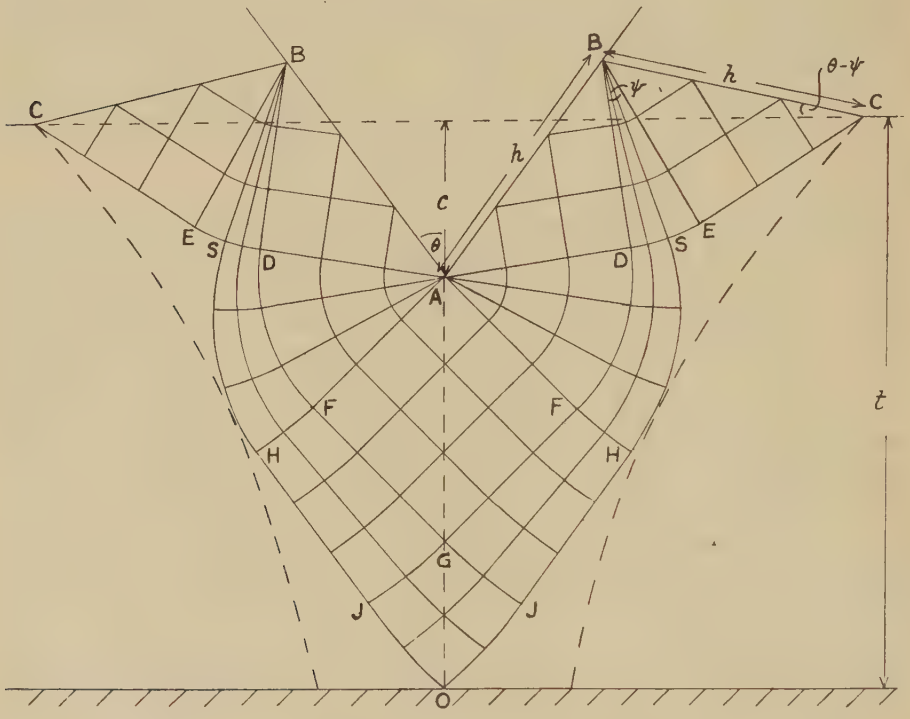

ABCDE does not constitute the whole plastic region. Beyond this field lies a further plastic zone where the material is stressed to the yield-point but remains rigid, being prevented from deforming by the constraint of the non-plastic matrix (Hill 1949). The state of stress and strain in the material undergoing deformation is independent of the distribution of stress in the rigid material. Consequently, there is no need to calculate the latter whenever it is evident that the rigid material is capable of supporting the stresses acting around its perimeter. This is necessarily so when a specimen is sufficiently large compared with the

localized area of deformation. It follows that conditions in the plastically-deforming zone are independent of the size of the specimen, provided only that it is sufficiently great. In particular, the configuration around a wedge remains geometrically similar (though the shape of the plastic boundary does not).

These conclusions are strictly valid only for a material that remains *rigid* whenever the maximum shear stress is less than k. In an actual solid, where Young's modulus E is finite, the deformation in the plastic region is dependent on the elastic distortion elsewhere. For example, the volume of the coronet is governed by the extent to which the elastic resilience of the whole specimen can accommodate the displaced material. Such departures from the behaviour of a plastic-rigid body are presumably only of order k/E, and the hardness should be independent of specimen size over a certain minimum, within normal experimental error (as is observed).

Fig. 2.

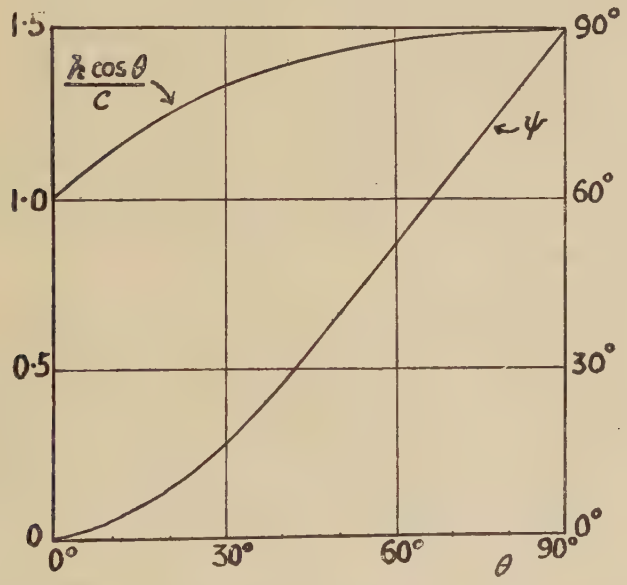

In a specimen whose thickness is small compared with its width, the plastic boundary moves relatively further from the indenter and nearer to the rear surface as indentation proceeds. When the specimen rests on a plane rigid foundation, it is a natural supposition (and one which is suggested by observations of the plastic distortion of the rear surface) that the relative expansion of the plastic zone is mainly concentrated directly below the indenter. At some stage of the indentation the element situated at the midpoint O of the rear surface is stressed to the yield limit. At a little later stage the plastic region contains all the material within a

certain area which lies below the indenter and intersects the rear surface over a finite length (the conjectured plastic boundary at this stage is indicated by broken curves in fig. 1). It may be proved (Hill 1949) that deformation is confined to the area ABCDE up to the moment when the plastic region has spread so far that it just includes the two slip-lines OS from O. Thereupon the constraint fails, the plastic core deforms, and the rigid ends are thrust apart, sliding over the foundation. The configuration round a wedge no longer remains geometrically similar and subsequent hardness measurements are spurious.

We now examine the criterion determining the critical depth of penetration. The slip-line field bounded by OS and AS is uniquely determined by the known shape of AS ; the particular position of S on ADEC depends, of course, on the ratio of AO to AB. The field having been calculated, Hencky's theorem determines the normal stresses acting across AO, and hence the total lateral thrust exerted on each half of the specimen by the stresses along OAB. The thrust vanishes when the foundation is smooth and the ends of the specimen are unconstrained. Now the field OSAS could always be formally constructed at any stage of the indentation, but only for one particular depth of penetration would the corresponding thrust across OAB vanish. Before this depth is attained, the plastic region can therefore not have spread sufficiently far to enclose the entire length of the slip-lines OS. Hence, as already stated, the material below the indenter must have remained rigid. The criterion for the critical penetration is therefore that there should be no resultant lateral thrust over OAB corresponding to a formal construction of the field OSAS.

§3. Calculation of the Critical Thickness.

Slip-line fields with a 5° mesh were constructed for smooth wedges of 60° and 120° total angle by the numerical method due to Hill and Lee (1946). The field OSAS consists of a region ADF where the slip-lines are radii through A and circular arcs ; a region DFHS defined by the circular arcs DF and DS of equal radius ; a uniformly stressed region AFG ; a region FGHJ where one family of slip-lines are straight ; and a region GJO defined by the slip-line GJ and the axis of symmetry.

If t is the minimum specimen thickness, it is found that $t/2h$ is equal to 1·04 for $\theta=30°$ and to 2·17 for $\theta=60°$. The corresponding distributions of normal stress across OA are shown in fig. 3 ; it will be observed that this stress is tensile immediately under a narrow wedge but compressive under a wide wedge. The stress in the rear surface is always tensile. When θ tends to zero, so that the indenter becomes a knife-edge, the pressure $2k$ along AB is balanced by a uniform tension πk across OA. $t/2h$ is therefore equal to $(\pi+2)/2\pi$ or 0·82 approximately. At the other extreme, when θ tends to 90°, the slip-line field becomes similar to that for a flat die, for which the critical $t/2h$ is 4·37 (Hill 1947). The relation

between the critical ratio $t/2h$ and the semi-angle θ is given in fig. 4*. The critical ratio of load to thickness is also shown; since this has a maximum value when $\theta \sim 60°$, the hardness of a given specimen can be measured over a greater range of loads with a 120° wedge than with any other.

Fig. 3.

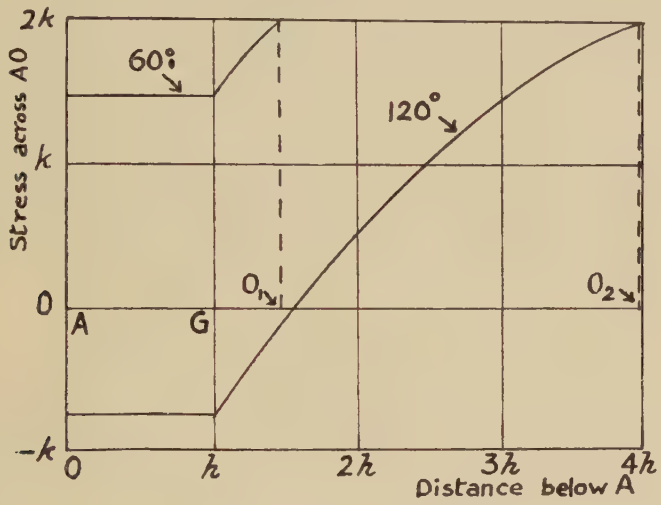

Fig. 4.

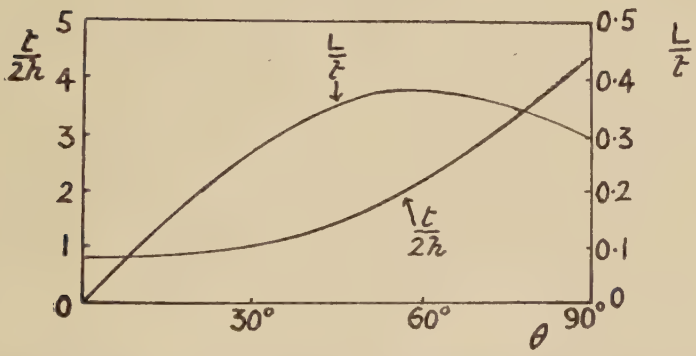

The effect of friction on the foundation is to delay the moment when the critical penetration is reached. Calculation shows, however, that the effect is so small as to have little practical importance for coefficients of friction less than 0·1. Lateral compressive forces applied to the sides of the specimen would be more effective (so long as they do not cause general yielding).

* For comparison, the critical ratio of specimen thickness to impression diameter is 3·14 when a semi-cylindrical cavity is expanded in the surface (Hill 1948).

The speed U with which the ends of the specimen slide sideways is determined by the following considerations. If the speed V of penetration is given, and U is assigned arbitrarily, the velocity at any point in the plastic region can be calculated from Geiringer's equations. In particular, the velocity in AFG, ABD, and BEC is uniform, so that the displaced surface BC remains straight during the next infinitesimal increment of penetration. (As the penetration continues, the part of the coronet above the element now at C remains straight, but the additional lower part is curved.) Corresponding to a slightly altered position of the surface, it must be possible to find a new plastic state of stress throughout the material which was plastic prior to the increment of penetration. Otherwise plastic material unloads during the incremental penetration and this is inconsistent with the assumption of continuing plastic flow implicit in the application of Geiringer's equations*. This is the condition which determines the true ratio U/V. A calculation of U/V has not been made by the writer.

§4. Calculation of the Critical Width.

In a specimen whose width is small compared with its thickness, the plastic region spreads out to the sides as indentation continues. At a certain penetration the plastic region (whose conjectured boundary is indicated by broken curves in fig. 5) just contains a complete slip-line HJKLM, extending from the axis of symmetry to the lateral surface (which it must meet at an angle of 45°). Up to this moment the plastic material below the indenter has been rigidly constrained. After this moment the rigid corners of the specimen are assumed to be displaced sideways by sliding over the slip-line KLM; for this to be possible, KLM must be of a suitable shape. Now the development of a plastic region having a boundary cut more than once by a slip-line family is not uniquely determined by the state of stress alone, but proceeds in such a way that certain conditions for the existence of displacements are satisfied (Hill 1950). It is reasonable to suppose, therefore, that the plastic region spreads out to the sides of the specimen in such a manner that the slip-line KLM is of the correct shape to permit a sideways displacement of the rigid corners. Since a rigid-body motion in a plane can only be a rotation about some instantaneous centre (which is at infinity for a pure translation), two rigid bodies can only slide over each other if the line of contact is a circular arc. Thus KL must be circular. We must also include a straight segment LM such that LMN is a region with straight slip-lines meeting the surface at 45°. The stress in LMN is a uniform compression $2k$ parallel to the surface, while the ensuing deformation caused by the rotation of the corner is a non-uniform shear parallel to LM.

* These remarks are of general significance for removing an apparent lack of uniqueness in many problems where a plastic-rigid body is assumed.

Since the nett angle turned through in going from M to H along the slip-line is zero, the hydrostatic components of the stress at H and M are equal; their value is $-k$, since the stress in LMN is a compression of amount $2k$. Hence H is the point on the axis at which the hydrostatic stress-component is $-k$ in the unique continuation of the field ABCDE. By Hencky's theorem, H lies on the slip-line through B which is inclined at an angle $\frac{1}{4}\pi - \frac{1}{2}(\theta - \psi)$ to BE. For θ less than about 50°, H coincides with A, and the slip-line HJKLM makes an angle $\frac{1}{4}\pi - \frac{1}{2}(\theta - \psi)$ with AD.

Fig. 5.

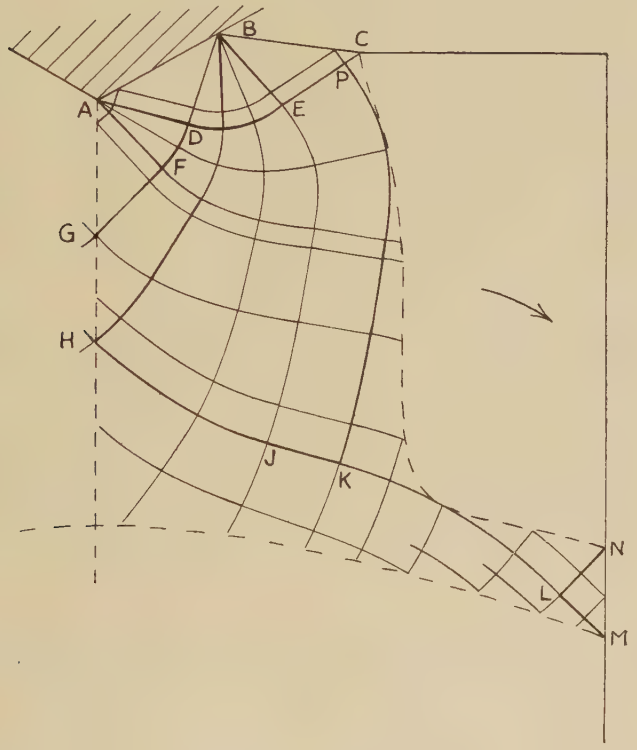

H having been fixed in this way, there are three unknown quantities to be calculated. These are the length b of JK (all slip-lines of this family of EJKP are of equal length), the radius r of KL, and the length a of LM. When these are known, the critical width of the specimen follows at once from simple geometry. To determine the three unknowns there are the three conditions for the equilibrium of the rigid corner, viz.: two conditions for the vanishing of the resultant force components, and one for the vanishing of the resultant couple. The resultant force and couple are calculated from the distribution of stress over the perimeter CPKLN, or, more conveniently, from the distribution over BAHJKLM

(the equilibrium of the region covered by the slip-line field is, of course, automatically ensured by the equations of Hencky used in constructing the field).

When the indenter is a knife-edge an explicit analytic solution is possible (fig. 6). The perimeter of the rigid corner has an axis of symmetry bisecting the angle at the corner. It may be shown without difficulty that

$$a/h=\sqrt{2}-\frac{4}{\pi}, \qquad b/h=\frac{4}{\pi}-\frac{1}{\sqrt{2}}, \qquad r/h=\frac{4}{\pi}.$$

Fig. 6.

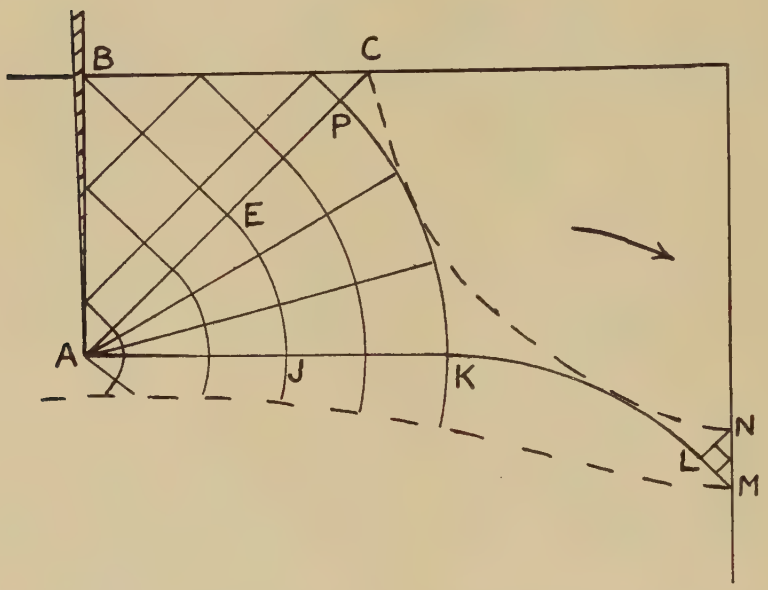

The critical width is therefore $2h(\pi+4)/\pi$ or about 4·54 times the depth of penetration. When $\theta=90^\circ$ (flat die) calculation gave the values

$$a/h=0{\cdot}95\,, \qquad b/h=0{\cdot}54\,, \qquad r/h=5{\cdot}67\,.$$

The critical width is 8·6 times the width of the die. M is 3·67 die-widths below the corner. When $\theta\sim50^\circ$ the point H coincides with A ($\theta+\psi\sim90^\circ$; see fig. 2). The corresponding values of a, b and r, were calculated to be

$$a/h=0{\cdot}205\,, \qquad b/h=0{\cdot}51\,, \qquad r/h=1{\cdot}92\,.$$

The critical width is about 4·5 times the width of the impression. M is $2{\cdot}14h$ below the corner.

§5. Conclusions.

The minimum dimensions for the two-dimensional model are somewhat greater than those for actual indenters. For example, the minimum thickness recommended with a 136° pyramid is about twice the diagonal

of the impression (Hankins and Aldous 1934). The difference is understandable since there is greater freedom of flow around a three-dimensional indentation. Moreover, the plastic zone penetrates less far, owing to the diffusion of stress concentrations through a relatively larger volume. The present calculations have, therefore, a limited practical value. The value of the investigation lies rather in its contribution to a general understanding of a hardness test, especially in showing why the hardness value is independent of specimen size, down to dimensions which are comparatively small in relation to the indentation. The investigation is also of fundamental interest in that it formulates methods for solving plane plastic problems of a kind different from any previously attempted.

Acknowledgments.

I am grateful to the Director of the British Iron and Steel Research Association for permission to publish the paper. I have received valuable help in the numerical computations from Messrs. G. Douglass and A. P. Green, of the Solid Mechanics Section of B.I.S.R.A.

References.

Field Foster, P., 1948, *Mechanical Testing of Metals and Alloys*, 4th Edition (London : Pitman & Sons), p. 161.

Hankins, G. A., and Aldous, C. W., 1934, *J. Inst. Metals*, **54**, 59.

Heyer, R. H., 1937, *Proc. Am. Soc. Test. Mat.*, **37**, 119.

Hill, R., 1947, *J. Iron & Steel Inst.*, **156**, 513 ; 1948, *Proc. 7th Int. Cong. App. Mech.* (London) ; 1949, *Quart. J. Mech. App. Maths.*, **2**, 40 ; 1950, *The Mathematical Theory of Plasticity*, (Oxford : Clarendon Press), Chap. IX.

Hill, R., and Lee, E. H., 1946, *Proc. 6th Int. Cong. App. Mech.* (Paris).

Hill, R., Lee, E. H., and Tupper, S. J., 1947, *Proc. Roy. Soc.* A, **188**, 273.

LXVIII. *On the Back Current in Blocking-Layer Rectifiers.*

By J. H. Gisolf,
Haarlem*.

[Received February 24, 1950.]

Summary.

This paper is based on the theory of the metal semiconductor contact of Schottky and of Davidov, and is meant (*a*) to make this theory applicable in practice to all existing semiconductor types, and (*b*) to introduce quantitatively the influence of the electric field at the interface on the threshold energy. It appeared to be useful to introduce an independent variable y, proportional to the reciprocal of the concentration of the conduction electrons. A differential equation of the Abel type is derived for the electric field in the semiconductor as a function of y. Taking into account the diminution of the threshold energy by the electric field at the interface, a relation is derived between the variable y and the electric field at the interface. The differential equation is given for the different types of semiconductors. When the differential equation is solved, the current-voltage characteristic can be found by numerical integration. Some examples are given. In the case of back currents, an asymptotic solution of the differential equation exists, which leads to a parametric representation of the current-voltage characteristic in the back direction. The shape of the back current characteristic is discussed. The differences between rectifiers of the selenium type and the crystal detectors are elucidated. Some remarks on the physical background of the electrical pretreatment of selenium rectifiers are made.

§1. Introduction.

The first theory of the blocking-layer rectifier, not based on *ad hoc* hypotheses, was given almost simultaneously by Davidov (1939) and by Schottky (1939). These theories differ in their mathematical form, but are based on the same physical conceptions (Gisolf 1942). They account satisfactorily for the current dependence of the resistance for forward and for small back currents. (The "forward" direction is the direction for which the resistance is low.) For larger back currents considerable deviations from the theory occur. The resistance first passes through a maximum and tends to vanish for large back currents. Schottky (1941) did mention the presumable cause of this deviation, namely that in consequence of the strong electric field in the semiconductor at the boundary of the metal electrode, the threshold energy for the transition

* Communicated by the Author.

of charge carriers from the metal to the semiconductor is diminished and the number of these particles in the semiconductor is increased. In the present paper a treatment of the above problem is given, which enables one to derive formulæ for the resistance of back currents with due allowance for the influence of the field on the threshold energy. The way by which this result is achieved may be outlined as follows. The concentration of the free electrons in the semiconductor is a univalent function of the distance x of the point under consideration from the surface of the electrode. Instead of x an independent variable y is introduced, which, except for a constant factor, is equal to the reciprocal of the concentration of the free electrons. From the fundamental formula of the electric field a differential equation is derived which gives the electric field strength in the semiconductor as a function of y for each value of the current density. The equation can be solved by numerical methods for the different types of semiconductors. A boundary condition is given by the field strength at a long distance from the electrode where $y=y_\infty$. Schottky's formula for the diminution of the threshold energy at the electrode as a function of the field strength together with the relation between the field strength and the variable y, leads to the value y_0 of the variable y at the electrode. The resistance and the capacity of the metal semiconductor contact are found as integrals of completely known functions of y between the limits y_0 and y_∞.

§2. Theoretical Picture of a Semiconductor.

In the following pages ordinary electrons with a charge $-e$, as well as " electron holes " with a charge $+e$ will be spoken of as " electrons ". It is possible to classify the rich variety of semiconductors on account of the electron energy scheme (Gisolf 1947). The following types may be cited :—

A. The concentration of the free or conduction electrons n_e is large compared to the concentration of the electron traps N_t. The free electrons originate from impurity atoms nearly all of which are ionized by the crystal lattice. These impurities may be a stoichiometric excess of metal or metalloid atoms (for electrons and electron holes respectively), similar to those constituting the crystal lattice. The concentration n_e is then practically independent of the temperature. The conductivity slightly increases with decreasing temperature.

B. Although only a fraction of the impurity atoms is ionized by the crystal lattice, the concentration of the free electrons n_e is still large compared with the concentration of the electron traps N_t. The degree of ionization increases with increasing temperature. The concentration of the free electrons, and in consequence the conductivity, increases exponentially with increasing temperature. A definite ionization energy can be attributed to the impurity atoms. This case *B* is the only one that is treated in textbooks though it rarely occurs in practice.

C. In this case the concentration of the conduction electrons n_e is small compared to the concentration of the electron traps N_t. One can assume, without loss of general applicability, that the impurity atoms are all ionized. The trapping energies are supposed to be practically homogeneously distributed over a range of energies ΔE, which is large compared to the Boltzmann energy kT. In this case the concentration of the free electrons, and consequently the conductivity, is again an exponential function of the temperature. The pseudo "ionization energy" deduced from this exponential dependence, however, now strongly depends on the concentration of the impurity atoms N_i and in such a way that it becomes a universal linear function of the logarithm of the conductivity (the Meyer rule).

The electrons of the semiconductor, which do not belong to the atoms of the normal lattice, are either bound to impurity atoms or are "free". In any case they are supposed to have a definite energy. The energy of a free or conduction electron will be denoted by E_e and the energy of an electron bound to an impurity atom by E_i. The concentration of the conduction electrons n_e is given by the formula

$$n_e = N_c/\{1+\exp(E_e-g)/kT\} \quad . \quad . \quad . \quad . \quad . \quad . \quad (1)$$

with

$$N_c = \left(\frac{2\pi m^* kT}{h^2}\right)^{3/2}, \quad . \quad . \quad . \quad . \quad . \quad . \quad . \quad . \quad (2)$$

In these formulæ m^* is the "effective" electron mass. m^* may be several times the normal electron mass but the exact value cannot be fixed. T is the absolute temperature; k is Boltzmann's constant and h is Planck's constant. $N_c \approx 10^{19}$ cm.$^{-3}$; g is the free energy per electron. In a stationary state the value of g is the same at every point.

The concentration n_i of the electrons bound to the impurity atoms with the energy E_i, is given by the analogous formula

$$n_i = N_i/\{1+\exp(E_i-g)/kT\}. \quad . \quad . \quad . \quad . \quad . \quad . \quad (3)$$

In this formula N_i is the concentration of the impurity atoms to which electrons can be bound with the energy E_i. With the abbreviation

$$y = \exp(E_e-g)/kT \quad . \quad . \quad . \quad . \quad . \quad . \quad . \quad . \quad (4)$$

the formulæ (1) and (3) can be written

$$n_e \quad N_c/(1+y) \approx N_c/y, \qquad (\text{for } n_e \ll 10^{19}). \quad . \quad . \quad . \quad . \quad (5)$$

$$n_i = N_i/\{1+y\exp(-E_e+E_i)/kT\} \approx N_i/y\exp(-E_e+E_i)/kT, \quad (\text{for } n_i \ll N_i)$$
$$. \quad . \quad . \quad (6)$$

When the contact surface of the metal and the semiconductor is flat, y only depends on the distance from the contact surface.

The space charge density ρ can readily be expressed in terms of the parameter y for each of the semiconductor types mentioned above. It is assumed that the impurity atoms in the crystal are electrically neutral

so long as they have not lost electrons by thermal dissociation. For the "traps", on the other hand, it is assumed that they are electrically neutral so long as they have not captured an electron. The following formulæ for the space charge density ρ are found :

For the case A : $$\rho = e(N_i - N_c/y). \quad . \quad . \quad . \quad . \quad . \quad . \quad . \quad . \quad . \quad . \quad (7)$$

For the case B : $$\rho = eN_i \frac{\{y^2 + y(1 - N_c/N_i) - N_c/N_i \exp \Delta E/kT\}}{\{y^2 + y(1 + \exp \Delta E/kT) + \exp \Delta E/kT\}}$$

$$\approx e \frac{\{N_i y^2 - N_c(y + \exp \Delta E/kT)\}}{y(y + \exp \Delta E/kT)}, \quad . \quad . \quad . \quad . \quad . \quad (8)$$

ΔE being the dissociation energy of the impurity atoms.

For the case C : $$\rho = e\{N_i - N_t(1 - kT/\Delta E \ln y) - N_c/y\}, \quad . \quad . \quad . \quad . \quad (9)$$

ΔE now being *the range* of the trapping energies of the electron traps.

The types *A*, *B* and *C* represent extreme cases. All practical cases are more or less intermediate. The bulk of the semiconductors belongs to type *C*. The discussion of this type is important for the theory of the crystal detectors. Cuprous oxide belongs most probably to type *B*. For selenium the situation is not clear. From measurements on single crystals one might conclude that selenium belongs to type *B*, with a rather small value of ΔE. For polycrystalline selenium ΔE strongly differs for variously treated samples, but it is always small. Since the value of y is large in the blocking layer, the formulæ (7) and (8) show that, when dealing with blocking layer problems, one may reckon selenium to class *A*, as has already been pointed out by Schottky (1939).

§3. Derivation of the Detector Equation.

In the semiconductor the following two fundamental equations hold universally.

(*a*) The Poisson equation

$$dF/dx = \rho(x)/\epsilon\epsilon_0. \quad . \quad . \quad . \quad . \quad . \quad . \quad . \quad . \quad . \quad (10)$$

(*b*) The "continuity equation" for the current

$$i = n_c e u F + kTu \, dn_c/dx, \quad . \quad . \quad . \quad . \quad . \quad . \quad . \quad . \quad (11)$$

where F is the electric field strength, ϵ is the dielectric constant of the semiconductor and $\epsilon_0 = 8{\cdot}859 \cdot 10^{-14}$, A sec/V cm. is the permittivity of free space, i is the current density, e is the value of the electronic charge, u is the electron mobility in the semiconductor.

The x-axis is perpendicular to the interface of the metal and the semiconductor, the positive direction pointing to the semiconductor. By means of formula (5), n_c in equation (11) can be expressed in terms of the parameter y. A simple transformation results in

$$dy/dx = (F - iy/euN_c)ey/kT, \quad . \quad . \quad . \quad . \quad . \quad . \quad . \quad (12)$$

y being a function of x only, equation (10) can be transformed in the following manner :

$$d\mathrm{F}/dy \,.\, dy/dx = \rho(y)/\epsilon\epsilon_0. \quad . \quad . \quad . \quad . \quad . \quad . \quad . \quad (13)$$

The function $\rho(y)$ is given by one of the formulæ (7), (8) or (9) according to the type of the semiconductor under consideration. Substituting (12) in (13) one obtains

$$d\mathrm{F}/dy \,.\, (\mathrm{F} - iy/eu\mathrm{N}_c)ey/k\mathrm{T} = \rho(y)/\epsilon\epsilon_0. \quad . \quad . \quad . \quad . \quad (14)$$

The solution of this non-linear differential equation gives F as a function of the parameter y.

Equation (14) can be shortened, by introducing an auxiliary quantity $f(y)$, defined in the following way :

$$f(y) = \mathrm{F}(y) - iy/eu\mathrm{N}_c. \quad . \quad . \quad . \quad . \quad . \quad . \quad . \quad (15)$$

Introducing (15) into (14), we have

$$df/dy = k\mathrm{T}/e\epsilon\epsilon_0 \,.\, \rho(y)/yf - i/eu\mathrm{N}_c \quad . \quad . \quad . \quad . \quad . \quad (16)$$

or

$$\boxed{df/dy = \chi(y)/f - f_c} \quad . \quad . \quad . \quad . \quad . \quad . \quad . \quad (17)$$

where

$$\chi(y) = k\mathrm{T}/e\epsilon\epsilon_0 \,.\, \rho(y)/y \quad . \quad . \quad . \quad . \quad . \quad . \quad . \quad (18)$$

and

$$f_c = i/eu\mathrm{N}_c = \text{constant}. \quad . \quad . \quad . \quad . \quad . \quad . \quad . \quad (19)$$

Equation (17) is the starting point for the crystal rectifier problem. It will be referred to as the " detector-equation ". It is a so-called Abel equation. The solutions cannot be expressed in terms of finite elementary functions. It is however very suitable for numerical integration. For each type of semiconductor the function $\chi(y)$ is completely known and can be tabulated once and for all. When the quantity $\mathrm{F}(y)$ is found as a function of y by integration of the detector equation, it leads to the desired information concerning the electric resistance, the capacity, etc., for each value of the current density i. (See § 5.)

The quantity $f(y)$ has an obvious physical meaning. It is that part of the electric field that is needed to maintain the differences in the concentration of the free electrons from point to point.

§ 4. The Boundary Conditions for the Solution of the Detector Equation.

At a large distance from the interface, the electron distribution in the semiconductor will be the same as if no metal were present. In practice, this " large " distance means about 1μ). According to formula (5) the concentration of the conduction electrons for $x \to \infty$ is given by

$$n_c(x \to \infty) = \mathrm{N}_c/y_\infty, \quad . \quad . \quad . \quad . \quad . \quad . \quad . \quad (20)$$

y_∞ is the value of y for $x = \infty$.

For $x\to\infty$ the electron distribution becomes homogeneous and in consequence $f(x\to\infty)\to 0$. Thus

$$\text{for } y\to y_\infty,\quad f(y)\to 0 \quad \text{and} \quad \chi(y)\to 0. \qquad (21)$$

Substituting (21) in the detector equation (17) one sees that for $y\to y_\infty$, df/dy becomes indefinite. We can abolish this indefiniteness by differentiation of the numerator and the denominator of the quotient χ/f. This gives for $(df/dy)_{y_\infty}$ a quadratic equation with the following solutions:

$$\left(\frac{df}{dy}\right)_{y_\infty}=\frac{-f_c}{2}\pm\sqrt{\frac{f_c^2}{4}+\left(\frac{d\chi}{dy}\right)_{y_\infty}}, \qquad (22)$$

$f(y)$ and df/dy are always negative and in (22) the sign must be chosen accordingly. The integration of the detector equation can be started at $y=y_\infty$. Because no great accuracy is wanted, the integration is readily performed.

For the case in which the current is zero, the constant f_c also becomes zero and the detector equation reduces to

$$df/dy=\chi/f \qquad (\text{for } i=0). \qquad (23)$$

This equation can be integrated immediately:

$$f^2(y)=2\int_{y_\infty}^{y}\chi(y)\,dy \qquad \text{for } i=0. \qquad (24)$$

§ 5. Calculation of the Characteristic Properties of the Metal-semiconductor Contact.

In the preceding section it was shown how, for a given semiconductor f can be calculated as a function of y for each value of the current density i. The next task will be to express the characteristic quantities such as the resistance, the capacity, etc., in terms of f and y.

The conductivity is given by the following formula:

$$\sigma=eun_c=eu\mathrm{N}_c/y \text{ ohm}^{-1}\text{ cm.}^{-1}. \qquad (25)$$

The barrier-layer resistance R_b is defined as the difference of the actual resistance per cm.^{2} and the resistance per cm.^{2} such as it would be if no metal were present. Thus

$$\mathrm{R}_b=\frac{1}{eu\mathrm{N}_c}\int_0^\infty (y-y_\infty)\,dx. \qquad (26)$$

From (12) it follows that

$$dx=k\mathrm{T}/e\,.\,dy/yf \qquad (27)$$

and thus:

$$\mathrm{R}_b=\frac{k\mathrm{T}}{e^2u\mathrm{N}_c}\int_{y_0}^{y_\infty}\frac{(y-y_\infty)}{yf}\,dy \text{ ohm cm.}^2, \qquad (28)$$

y_0 is the value of y at $x=0$.

Multiplying R_b by i one finds the barrier-layer tension U_b. U_b is that part of the applied voltage that appears across the barrier-layer.

$$U_b = \frac{kTi}{e^2 u N_c} \int_{y_0}^{y_\infty} \frac{(y-y_\infty)}{yf}\, dy \text{ volt.} \quad . \quad . \quad . \quad . \quad . \quad (29)$$

The electric field strength at the surface of the metal F_0 follows from (15):

$$F_0 = f(y=y_0) + iy_0/euN_c \text{ volt cm.}^{-1}. \quad . \quad . \quad . \quad . \quad . \quad (30)$$

The barrier-layer capacity C_b is given by

$$C_b = \epsilon\epsilon_0\, dF_0/dU_b \text{ farad. cm.}^{-2} \quad . \quad . \quad . \quad . \quad . \quad (31)$$

and follows therefore from (29) and (30).

§ 6. The Value of y_0 at the Electrode.

In order to calculate the characteristic quantities of the blocking layer with the help of the formulæ of the preceding section, the value y_0 at the electrode must be known. This is synonymous with the assertion, that the concentration of the free electrons in the semiconductor at the electrode must be known.

The electrons in the semiconductor at the boundary of the metal are in thermodynamical equilibrium with the electrons inside the metal. *It is assumed that this equilibrium is not disturbed even by the largest current.* The equilibrium concentration of the free electrons at the interface is determined by the threshold energy $e\phi$ for the transition of electrons from the metal to the semiconductor. As the top of the occupied energy levels in the metal coincides with the free energy per electron g introduced in (1), this threshold energy is $k\mathrm{T} \ln y_0$, as can be seen from (4). Thus

$$e\phi = k\mathrm{T} \ln y_0. \quad . \quad . \quad . \quad . \quad . \quad . \quad . \quad . \quad (32)$$

Now it is known that under the influence of an electric field F_0 at the boundary of the metal, the threshold energy decreases by $e\sqrt{(-eF_0/\epsilon\epsilon_0)}$. (See, for instance, *Handbuch der Physik*, xxiv., **2**, p. 437.)

This is a consequence of the "image force". If Y_0 is the value of y at the interface in absence of any electric field, then

$$e\sqrt{(-eF_0/\epsilon\epsilon_0)} = e(\phi_0 - \phi) = k\mathrm{T} \ln Y_0/y_0. \quad . \quad . \quad . \quad . \quad (33)$$

Eliminating F_0 from this equation with the help of formula (15) one gets

$$\boxed{f_0 + iy_0/euN_c = -k^2\mathrm{T}^2\epsilon\epsilon_0/e^3 \,.\, \ln^2 (Y_0/y_0).} \quad . \quad . \quad . \quad (34)$$

The quantity $k\mathrm{T} \ln Y_0$ might be called the "true" threshold energy. It is a property of the combination of the particular metal and semiconductor under consideration and must be known *a priori* in order to carry through the preceding calculations. The equation (34) describes the quantity f_0 as a function of y_0. The point of intersection of the curve representing f_0 as a function of y_0 (formula (34)) and the curve representing f as a function of y (detector equation, formula (17)) gives the values of

y_0 and f_0 which are needed to apply the formulæ (28), (29) and (30). With this result the mathematical solution of the blocking-layer problem, with due allowance for the field effect is obtained.

In the next section the method will be demonstrated with the aid of some examples. In the following section it will be shown that for large back currents an asymptotic solution of the detector equation exists which enables us to calculate the characteristic quantities of the blocking-layer without numerical integration. This asymptotic solution will then be used in the discussion of the properties of the blocking-layers at large back currents.

§ 7. Some Examples.

In the following examples the values of the different constants, such as the dielectric constant ϵ and the electron mobility u, are not specific for a particular material, but do represent plausible values and are chosen in such a way as to make the different coefficients of the detector equation simple numbers.

For N_c we take the value 10^{-19} cm.$^{-3}$ and for u the value $u=6{\cdot}3$ cm.^{2} V^{-1} sec.$^{-1}$, which makes $euN_c=10$. For ϵ the value $\epsilon=4{\cdot}55$ is chosen and hence $kT/\epsilon\epsilon_0=10^{-8}$ V^2 cm. for T$=293°$ K.

The following examples refer to semiconductors of the types A and C. For both, the "true" threshold energy $e\phi_0$ is taken as 0·349 eV., which gives $Y_0=10^6$ at T$=293°$ K. For the semiconductor of type C the value ΔE is arbitrarily chosen as 0·582 eV. ($=23\,kT$). The concentration of the electron donor impurity atoms and the concentration of the electron traps are chosen in such a way as to give both semiconductors at room temperature the same conductivity when no metal is present. This means that both will have the same y_∞. For y_∞ we take the value 10^4. At a large distance from the metal, that is to say for $y=y_\infty$, $\sigma=10^{-3}$ ohm cm. (see formula (25)) and the space charge denisty ρ is zero. Thus formula (7) for the semiconductor of type A gives $N_i=10^{15}$ cm.$^{-3}$ and for the semiconductor of type C formula (9) gives $N_i-0{\cdot}6N_t=10^{15}$ cm.$^{-3}$. If the arbitrary value $N_t=10^{18}$ cm.$^{-3}$ is chosen for N_t, it follows that $N_i=6{\cdot}01\ 10^{17}$ cm.$^{-3}$. The numerical integration of the equation (17) has been performed by means of a very straightforward method, due to Horst van Sanden (1946). The integrations are carried through for a number of positive and negative values of i.

In the Tables I. and II. some of the results are summarized with the purpose of demonstrating that two semiconductors, which are alike from the electrical point of view, may behave quite differently as rectifiers in contact with the same metal even when the threshold energy is also the same. For the type C semiconductor the blocking-layer resistance is much less than for the type A semiconductor and for small current densities the direction of the rectification is opposite in the two examples, as can be seen from the current-voltage characteristics in fig. 1. These differences are brought about by the much larger space charge density in the case of the type C semiconductor and its strong current dependence.

TABLE I.

Type A : $Y_0=10^6$; $N_i=10^{15}$ cm.$^{-3}$.

i A cm.$^{-2}$	R Ohm cm.^{2}	y_0	F_0 V. cm.$^{-1}$	ρ_0 el. charges	$\phi_0-\phi$ volt
+10	$1{\cdot}08\times10^{-2}$	$1{\cdot}00\times10^6$	$+9{\cdot}02\times10^3$	$9{\cdot}9\times10^{14}$	0
+1	$4{\cdot}36\times10^{-2}$	$2{\cdot}45\times10^5$	$-3{\cdot}20\times10^3$	$9{\cdot}9\times10^{14}$	0·036
0	$6{\cdot}40\times10^{-2}$	$1{\cdot}48\times10^5$	$-5{\cdot}93\times10^3$	$9{\cdot}3\times10^{14}$	0·048
−1	$8{\cdot}10\times10^{-2}$	$8{\cdot}06\times10^4$	$-9{\cdot}80\times10^3$	$8{\cdot}8\times10^{14}$	0·064
−10	$5{\cdot}40\times10^{-2}$	$2{\cdot}28\times10^4$	$-2{\cdot}31\times10^4$	$5{\cdot}6\times10^{14}$	0·095

TABLE II.

Type C : $Y_0=10^6$; $N_i=6{\cdot}10^{17}$ cm.$^{-3}$; $N_t=10^{18}$ cm.$^{-3}$; $\Delta E=0{\cdot}582$ eV.

i A cm.$^{-2}$	R Ohm cm.^{2}	y_0	F_0 V. cm.$^{-1}$	ρ_0 el. charges	$\phi_0-\phi$ volt
+10	$2{\cdot}38\times10^{-3}$	$5{\cdot}70\times10^4$	$-1{\cdot}34\times10^4$	$7{\cdot}54\times10^{16}$	0·073
+1	$1{\cdot}65\times10^{-3}$	$2{\cdot}93\times10^4$	$-2{\cdot}02\times10^4$	$4{\cdot}64\times10^{16}$	0·089
0	$1{\cdot}60\times10^{-3}$	$2{\cdot}76\times10^4$	$-2{\cdot}08\times10^4$	$4{\cdot}36\times10^{16}$	0·091
−1	$1{\cdot}53\times10^{-3}$	$2{\cdot}60\times10^4$	$-2{\cdot}15\times10^4$	$4{\cdot}11\times10^{16}$	0·094
−10	$1{\cdot}16\times10^{-3}$	$1{\cdot}80\times10^4$	$-2{\cdot}62\times10^4$	$2{\cdot}49\times10^{16}$	0·101

Fig. 1.

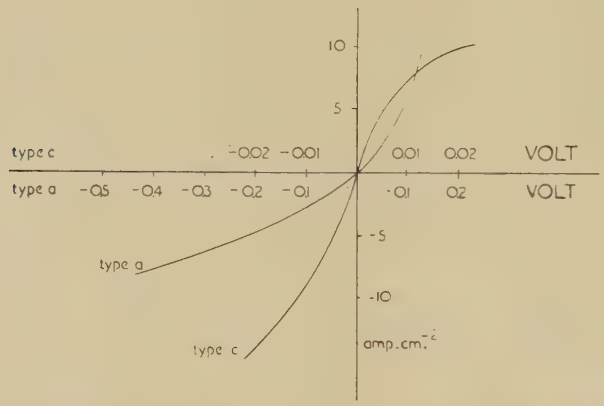

The barrier-layer tension as a function of the current density of two crystal-rectifiers of the A-type and the C-type respectively.
For the A-type : $Y_0=10^6$; $N_i=10^{15}$ cm.$^{-3}$.
For the C-type : $Y_0=10^6$; $N_i=6{\cdot}10^{17}$ cm.$^{-3}$; $N_t=10^{18}$ cm^{-3} ; $\Delta E=0{\cdot}582$ eV.

§ 8. AN ASYMPTOTICAL SOLUTION OF THE ABEL EQUATION.

Consider the case in which the constant f_c in the differential equation (17) is negative. Physically this means that a back-current flows. When y is increased to infinity, the function $\chi=\rho(y)/y$, tends to zero as can be seen from the formulæ (7), (8) and (9). f being always negative, df/dy cannot tend to a finite positive value and therefore χ/f cannot become zero for large values of y. But then f and df/dy must go to zero with increasing y and thus the differential equation reduces to

$$f(y)=\chi(y)/f_c. \quad . \quad . \quad . \quad . \quad . \quad . \quad . \quad . \quad (35)$$

Substituting (35) into (28) and considering that $y \gg y_\infty$, one finds for the back-resistance the approximation

$$R_b = \frac{kT}{e} \frac{i}{(euN_c)^2} \int_{y_0}^{y_\infty} \frac{dy}{\chi(y)}. \quad \ldots \ldots \quad (36)$$

The above approximation holds as well for large values of y, as for large negative values of i. In this approximation the equation (34) reduces to the following transcendental equation for y_0 :

$$iy_0/euN_c = -k^2T^2\epsilon\epsilon_0/e^3 \cdot \ln^2 (Y_0/y_0). \quad \ldots \ldots \quad (37)$$

In the next section the above approximation will be used to calculate the back-current characteristic of the contact of a metal with a semiconductor of the A-type.

§ 9. The Back-current Characteristic for a Semiconductor of the A-type.

For a semiconductor of the A-type, equation (35) reduces to

$$f = \frac{kTeuN_cN_i}{\epsilon\epsilon_0 i} \cdot \frac{(y-y_\infty)}{y^2} \quad \ldots \ldots \quad (38)$$

and (29) reduces to

$$U_b = -\frac{\epsilon\epsilon_0}{2eN_i(euN_c)^2} \cdot i^2(y_0^2 - y_\infty^2). \quad \ldots \ldots \quad (39)$$

From equations (37) and (39) the equation for the back-current characteristic can be derived, computing y_0 from (39) and substituting in (37). For practical calculations, however, it is more convenient to consider equations (37) and (39) as a parameter representation of the back-current characteristic. For each chosen value of y_0 these equations give the corresponding values of i and U_b.

When the back-current increases, the value of y_0 decreases, as can be seen when computing di/dy from (37). Thus in (39) the factor $(y_0^2 - y_\infty^2)$ will decrease when i^2 increases and the possibility of a maximum in the border-layer tension exists. With the aid of (37), i can be eliminated from (39). For the occurrence of a maximum for U_b dU_b/dy_0 must be zero. This leads to the following transcendental equation for y_0^*, the value of y_0 for which the barrier-layer back tension attains its maximum :

$$\ln Y_0/y_0^* = 2(y_0^* - y_\infty^2)/y_\infty^2. \quad \ldots \ldots \quad (40)$$

Substituting the value of y_0^* found from this equation into (37) one finds the corresponding value of the back-current i^*, and substitution of y_0^* and i^* into (39) gives the maximum U_b^* of the barrier-layer tension. Equation (40) can be solved graphically in a simple way.

Some examples :

	N_i	Y_0	y_0^*	U_b^*	i^*
(*a*)	10^{15} cm.$^{-3}$	10^7	$2{\cdot}03 \times 10^4$	$-3{\cdot}71$ volt	-30 A/cm.^{2}
(*b*)	10^{15} cm.$^{-3}$	$1{\cdot}4 \times 10^{10}$	$2{\cdot}62 \times 10^4$	-100 volt	-107 A/cm.^{2}
(*c*)	10^{15} cm.$^{-3}$	10^{12}	$3{\cdot}07 \times 10^4$	-279 volt	-157 A/cm.^{2}

The voltage maximum in the back direction cannot be observed on selenium or cuprox rectifiers because at current densities much smaller than those at which the maximum would occur, the rectifier would have been disturbed by heat. The maximum is observable on crystal rectifiers when high-frequency voltage pulses are applied (Torrey and Whitmer 1948). The maximum is found at a voltage of some 100 or 200 volts. The value of the current density in crystal rectifiers of the whisker-contact type is difficult to estimate, because the contact area between the whisker and the crystal is not exactly known. At any rate, the back-current densities at high back voltages can be estimated at magnitudes of a hundred A/cm.^{2} or so.

Fig. 2.

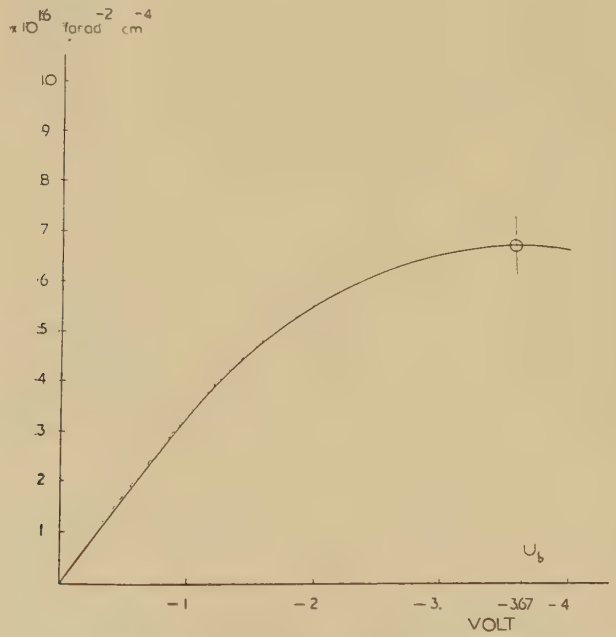

$1/C_b^2$ of a crystal rectifier of the A-type as a function of the back-voltage U_b. $Y_0=10^7$; $N_i=10^{15}$ cm.$^{-3}$.

The example (*a*) corresponds to a rather bad rectifier ; the example (*b*) corresponds to a modern high-inverse-voltage crystal detector and the example (*c*) corresponds to a rectifier of the selenium type.

The *barrier-layer capacity* C_b follows from (31) :

$$dF_0/dU_b=(dF_0/dy_0)/(dU_b/dy_0), \quad . \ . \ . \ . \ . \quad (41)$$

dF_0/dy_0 follows immediately from (33) and dU_b/dy_0 follows from (39), when i is eliminated with the aid of (37).

As an example $1/C_b^2$ is calculated as a function of U_b for a semiconductor of the A-type with $N_i=10^{15}$ cm.$^{-3}$ and $Y_0=10^7$, (see fig. 2).

For small back-voltages $1/C_b^2$ is the same linear function of the back-voltage as has been found by Schottky (1941–1942).

For large back-voltages deviations from linearity are observed which agree qualitatively with the calculated curve of fig. 2. The curve has a maximum analogous to the maximum in the current-voltage characteristic in the back direction.

The maximum occurs at a back-voltage U_b^{**} corresponding to a value y_0^{**} in the parameter representation of (37) and (39), *i. e.* to the value which is a solution of the transcendental equation

$$\ln Y_0/y_0^{**}=\tfrac{4}{3}(y_0^{2**}-y_\infty^2)/y_\infty^2. \quad . \quad . \quad . \quad . \quad . \quad . \quad (42)$$

In the example of fig. 2 one finds $y_0^{**}=2{\cdot}35\times10^4$, and substituting this value into (37) one finds $i^{**}=-25{\cdot}3$ A/cm.$^{-2}$. Substituting y_0^{**} and i^{**} into (39) one finds $U_b^{**}=-3{\cdot}67$ V. Just as with the maximum in the current-voltage characteristic it is to be expected that the maximum in the $(1/C_b^2, U_b)$ curve will only be observable with short voltage-pulses. As far as the author is aware, such a maximum has not yet been observed †.

§ 10. The Rectifier of the Selenium-type.

Among the crystal rectifiers used in practical applications two quite different types can be discerned: the selenium and the cuprous oxide rectifiers on the one side and crystal detectors on the other. The principal difference lies in the fact that the crystal detector operates at 10^4 or 10^5 times as large a current density as the selenium or the cuprous oxide rectifier. That the applied current density is of preponderant influence on the unipolar conductivity of a metal semiconductor contact, will be clear when comparing, for example, fig. 1 and fig. 3. Most semiconductors in contact with a fine metal point, have an asymmetrical current-voltage characteristic, when the current density is made sufficiently high. This is effected by touching the crystal very loosely, so that the contact area is very small. Extremely few semiconductors have good rectifying properties at as low a current density as about a milliampere per cm.^{2}. Only two are used in practice, viz. selenium and cuprous oxide.

For a good rectifier of the selenium or cuprous oxide type, it is claimed that at a back-voltage of about 10 volt, the back-current will not exceed one milliampere per cm.^{2}. The contact being characterized by the two parameters Y_0 and N_i, one can ask for which pairs of values of these parameters a metal semiconductor contact will satisfy this requirement. In the formulæ (37) and (39) we substitute for i the value -10^{-3} amp cm.$^{-2}$ and for U_b the value -10 volt and thereupon these equations are solved for Y_0 and N_i. This is performed by putting N_i arbitrarily equal to integral powers of ten and computing the corresponding values of Y_0. The pairs of values thus obtained, together with some other calculated

† *Note added in proof.*—R. N. Smith (1946, *Phys. Rev.*, **69,** 683), reports that the contact capacity of Si-detectors, plotted as a function of the voltage, shows a minimum at a backvoltage of 0·5 volt.

features of the contact, are tabulated in Table III. Columns 1 and 2 give N_i and Y_0. Column 3 gives the value of ϕ_0 corresponding to Y_0. Column 4 gives the value of y_0. Column 5 gives the electric field at the electrode. In column 6 V_d the so-called " diffusion-potential " is tabulated, as derived from

$$V_d = kT \ln Y_0/y_\infty = 0{\cdot}058 \log Y_0/y_\infty \text{ volt.} \quad . \quad . \quad . \quad . \quad (43)$$

Column 7 gives the conductivity σ of the semiconductor.

It must be kept in mind, that the figures in this table are not calculated with values of ϵ, u and m^* which hold exactly for selenium ; these figures are therefore only meant as an illustration. The quantities that are open to experimental check are : N_i (from the voltage dependence of the capacity) ; V_d (from the current-voltage characteristic in the forward-direction) ; and σ (also from the current-voltage characteristic in the forward-direction). The figures inside the framed part of Table III. agree with experimental observations on actual rectifiers.

Table III.

N_i in cm.$^{-3}$	Y_0	ϕ_0 in volt	y_0	F_0 in volt cm.$^{-1}$	V_d in volt	σ in Ohm^{-1} cm.$^{-1}$
10^{16}	$4{\cdot}26\times10^{28}$	1·66	$2{\cdot}81\times10^{10}$	$2{\cdot}81\times10^{6}$	1·61	1
10^{17}	$1{\cdot}39\times10^{20}$	1·17	$8{\cdot}88\times10^{9}$	$8{\cdot}88\times10^{5}$	1·05	10
10^{16}	$1{\cdot}53\times10^{14}$	0·82	$2{\cdot}81\times10^{9}$	$2{\cdot}81\times10^{5}$	0·65	10^{2}
10^{15}	$1{\cdot}47\times10^{12}$	0·71	$8{\cdot}88\times10^{8}$	$8{\cdot}88\times10^{4}$	0·48	10^{3}
10^{14}	$1{\cdot}84\times10^{10}$	0·60	$2{\cdot}81\times10^{8}$	$2{\cdot}81\times10^{4}$	0·31	10^{4}
10^{13}	$9{\cdot}24\times10^{8}$	0·52	$8{\cdot}88\times10^{7}$	$8{\cdot}88\times10^{3}$	0·17	10^{5}
10^{12}	$1{\cdot}16\times10^{8}$	0·47	$2{\cdot}98\times10^{7}$	$2{\cdot}98\times10^{3}$	0·062	10^{6}
10^{11}	$1{\cdot}46\times10^{9}$	0·53	$1{\cdot}09\times10^{8}$	$1{\cdot}09\times10^{4}$	0·068	10^{7}

In fig. 3 the back-current characteristic is drawn for a rather arbitrary example, as calculated according to § 9. The decreasing back-resistance with increasing back-voltage is a common experience on selenium rectifiers.

Surveying Table III. the most striking feature is the small range for the threshold potential ϕ_0 in which rectifiers are actually realized. This is the more astonishing, as good selenium rectifiers can be made with a rather large variety of electrode metals. Now, it is known that every selenium rectifier gets its rectifying properties not until it has been subjected to an electrical treatment. Usually a constant back-current is forced through the rectifier, the back-voltage increasing in the course of the treatment until the desired back-voltage is reached. The question arises as to which of the two characteristic parameters Y_0 and N_i is affected by this treatment. It has been suggested (F.I.A.T. Report), that during the electrical treatment under the influence of the electric field the impurity atoms, which are assumed to be electrically negative, are driven from the semiconductor to the metal. There they should either be stored in a very thin layer at the interface, or be taken up by the metal, but in all events to be put out of action. A reduction of the impurity atoms will increase the back resistance.

The curve of fig. 4 represents the back-voltage for a back-current of 10^{-3} A/cm.$^{-2}$, as a function of the concentration of the impurity atoms at an arbitrarily chosen value of Y_0. As can be seen from this curve, which would describe the falling off of the concentration N_i during the electrical treatment, the concentration of the impurity atoms must be diminished by a factor $\sim 10^2$, to compensate a " mismatch " in the threshold potential ϕ_0 of $\sim 10^{-1}$ volt. Curves as of fig. 4 have been calculated for very different values of Y_0, leading to practically the same result. This result makes it rather improbable that the effect of the electrical pretreatment is due to a diminution of the impurity atoms. The scanty experimental data concerning the change of N_i during the electrical treatment show a decrease of N_i during the last stage of the electrical treatment of a factor 5 at most.

Fig. 3.

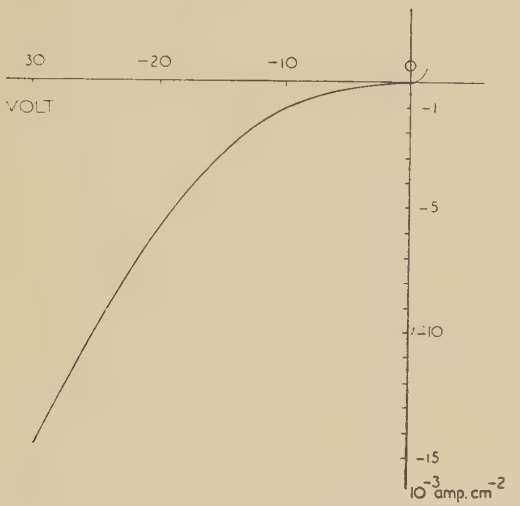

The barrier-layer tension U_b as a function of the back-current of a crystal rectifier of the A-type. $N_i = 10^{15}$ cm.$^{-3}$; $Y_0 = 1{\cdot}47 \times 10^{12}$. This example is meant to represent the behaviour of a normal Selenium rectifier.

It is conceivable that the observed influence of the electrical pretreatment on the concentration of the impurity atoms is only a secondary effect and that the primary effect is an increase of the threshold potential ϕ_0. One might for instance suppose that during the treatment under the influence of the electric field at the boundary of the metal, metal ions enter the selenium, building up a double layer at the interface, by which the threshold potential ϕ_0 for electron holes is increased. In this assumption the curve of fig. 5 is calculated for $N_i = 10^{15}$ cm.$^{-3}$ and $i = 10^{-3}$ A/cm.$^{-2}$. It appears that an increase of ϕ_0 of 0·1 volt only, can raise the back-voltage to an enormous extent. It is from present day experimental knowledge not possible to decide between the two suggestions. In virtue of the foregoing considerations the author attaches the greatest probability to the last.

From Table III. it is evident that the chance that an arbitrary combination of a metal and a semiconductor will be a good rectifier, is extremely small, and so is the number of the actual technically useful combinations. The copper-cuprous-oxide rectifier is a case of fortunate coincidence, very sensitive to traces of admixtures and the thermal pretreatment. The great technical success of the selenium rectifier is due to the possibility of adapting it to its purpose by the simple electrical pretreatment, and this possibility is linked up with the extraordinary mobility of foreign ions in

Fig. 4.

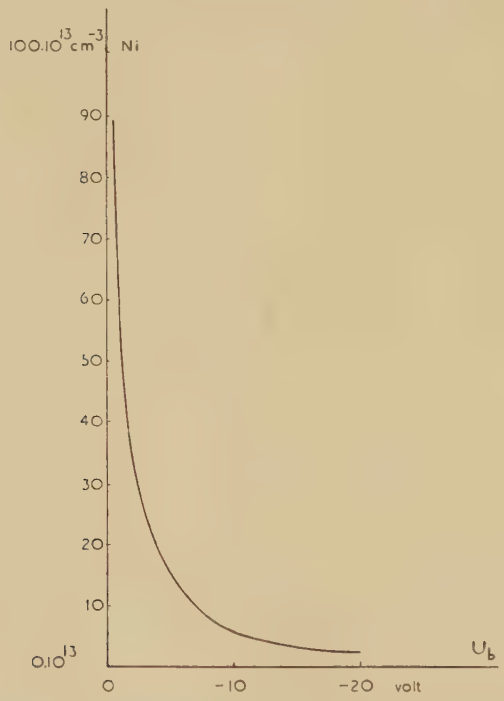

The back-voltage at a current density of 10^{-3} A$\times$cm.$^{-2}$ as a function of the concentration of the impurity atoms N_i for a rectifier of the A-type, with $Y_0=10^{10}$.

hexagonal selenium (Torrey and Whitmer 1948). But this merit is also its weakness, for the electric fields during the normal operation of the rectifier give rise to the same effect as those during the electrical pretreatment and this results in a sometimes very appreciably increasing resistance both in the forward and in the back direction.

In connection with the above considerations the effect of artificial barrier-layers, which are sometimes applied, for instance in the form of a thin film of lacquer between the selenium and the metal, can easily be

explained. When the thin lacquer film is pierced at several spots, the local current density in the different parallel current paths is much higher than it would have been, when the same current was homogeneously distributed over the whole cross-section of the rectifier. It follows from the shape of the current-voltage characteristic that the rectifier-effect is strongly favoured by an increase of the current density. The effect of the pierced insulating film is thus essentially the same as that of a loosely applied whisker contact.

Fig. 5.

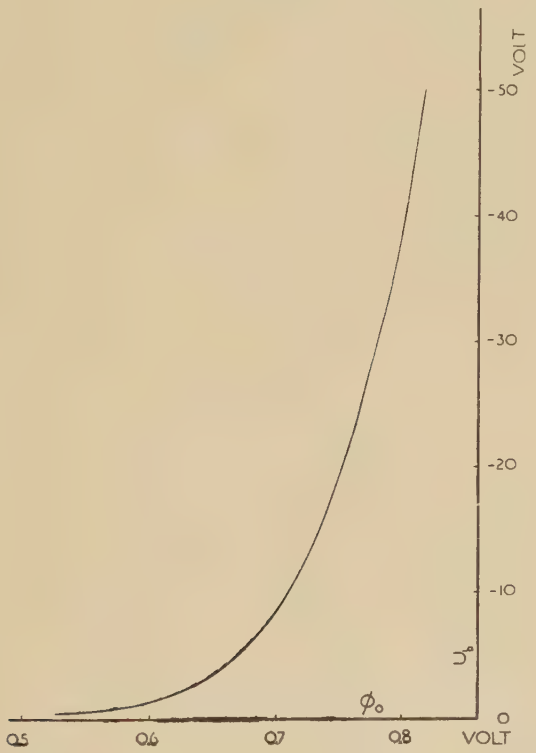

The back-voltage at a current density of 10^{-3} A $\times$ cm.$^{-2}$ as a function of the threshold potential ϕ_0 for a rectifier of the A-type with a concentration of the impurity atoms N_i of 10^{15} cm.$^{-3}$.

References.

Davidov, B., 1939, *J. Phys., U.S.S.R.*, **1**, 167.
F.I.A.T. Report on Selenium Dry Rectifier Development. Final Report No 706.
Gisolf, J. H., 1942, *Ned. T. Natuurk.*, **9**, 49 ; 1947, *Ann. Physik* 6 *Folge*, **1**, 3.
Sanden, Horst van, 1946, *Praxis der Differentialgleichungen.*
Schottky, W., and Spenke, E., 1939, *Wiss. Veröff Siemens-Werke*, **18**, 225.
Schottky, W., 1941–1942, *Z. Phys.*, **118**, 539.
Torrey, H., and Whitmer, Ch., 1948, *Crystal Rectifiers*, Chapter 12, New York.

LXIX. *The Electrical Conductivity of Bismuth Fibres.*— II. *Anomalies in the Magneto-Resistance.*

By B. Donovan and G. K. T. Conn,
Department of Physics, The University of Sheffield*.

[Received May 19, 1950.]

Summary.

In examining the magneto-resistance of thin fibres of bismuth, which are known from previous work to approximate to single crystals, it was found that a considerable proportion of these, about 10 per cent, showed a decrease in the resistance on application of a magnetic field. The effect is only present in fields of the order of 1000 oersteds or less and is of the order of $10^{-4}\rho_0$. The influence of direction of current, direction of field and orientation of the crystal axes is examined. It is considered that these observations provide the first unequivocal evidence of the existence of a longitudinal Hall coefficient. Used in conjunction with the theory of conduction in anisotropic solids, it is possible to indicate the appropriate crystal orientation. It has not, as yet, been possible to designate this with accuracy.

§ 1. Introduction.

In the first paper of this series (Donovan and Conn 1949), the initial results of an investigation into the magneto-resistive behaviour of bismuth fibres were discussed, and particular attention was paid to the elucidation of the structure of the specimens. Comparison of the results with those obtained for single crystals (Stierstadt 1933) led to the conclusion that the fibres were, with certain exceptions, single crystals with the main cleavage plane parallel to the fibre axis. The exceptions were provided by the low-resistance (*i.e.* the thicker) fibres and it seemed feasible that these should possess a less highly developed crystal structure; their magneto-resistive behaviour was not radically different from that of the high-resistance fibres, but was sufficiently distinctive to enable positive identification to be made.

In the course of this investigation certain anomalous results were obtained and it is the purpose of the present paper to discuss these. The essential feature is that, under certain circumstances, the change in resistance resulting from the application of the magnetic field may be negative, or, in other words, the change in resistance may reverse in sign when the direction of the magnetic field is reversed. The possibility of such an "Umkehreffekt" has been discussed in a number of theoretical papers, but no conclusive experimental evidence has hitherto been reported. The work of Kapitza

* Communicated by Professor W. Sucksmith, F.R.S.

(1928) and others has lead to the conclusion that the change in resistance is proportional to the square of the field strength in weak fields and tends gradually to a linear relation at very high field strengths. The results discussed below indicate that the resistance cannot be represented simply as a quadratic function of the field strength and suggest that a linear term is also present which outweighs the quadratic term below a certain critical field strength. A preliminary notification of the present work has already appeared (Conn and Donovan 1948).

This paper does not contain a detailed treatment of the "Umkehreffekt" as such, but presents experimental results which may be regarded as evidence of its existence in bismuth; in the absence of sufficiently extensive experimental data, a complete interpretation cannot be attempted, but it is felt that a qualitative explanation can with advantage be given.

§ 2. Experimental Results.

The preparation and mounting of the fibres, and the experimental technique employed, have been described in the previous paper (Donovan and Conn, *loc. cit.*). The same potentiometer arrangement was used in the present series of measurements and it was again found convenient to use the galvanometer as a continuous recorder of potential difference. In the earlier experiments, the change in resistance of the specimen was determined as a function of its orientation with respect to the magnetic field, which remained constant for a given "cycle." In the experiments to be described the fibre was maintained in a fixed position with respect to the field and its resistance was obtained as a function of the field strength

At low field strengths the residual magnetism of the pole-pieces presents difficulties and it was deemed advisable to employ a source of magnetic field which did not involve the use of iron cores. Two large coils were available, each wound with 1790 turns, the outer diameter being 36 cm. and the inner diameter 12 cm. These were supported coaxially, as in an Helmholtz arrangement. With a separation of 3·8 cm. a field of 120 oersteds per ampere was obtained at the centre of the gap. Owing to the small dimensions of the specimens, no difficulties arising from inhomogeneities of the field were encountered.

With this arrangement the procedure of varying the field was considerably simplified.

It will be convenient to refer to the ϕ and θ orientations already introduced (Donovan and Conn, *loc. cit.*) and fig. 1 has been reproduced to make the notation clear. In both cases the axis of rotation is perpendicular to the magnetic field; the axis of the fibre is parallel to, and perpendicular to the axis of rotation in the ϕ and θ cases respectively. In the latter case, therefore, the fibre rotates in a plane parallel to the magnetic field.

In the ϕ case the anomalous behaviour has appeared in certain fibres and is illustrated in fig. 2 which shows the change of resistance plotted against field strength for a fibre whose orientation corresponds to the minimum of the ϕ curve. The fibre had a zero-field resistance of 170 ohms. It will be

seen that for field strengths less than approximately 350 oersteds the change in resistance is negative and the minimum value occurs in the neighbourhood of 180 oersteds. The decrease in resistance is extremely small but,

Fig. 1.

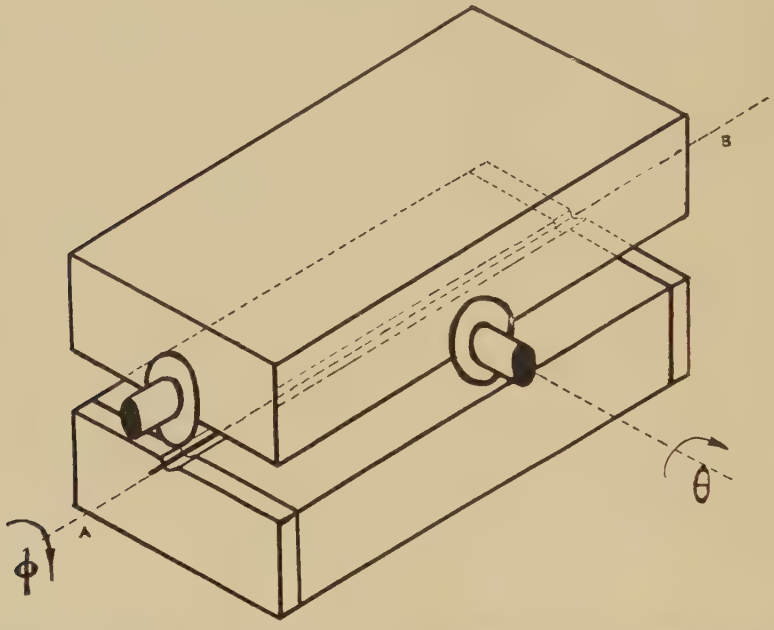

Isometric drawing of the holder. AB is the axis of the fibre and the ϕ-axis.

Fig. 2.

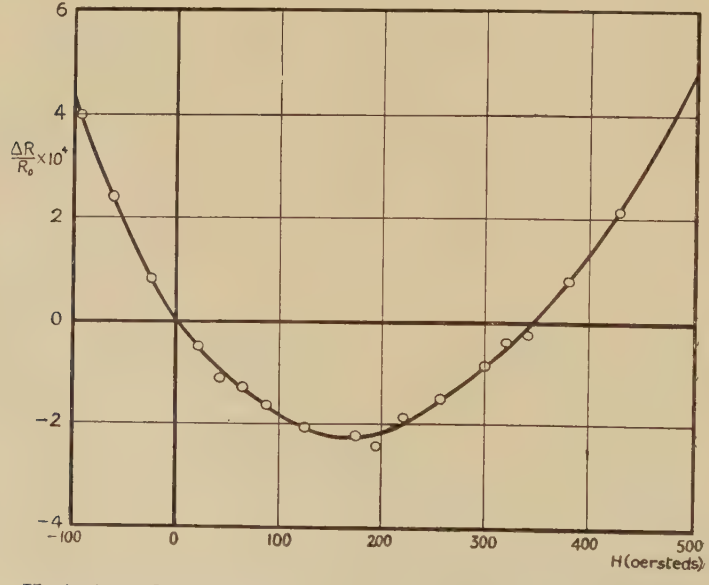

Variation of resistance with field-strength for 170 ohm fibre.

by virtue of the comparatively high resistance of the specimen and the sensitivity of the arrangement, it is easily detected and is readily reproducible.

It should be emphasized that this phenomenon is not characteristic of bismuth fibres *per seq*, and in fact only a fraction of the order of 10 per cent of the fibres exhibited this effect. For this minority the effect was quickly and convincingly demonstrated. Having balanced the potentiometer in the absence of a magnetic field, a suitable permanent magnet is brought up to the specimen and the galvanometer observed.

All the fibres which showed the negative change in resistance did so when the orientation corresponded to the minimum of the ϕ curve. With one exception, which will be referred to later, no such effect was observed

Fig. 3.

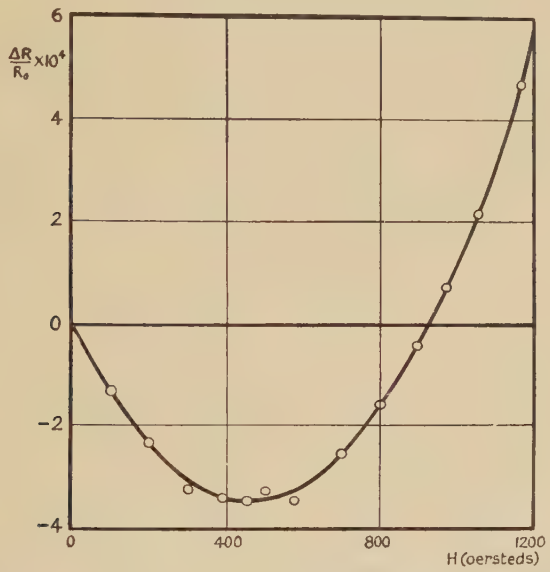

Variation of resistance with field-strength for 6 ohm fibre.

when the orientation corresponded to the maximum of the ϕ curve. The significance of these two extreme positions lies in the fact that they represent simple orientations of the main cleavage plane with respect to the field (Stierstadt 1933, Donovan and Conn *loc. cit.*). No negative change in resistance was observed in any fibre when its axis was parallel to the field (θ-orientation).

Considerable variation was apparent in the order of magnitude associated with the anomaly. In particular, the range of field strength over which the resistance change was negative varied widely from one specimen to another; the limits of the critical or "change-over" field strength were roughly 300 to 1000 oersteds. No useful purpose will be served by including a large number of experimental curves, but a further example may be given (fig. 3) illustrating a wider range of negative resistance change.

The critical field strength in this case is approximately 930 oersteds. The fibre had a zero-field resistance of 6 ohms and again was set at the minimum of the ϕ curve.

The magneto-resistive behaviour of the fibres which did not exhibit the effect in question was quite consistent, and is illustrated in fig. 4, which was obtained with a representative " orthodox " specimen. The change of resistance for weak fields is shown for orientations corresponding to the maximum and minimum of the ϕ curve

Finally, we give curves (fig 5) obtained with a fibre which was unique in its behaviour and which provided the solitary exception previously mentioned. This fibre had a zero-field resistance of 46 ohms and was remarkable in two respects: (*a*) the decrease in resistance was about fifty times larger than that obtained in other cases and (*b*) the decrease in

Fig. 4.

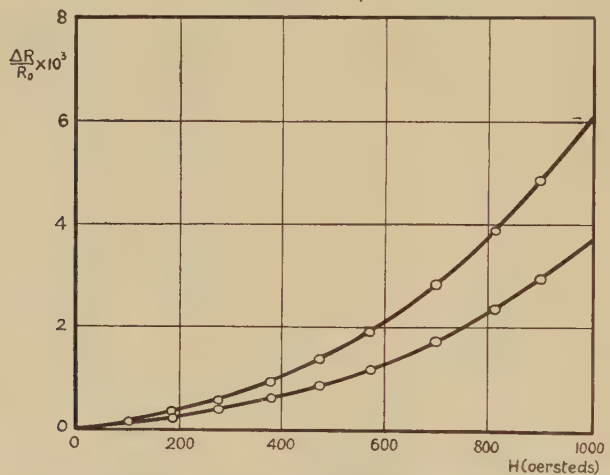

" Orthodox " magneto-resistance effect in weak fields. The upper and lower curves represent the maximum and minimum respectively of the ϕ cycle.

resistance was obtained with orientations corresponding to the maximum as well as the minimum of the ϕ curve. The critical field strengths in these two cases are approximately 1300 and 1700 oersteds respectively, and these are considerably greater than any other observed values.

§ 3. Possible Errors.

In view of the small magnitude of the decrease in resistance, and the nature of the phenomenon, suspicion is at first to be directed towards possible sources of experimental error. The various effects, however, which might conceivably give rise to spurious results can be discussed, if not with finality, at least with sufficient cogency to enable the "Umkehreffekt " to be regarded as genuine.

The possible sources of error which are relevant in magneto-resistance measurements have been enumerated by Thompson (1938). Of these, the most serious is undoubtedly due to the presence of the transverse Hall effect. If the electrodes are attached to the specimen in such a way that they do not lie on a line of current flow, then, when the magnetic field is applied, a component of the Hall e.m.f. will appear across the terminals. Such a misalignment is illustrated, in exaggerated form, in fig. 6 (*a*) which represents a section through a specimen perpendicular to the magnetic field. The Hall e.m.f. reverses, of course, when the field is reversed and the majority of previous workers have used mean values obtained from the two directions of the field. Under these circumstances the resistance change

Fig. 5.

Variation of resistance with field-strength for 46 ohm fibre.

must necessarily be a symmetrical function of the field and no "Umkehreffekt" could have been detected. Moreover, it should be pointed out that the decrease in resistance is associated essentially with weak fields and that, in the past, more attention has been paid to investigations in strong fields, or at low temperatures, where the resistance changes are very large.

As mentioned in the previous paper already referred to, specimens in the form of fibres possess the distinctive advantage of combining the structure of a single crystal with a resistance value suitably high for accurate measurements. In addition, the shape of the specimens is such as to

minimize the influence of transverse effects, and in this respect fibres are superior to the previous types of single crystal, such as triangular prisms (Stierstadt 1933) and plates (Thompson 1938). Two other reasons may be adduced for believing that the Hall effect referred to above is not responsible for the observed negative resistance change. Firstly, the electrodes are not " localized " at points on the specimen, as would be the case for instance with fine wires ; the method of construction ensures that contact is made over the whole cross-section, as shown in fig. 6 (*b*). Thus any effects due to the type of misalignment depicted in fig. 6 (*a*) are eliminated. Secondly, the effect is not universal and it is difficult to see how such a general explanation as the Hall effect can be valid when about 90 per cent of the fibres show no indication of the phenomenon.

Fig. 6.

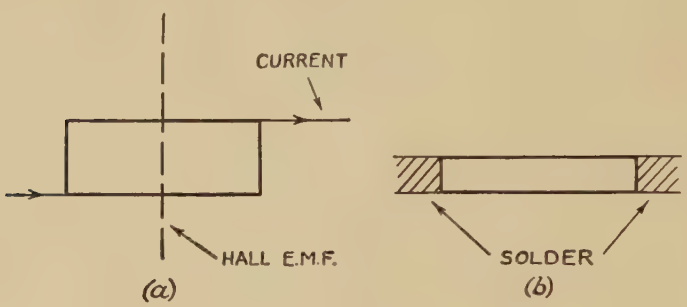

(*a*) Possible misalignment of specimen. Magnetic field perpendicular to plane of paper.
(*b*) Type of mounting used for fibres.

The evidence indicates an explanation in terms of the crystal structure of the specimen, and suggests that the " anomalous " fibres are characterized by departure from the general structure discussed in the previous paper. Whereas in the majority of fibres the main cleavage plane is parallel to the fibre axis, it seems reasonable to suppose that in the " anomalous " cases this no longer applies, and the main cleavage plane is inclined at a small angle to the axis. Small variations in this angle might well account for the different values of the " change-over " field strength observed.

It is natural to seek confirmation of such conclusions by examining the X-ray diffraction of these fibres. A preliminary investigation undertaken through the kind co-operation of Mr. R. B. Shepherd has served to clarify the problem but it cannot be said as yet to have yielded clear evidence. The inclination of the cleavage plane to the axis, upon which our interpretation is based, is sufficiently small to make discrimination difficult by X-ray methods and, bearing in mind that the fibres are of the order of 10^{-3} cm. in diameter, it would appear that this corroboration, which is clearly desirable, is likely to require a separate investigation in itself.

§ 4. Outline of Previous Work.

Before any discussion of the foregoing experimental results is attempted, it is necessary to give a brief survey of the existing literature. The theoretical approach may be directed along one of two lines: the starting point may be either the classical equations of conduction in an anisotropic medium, or the quantum mechanical formulation of transport phenomena. The latter method of treatment has not, hitherto, proved particularly satisfactory in the case of bismuth, as the effect of the crystal symmetry has not been rigorously investigated.

The negative change in resistance would be readily explicable if the Hall effect contained a longitudinal as well as a transverse component, *i. e.* if an e.m.f. were produced *parallel* to the current flow. This must not be confused with the spurious Hall effect due to a bad experimental arrangement considered above. Such a longitudinal Hall effect would give rise to a resistance change whose sign depends on the direction of the magnetic field. The transverse character of the Hall effect was postulated by Voigt (1928) but the consequences of removing the restriction were examined by Kohler (1934) following some experimental results on the Hall effect (Verleger 1932) which could not be reconciled with Voigt's treatment. In view of the considerable experimental evidence supporting the Voigt theory, Shoenberg (1935) was led to suggest that Verleger had incorrectly described his experiments and that in fact the discrepancy was not genuine. Shoenberg dealt with some of the implications of Kohler's work and endeavoured to obtain experimental evidence by means of a magneto-resistance experiment with a bismuth crystal. No indication, however, of a longitudinal Hall effect was forthcoming.

A more detailed theoretical investigation of the magneto-resistance effect, based on Kohler's work, was carried out by Meixner (1939). Starting with the general expression for the resistance, in terms of odd as well as even powers of the field strength, Meixner showed that an "Umkehreffekt" could occur in anisotropic substances, for certain orientations of the current, field and crystal axes. In bismuth, when the conditions for maximum "Umkehreffekt" are fulfilled, the linear term should out-weigh the quadratic term for field strengths less than about 6700 oersteds and the change of resistance should be negative.

In a later paper Meixner (1941) made a comprehensive examination of electrical transport phenomena, from the quantum mechanical standpoint. This treatment, which was quite general, led to the result that neither the electrical nor the thermal conductivity was dependent upon the direction of the magnetic field. Any "Umkehreffekt" was thus inexplicable on this basis, but, in surveying the experimental results on the Hall effect in bismuth, Meixner admitted that the question must be regarded as still open. Some significance is to be attached to the fact that an "Umkehreffekt" of thermal conductivity, also excluded by Meixner's theory, has been observed in bismuth by Grüneisen and Gielessen (1936). It would appear that the quantum mechanical formulation necessarily involves

assumptions that render it invalid in the case of bismuth. In a further application of the electron theory of metals, Kohler (1941) suggested that a possible explanation of these discrepancies might lie in the neglect of the quantization of the electron paths in the magnetic field.

The only previous experimental evidence of this effect for bismuth has been reported by Casimir and Gerritsen (1941). Their measurement showed that the resistance was actually a function of the direction of the field, for a single crystal at 77·3° K. Casimir and Gerritsen concluded, however, that the cause was spurious, since a similar " Umkehreffekt " was found with a crystal orientation which was precluded on theoretical grounds. No reference was made to Shoenberg's paper and, as no details of the experimental arrangement were given, the interpretation of the results cannot profitably be discussed.

§ 5. Discussion of Results.

We examine now the implications of the relevant theoretical results (Shoenberg 1935) for various special cases and conclude by advancing a tentative explanation to account for the results in the second section of this paper.

The most general expression for the Hall effect is

$$E_i = R_{ikl} J_k H_l, \qquad \text{(i)}$$

where **E**, **J**, **H** are vectors denoting the electric field responsible for the Hall e.m.f., the current density and the magnetic field respectively. The R_{ikl} are governed by the symmetry of the crystal and in the case of bismuth it has been shown by Kohler (1934) that there are only four independent constants:

$$\left.\begin{aligned} R_{231} &= -R_{132} = R_1, \\ R_{312} &= -R_{321} = R_2, \\ R_{123} &= -R_{213} = R_3, \\ R_{111} &= -R_{122} = -R_{212} = -R_{221} = R_4. \end{aligned}\right\} \qquad \text{(ii)}$$

If there is no longitudinal Hall effect, then $R_{ikl} = -R_{kil}$ and it follows from (ii) that

$$R_1 = R_2 \quad \text{and} \quad R_4 = 0 \qquad \text{(iii)}$$

In the subsequent application to the bismuth crystal, we shall use a rectangular cartesian system of axes with OZ parallel to the principal (trigonal) axis and OX parallel to one of the binary axes. The main cleavage plane is thus the (x, y) plane. In the experiments which concern us, the magnetic field is invariably perpendicular to the current flow. For this case Shoenberg has shown that a longitudinal Hall effect, which is implicit in equation (i), produces a change in the specific resistance given by

$$\begin{aligned} \Delta\rho = H[&(R_2 - R_1) \cos\alpha \sin\alpha \sin\chi \\ &- R_4 \sin^2\alpha(\sin\chi \sin 3\zeta + \cos\chi \cos\alpha \cos 3\zeta)] \end{aligned} \qquad \text{(iv)}$$

Here α is the angle between the principal axis and the current direction, ζ is the angle between the binary axis and the projection of the current vector on the main cleavage plane, and χ is the angle between the magnetic field and the projection of the principal axis on the plane normal to the current vector. The significance of these angles can be seen from fig. 7 (*a*). Expression (iv) represents a magneto-resistive effect which is linear in H, and the change in the observed resistivity when the field is reversed should be $2\,\Delta\rho$. If the current flow is perpendicular or parallel to the main cleavage plane ($\alpha=0°$ or $90°$) then the effect vanishes, as is also the case in polycrystalline material.

In Shoenberg's own experiment $\alpha=45°$, $\zeta=17°$ and χ was varied by rotating the magnet. Reversal of the magnetic field produced no detectable change in resistance for any value of χ and the essentially transverse nature of the Hall effect was regarded as established. However, only one value of magnetic field (13,700 oersteds) was used and it is probable that this was too high for the effect to appear. The effect is exceedingly small and is clearly more easily detected in weak fields where the orthodox magnetic resistance is not large.

In the orientation discussed by Meixner (1939) the magnetic field is parallel to one of the binary axes and the current is restricted to the (y, z) plane. Thus $\chi=\zeta=90°$ and equation (iv) reduces to

$$\Delta\rho/\mathrm{H}=(\mathrm{R}_2-\mathrm{R}_1)\cos\alpha\sin\alpha+\mathrm{R}_4\sin^2\alpha \quad . \quad . \quad . \quad . \quad \text{(v)}$$

For $\alpha=45°$ (see fig. 7 (*b*)) this expression has a maximum value in agreement with Meixner. An identical arrangement, with $\alpha=45°$, was used by Casimir and Gerritsen (1941), and produced an apparent "Umkehreffekt"; however, such an effect was also obtained when the magnetic field was perpendicular to the binary axis, which disagrees with the theory.

In discussing our own experimental results, the significance of the ϕ resistance curves must be borne in mind. Stierstadt (1933) has shown that in P_1 ($\perp$) crystals (current flow perpendicular to a binary axis) the resistance in moderately low fields is controlled by the orientation of the (111) plane, *i. e.* the main cleavage plane. When this is parallel to the field the resistance has a maximum value, and when it is perpendicular to the field the resistance has a minimum value. Further, in P_1 ($\parallel$) crystals, that is, current flow parallel to binary axis, the controlling influence on the resistance is exerted by the $(11\bar{1})$ plane, *i. e.* the subsidiary cleavage planes. The behaviour of these planes is opposite to that of the main cleavage plane. For example, if one of the subsidiary cleavage planes is parallel to the field the resistance has a minimum value. In this case the inclination of the main cleavage plane to the field is approximately 71° and therefore it is clear that in any P_1 type crystal the minimum of the ϕ curve represents a state of affairs in which the main cleavage plane is roughly perpendicular to the field; at any rate the departure must be less than 20°.

Returning to fig. 7 (*b*), we see that if the current vector $\mathbf{j}$ is parallel to the y-axis we have a normal P_1 ($\perp$) crystal with a main cleavage plane

parallel to the field, *i. e.* at the maximum of the ϕ curve. If **J** is restricted to the (x, y) plane, any type of P_1 crystal can be represented and as $\alpha = 90°$ in every case no "Umkehreffekt" is possible. As it has already been established in the previous paper that in these bismuth fibres the main cleavage plane is parallel to the axis and hence parallel to the current flow, we see why the majority of fibres do not exhibit this effect.

The explanation of the anomalous behaviour of the minority described in § 2 would seem to lie in the exceptional nature of the crystal structure of these fibres. In drawing the fibre the main cleavage plane has become tilted with respect to the normal orientation, with the result that the current flow is no longer parallel to the main cleavage plane and α is no longer 90°. This displacement must necessarily be quite small and of the order of a few degrees.

We consider first the orientation corresponding to the maximum of the ϕ curve. In P_1 ($\perp$) crystals the main cleavage plane is parallel to the

Fig. 7.

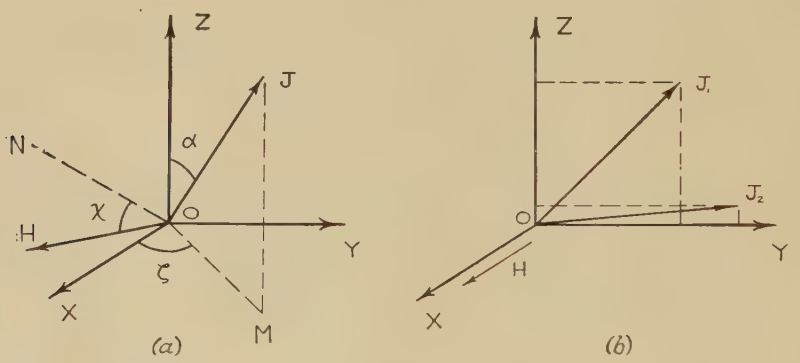

Orientation of current J and magnetic field H with respect to crystal axes, OZ parallel to principal axis; OX parallel to binary axis.

(*a*) General case; OM is projection of J on (x, y) plane; ON is projection of z-axis on plane normal to J.

(*b*) Special case with J in (y, z) plane and H parallel to OX. J_1 and J_2 correspond to values of 45° and approximately 85° respectively for α.

field and, as shown in fig. 7 (*b*), the current vector is displaced slightly from the y-axis although still remaining in the (y, z) plane. For this case, therefore, equation (v) will apply. In P_1 ($\parallel$) crystals, and intermediate cases, both **H** and **J** will be inclined to the main cleavage plane and no corresponding simplification of equation (iv) can be made.

Next we consider the orientation corresponding to the minimum of the ϕ curve. In true P_1 ($\perp$) crystals the main cleavage plane would be perpendicular to the field; in imperfect P_1 ($\perp$) crystals, that is to say, crystals possessing a fault in accordance with the conjecture made above, this will no longer by the case, but the principal axis will be in the plane

defined by **H** and **J**. It may be instructive to consider this orientation, which is shown in fig. 8 with the crystal fault intentionally exaggerated. If the principal axis lies in the plane of **H** and **J**, then $\chi=0$ and this restriction alone causes (iv) to reduce to

$$\Delta\rho/H=-R_4 \sin^2\alpha \cos\alpha \cos 3\zeta \quad . \quad . \quad . \quad . \quad . \quad . \quad \text{(vi)}$$

The " Umkehreffekt " is controlled by α, *i.e.* the magnitude of the crystal fault, and by ζ, which is determined by the position of the binary axis. In crystals of the quasi-P_1 ($\perp$) type, the binary axis is normal to the current* and $\zeta=90°$. Hence the resistance change should be normal. For all other orientations of the binary axis expression (vi) has a finite value.

In crystals of the quasi-P_1 ($\parallel$) type the position is complicated by the fact that the principal axis is inclined at an angle of approximately 19° to the plane containing **H** and **J**. For intermediate P_1 crystals the angle will have some value between 0 and 19° and, since α, χ and ζ are all finite for these cases, equation (iv) must be used as it stands.

Fig. 8.

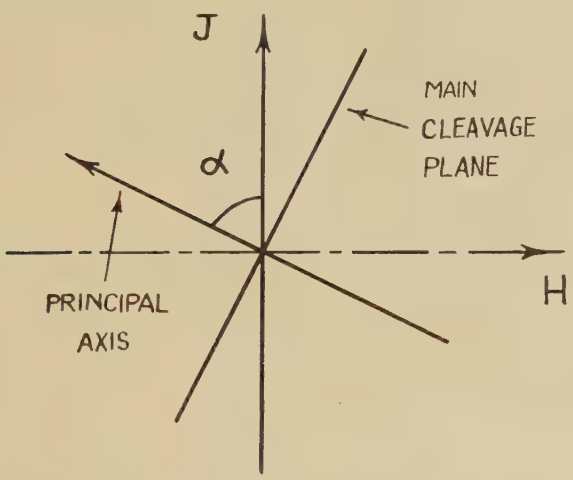

Crystal fault (exaggerated) in which main cleavage plane is not perpendicular to magnetic field. The principal axis, current J and field H all lie in one plane.

Conclusion.

The nature of the specimens we have used confers two very real advantages in exploring the reality of such an " Umkehreffekt." The preparation of crystals of such a relatively high resistance enables one to examine with care and precision any departures from the normal behaviour. This benefit is to some extent obtained at the expense of exactness in specifying

* In this case fig. 8 represents a section in the (y, z) plane.

to which crystalline category any given fibre belongs. Furthermore the size and the method of mounting would seem to eliminate the possibility that such observed effects were due to a component of transverse Hall coefficient.

It is difficult to resist the conclusion that the evidence here presented confirms the existence in these specimens of a longitudinal component of the Hall coefficient. Because there is at the moment an inevitable lack of precision in our specification of the category of any given fibre, we can go no further than the above qualitative interpretation setting out the various possibilities which can give rise to an " Umkehreffekt." With reference to the order of magnitude, it is relevant to quote Casimir and Gerritsen (*loc. cit.*) : "A linear term would lead to a decrease of resistance at low fields but . . . . this decrease would only amount to $2 \times 10^{-4} \rho_0$." The results illustrated in figs. 2 and 3 are in striking agreement with this prediction.

References.

Casimir, H. B. G. and Gerritsen, A. N., 1941, *Physica, 's Grav.*, **8,** 1108.
Conn, G. K. T. and Donovan, B., 1948, *Nature, Lond.*, **162**, 336.
Donovan, B. and Conn, G. K. T., 1949, *Phil. Mag.*, [7], **40,** 283.
Grüneisen, E. and Gielsessen, J., 1936, *Ann. Phys. Lpz.*, **26,** 449.
Kapitza, P., 1928, *Proc. Roy. Soc.* A, **119,** 358.
Kohler, M., 1934, *Ann. Phys. Lpz.*, **20,** 878, 891; 1941, *Ibid.*, **40,** 601.
Meixner, J., 1939, *Ann. Phys. Lpz.*, **36,** 105 ; 1941, *Ibid.*, **40,** 165.
Shoenberg, D., 1935, *Proc. Camb. Phil., Soc.*, **31,** 271.
Stierstadt, O., 1933 a, *Zeits. f. Physik*, **80,** 636 ; 1933 b, *Ibid.*, **85,** 310.
Thompson, N., 1938, *Proc. Roy. Soc.* A, **164,** 24.
Verleger, H., 1932, *Zeits. f. Physik*, **76,** 760.
Voigt. W., 1928, *Lehrbuch der Kristallphysik* (Leipzig : Teubner).

LXX. *The Experimental Determination of the Geomagnetic Radial Variation.*

By S. K. Runcorn, A. C. Benson and A. F. Moore,
The Dept. of Geodesy and Geophysics, Cambridge *
and
D. H. Griffiths,
University, Manchester †.

[Received June 8, 1950.]

Abstract.

Theories of the origin of the dipole components of the Earth's main magnetic field are of two types; distributed theories attribute it to a fundamental property of rotating matter, core theories to current systems within the core. The variation with depth below the surface of the horizontal field intensity is different for the two theories. Experimental values are given for this variation, obtained by measurements in coal mines, which are near to the values predicted by a core theory, and significantly different from those predicted by a distributed theory. The magnetic effects of the sedimentary rocks and magnetic anomalies due to the basement rocks are shown to have negligible results on the measurements.

It has been suggested, notably by Blackett (1947 and 1949), that the axial dipole component of the geomagnetic field might be a fundamental property of any rotating spherical mass; the non-dipole part of the field (about 15 per cent) arising from subsidiary processes such as induction. The other possible theory of the geomagnetic field suggests that it is due to the flow of electric currents maintained by thermo-electromotive forces or by dynamo action; these must be confined to the deep interior of the earth, where the electrical conductivity seems likely to be appreciably higher than that of the surface rocks. It is convenient to call the former a Distributed Theory and the latter a Core Theory.

Bullard suggested that it might be possible to decide between these two theories by measurements of the change with depth inside the earth of the horizontal and vertical components of the geomagnetic field. Preliminary measurements were made in mines in South Africa (Hales and Gough 1947) and in Lancashire (reported by Chapman 1948 a). Much more extensive measurements have now been made in the coal mines of this country and methods of establishing the significance of the results, which were lacking in the earlier work, have been developed.

---

* Formerly at the Physical Laboratories of the University of Manchester.
† Communicated by the Authors.

Were the distribution of the Earth's field exactly that of a dipole, the field components would vary radially according to an inverse cube law except in regions where the field vector is rotational. For a core theory such a region (of electric current flow) is inaccessibly deep within the Earth. The simplest interpretation of a distributed theory—though perhaps not the only one—is that the whole Earth is a region of virtual current flow, having magnetic but not electrical effects. Runcorn (1948) and Chapman (1948 b) calculated, for the two groups of theories, the differences (ΔZ, ΔH) between the vertical and horizontal field components at a small depth "d" below the Earth's surface (Z_d and H_d respectively) and the vertical and horizontal components at the surface (Z_0 and H_0 respectively). They showed that though for a Core Theory, if R is the radius of the Earth,

$$\Delta Z = Z_d - Z_0 = + \frac{3{\cdot}0\,.\,d}{R}\,.\,Z_0$$

and

$$\Delta H = H_d - H_0 = + \frac{3{\cdot}0\,.\,d}{R}\,.\,H_0,$$

a Distributed Theory, assuming the density of the surface rocks is 2·7, gives

$$\Delta Z = Z_d - Z_0 = + \frac{3{\cdot}0\,.\,d}{R}\,.\,Z_0,$$

$$\Delta H = H_d - H_0 = - \frac{6{\cdot}5\,.\,d}{R}\,.\,H_0.$$

The essential problem of the experiment is to find conditions in which measured differences of the geomagnetic components between a point on the Earth's surface and a point underground may be attributed to the main field and not to anomalies. For though the geomagnetic field is mainly a dipole field, the gradients of its components over small distances at the surface may be very different from the dipole gradients. Thus in England, while the surface gradients to be expected from the dipole field are of the order of 5 gammas per kilometre (1 gamma $= 10^{-5}$ gauss), the observed gradients in some regions may be of the order of hundreds of gammas per kilometre. These anomalous gradients seem to arise from surface features of the igneous basement rocks or from horizontal changes in their magnetite content; the sedimentary layers above usually producing little effect.

Therefore in regions where geological data indicates that the probable minimum depth at which extensive bodies of igneous rock are likely to occur is greater than 8000 feet, as in South Lancashire and Yorkshire, the gradients of the field components over distances of a few thousand feet, both along the Earth's surface and vertically, should be sensibly linear. If this is so, then the effect of anomalies arising from the basement rocks on the measured values of ΔZ and ΔH can be estimated by a surface survey and allowed for, if necessary.

For at any point where there is no current density (real or virtual) the gradients of the geomagnetic field along the 3 axes of a rectangular coordinate system are related by 4 equations, because

$$\text{curl } \mathbf{H}=0 \qquad \text{and} \qquad \text{div. } \mathbf{B}=0.$$

Such an equation is

$$\frac{d\mathrm{H}}{dz}=\frac{d\mathrm{Z}}{dx},$$

where z is a vertical distance and x a distance along a tangent to a line of longitude at the point.

The measurement of the surface gradients may prove difficult as the values of the field at points on the surface are likely to be perturbed by the field of igneous boulders in the drift clay, thus some scatter of the points from a straight line has to be expected. Also the measurements may be made impossible owing to the vicinity of built up areas. Thus the preliminary measurements at the Parsonage Colliery at Leigh in Lancashire are of less interest because no adequate surface survey could be made in the region.

It is difficult to find useful sites in mines as steel arches and rails are used in almost all passages and even if these are cleared some iron is usually buried. Passages also have to be a sufficient distance from the large concentrations of steel near the shafts, so that no gradient is detectable along the passage. Only then can the geomagnetic field in the passage be assumed to be free from man made disturbances. Only a very few of the cleared sites proved to be free of buried iron.

Measurements of the vertical and horizontal components are made to an accuracy of 1 gamma by the quasi-absolute B.M.Z. (magnetometric zero balance) and Q.H.M. (quartz horizontal magnetometer) respectively which were developed by Dr. La Cour at the Danish Meteorological Institute. The temperature coefficients of the instruments must be known accurately and frequently checked in the laboratory, because their values are of the order of 10 gammas per degree centigrade and the difference in temperature between the surface and underground sites may be as much as 30° centigrade. For a determination of ΔH and ΔZ measurements of H and Z are taken on the surface at a fixed point, the instruments are then taken to the underground site, the measurements repeated, and finally a further series is taken at the surface site. Throughout the experiment, instruments are left on the surface to record the temporal change in the geomagnetic field so that a correction for this may be applied to the results. The surface survey was made by H and Z variometers of the Schmidt balance type over a grid of 4·5 kms. around the surface site and from these measurements the surface gradients were computed and the value of the field at the surface site was corrected for any local anomaly.

The results of the measurements are shown in Tables I.–V. Table I. shows the position of the underground and surface sites where measurements were made, the depth of the former and the height above Ordnance Datum of the latter. The distances of these sites from the shafts and the steel materials and buildings associated with them are also given. Only in the case of the Nook surface site is there any interference, due to railway-sidings, and the correction for this is determined from the surface survey of the area. This Nook surface site was also used as the surface site for the Astley Green measurements, the necessary correction again being found from the surface survey of the area.

Table I.

Colliery	Latitude and longitude and National grid coordinates of underground site	National grid coordinates of surface site	Depth of underground site (feet)	Height above O.D. of surface (site) (feet)	Distance from shafts of underground site (yards)	Distance from shafts of surface site (yards)
Hickleton Main (near Doncaster, Yorks.).	53° 32′ 42″ N. 1° 17′ 36″ W. 44684056	44704065	2520	210	515	1200
Nook (near Leigh, Lancs.).	53° 29′ 50″ N. 2° 28′ 0″ W. 36924004	36914009	2930	100	560	410
Astley Green (near Leigh, Lancs.).	53° 28′ 40″ N. 2° 26′ 48″ W. 37053980	36914009	2859	64	1900	410

Table II. shows the results of the surface survey of the Lancashire and Yorkshire Areas. Values of H and Z on a kilometer grid covering a square with sides 4·5 km. from the surface base were used to compute, by a least squares method, the field gradients along each grid line. The gradients along the lines of latitude and longitude were then averaged. Figs. 1–4 show plots of H and Z against distances along lines of longitude (x) and along lines of latitude (y). The drawn straight line and the values given on the graph were derived by the method of least squares. The survey in South Lancashire was less satisfactory than that in Yorkshire, as small hamlets prevented measurements being made near certain of the grid points and the East–West gradient is rather large. However the corrections involved in ΔH and ΔZ are small.

TABLE II.

Surface Gradients of Geomagnetic Elements.

Colliery	Theoretical value of gradient of Z γ/km.	Experimental value of gradient of Z γ/km.	Theoretical value of gradient of H γ/km.	Experimental value of surface gradient of H γ/km.
	Variation with Latitude (Positive to North).			
Hickleton	+5·0	+5·0±0·3	−4·0	−3·4±0·5
Nook and Astley Green	+5·0	+4·0	−4·0	−6·0
	Variation with Longitude (Positive to East).			
Hickleton	0	+1·6±0·5	0	+1·2±0·6
Nook and Astley Green	0	+3·2	0	−8·0

Fig. 1.

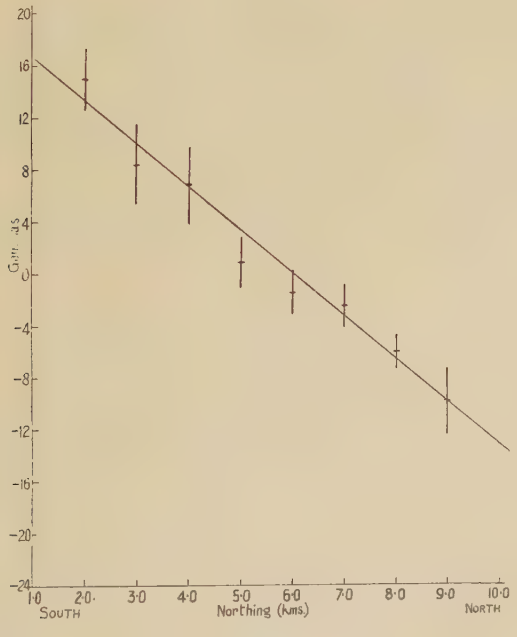

Hickleton Surface Survey.

Variation of H with latitude $\frac{\partial H}{\partial x} = -3{\cdot}4 \pm 0{\cdot}5\gamma$/km.

Fig. 2.

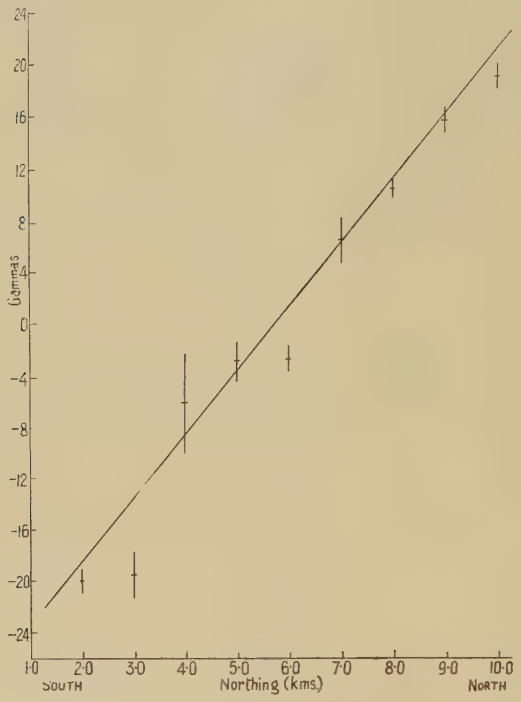

Hickleton Surface Survey.

Variation of z with latitude $\dfrac{\partial Z}{\partial x} = +5{\cdot}0 \pm 0{\cdot}3\gamma$ / km.

Fig. 3.

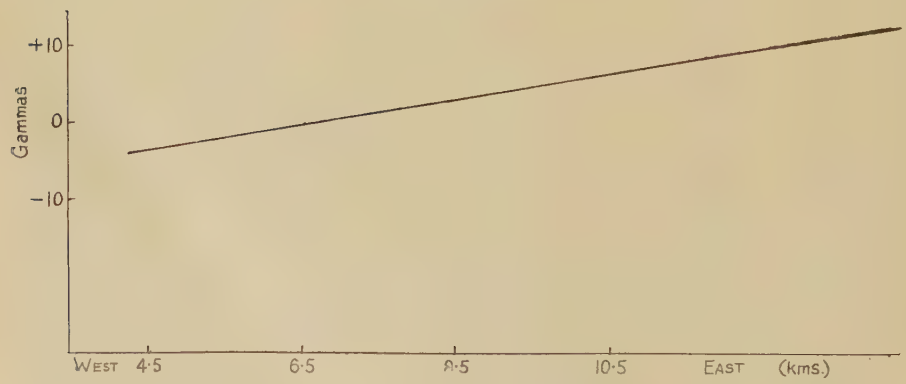

Hickleton Surface Survey.

Variation of z with longitude $\dfrac{\partial Z}{\partial y} = +1{\cdot}6 \pm 0{\cdot}5\gamma$ / km.

The effects on the measurements of the induced magnetism of the sedimentary rocks was examined. From boreholes and shafts in Lancashire and Yorkshire representative collections of strata samples were obtained and the magnetic susceptibilities of the specimens were determined with an astatic magnetometer. Table III. gives the average susceptibilities for the different types of rock.

Fig. 4.

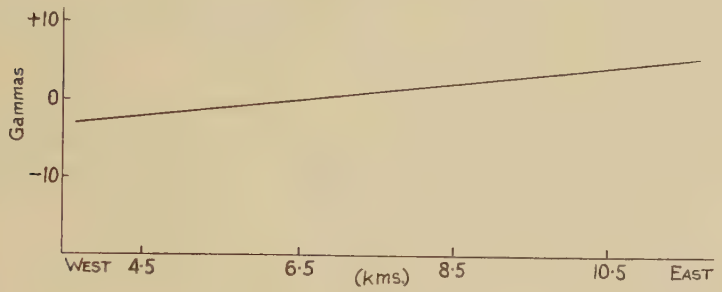

Hickleton Surface Survey.

Variation of H with longitude $\frac{\partial H}{\partial y} = +1{\cdot}2 \pm 0{\cdot}6\gamma$ | km.

Table III.

(K is volume magnetic susceptibility.)

Locality	Mudstones, shales and siltstones		Sandstones		Fireclays		Ironstones	
	Number of samples	Average K.10^6	Number of samples	Average K.10^6	Number of samples	Average K.10^6	Number of samples	Average K.10^6
Lancashire	40	23·5	21	14·5	7	19·4	14	56·7
Yorkshire	60	23·4	11	11·7	6	14·1	4	69·7

Calculations were made of the magnetic effects of the strata at Hickleton, Assuming that the various beds have uniform susceptibility and thickness. the vertical field components due to each bed at the surface and the underground observation points could be determined, if the horizontal extent of the bed were known. The effects could then be summed for the whole succession, the difference in the underground and surface values being a measure of the anomaly in ΔZ. The horizontal extent of each bed is not known, but if it is assumed to be that for which its effect is a maximum, we get an anomaly which cannot possibly be exceeded but which is certain to be very greatly overestimated. A more realistic estimate is obtained by computing an average value of the anomalies which would be produced by beds of all sizes up to a certain arbitrary

maximum. The "maximum" and "average" anomalies in ΔZ are shown in Table IV. The susceptibilities of the strata from the surface down to 2700 ft. have been measured and the susceptibilities of the strata beneath these down to the base of the Coal Measures at 4000 ft. have been estimated. The effect of all the sediments below the Coal Measures is negligible.

Table IV.

Thickness of Strata over which the effect is summed (feet from surface)	Vertical Component of Magnetic Fields due to Strata (gammas)					
	Maximum Effect			Average Effect		
	At surface	Underground (2367 feet)	Difference	At surface	Underground (2367 feet)	Difference
0–2728	+16	+30	+14	+5	+7	+2
2728–4000	0	+4	+4	0	+4	+4
Total			+18			+6

Table V.

(Positive Values denote Increase in Component with Depth).

	Theoretical ΔZ Both theories γ	Experimental ΔZ γ	Theoretical ΔH Core γ	ΔH Distributed γ	Experimental ΔH γ
Hickleton	+16	$+11\pm3$	+6	−13	$+22\pm2$
Nook	+19	$+11\pm3$	+8	−16	$+7\pm2$
Astley Green	+18	$+18\pm3$	+7	−15	$+10\pm3$

Table V. shows the expected change with depth of the horizontal and vertical components on both the distributed and core theories together with the final experimental values. The measured values have been corrected so that they represent the difference between the components in the mine and at a point immediately above on the surface. The values of the geomagnetic components to be used at the surface are deduced from the surface survey and those underground from the survey of the passage in which the site is situated. It will be seen that the measuremets are near to those predicted for a Core Theory and do not support

a Distributed Theory. Only in the case of the ΔH values at Hickleton do the results deviate significantly (*i. e.* by twice the standard deviation) from the prediction of a Core Theory.

Twenty sites in various mines have been magnetically surveyed but only six have been found to be free from buried iron. The result of the experiments in three of these sites has been described above. The experiment is proceeding in two more mines in the Doncaster area in order to obtain more ΔH measurements and a site in a colliery near Sunderland, Co. Durham is also being used. The detailed experimental results will be published elsewhere.

The experiments were done mainly from the Physics Dept. of Manchester University but are being continued from the Dept. of Geodesy and Geophysics of the University of Cambridge. We wish to thank Professor P. M. S. Blackett for his support and interest and Dr. Bruckshaw, the Danish Meteorological Institute, the Air Ministry, the Royal Greenwich Observatory, Dr. Veldkamp and Professor Whetton for the loan of instruments at various stages in the work. We are also grateful to the National Coal Board and its officials for providing facilities for the experiments and to many undergraduates of Manchester University for their assistance in the measurements.

References.

Blackett, P. M. S., 1947, *Nature, Lond.*, **159,** 658; 1949, *Phil. Mag.* [7], **40,** 125.

Chapman, S., 1948 a, *Nature, Lond.*, **161,** 462; 1948 b, *Annales de Geophysique*, **4,** 109.

Hales, A. L., and Gough, D. I., 1947, *Nature, Lond.*, **160,** 746.

Runcorn, S. K., 1948, *Proc. Phys. Soc.*, **61,** 373.

LXXI. *Energies and Widths of Domain Boundaries in Ferromagnetics.*

By B. A. Lilley,
Physics Department, University of Leeds*.

[Received May 30, 1950.]

Abstract.

A systematic treatment is given of the energies and widths of domain boundaries in ferromagnetics; it covers cubic crystals, with positive or negative magneto-crystalline anisotropy coefficients, and crystals with a single easy direction of magnetization. This extends the investigations of Bloch (1932), Landau and Lifshitz (1935), Lifshitz (1944) and Néel (1944) on cobalt and iron, and enables estimates to be made of the energies and widths of domain boundaries in nickel. The effect of magneto-elastic anisotropy energy is considered. Theoretical values of the energies and widths of the more important types of boundary in nickel, iron and cobalt are calculated.

§1. Introduction.

A ferromagnetic material is, in general, divided into elementary domains in each of which the spontaneous magnetization vector, $\mathbf{I}_0$, is constant, except possibly for small fluctuations in direction or intensity which may be neglected in the present calculations. The magnitude of $\mathbf{I}_0$ is the same in all the domains and is equal, to a good approximation, to the saturation intensity of the material at the temperature considered; the direction of $\mathbf{I}_0$ varies from domain to domain. The transition region between contiguous domains is known as a boundary or wall and in it $\mathbf{I}_0$ rotates from its direction in one domain to that in the other.

Estimates of the energy associated with domain boundaries and of their effective thickness were first made by Bloch in 1932. Since then the treatment has been refined and further developed by Landau and Lifshitz (1935), Néel (1944) and Lifshitz (1944). Landau and Lifshitz considered a crystal, such as hexagonal cobalt, with a single easy direction of magnetization; Néel and Lifshitz considered body-centred cubic iron, for which the easy directions lie along the cube edges, corresponding to a positive magneto-crystalline anisotropy coefficient.

The aim of this paper is to obtain more general formulae from which results may be obtained for all the particular cases of interest, and to apply similar methods to the more difficult problem of nickel, which has not previously been considered. For nickel, which has a face-centred

* Communicated by Professor E. C. Stoner, F.R.S.

structure, the easy directions lie along the cube diagonals, corresponding to a negative magneto-crystalline anisotropy coefficient. Most ferromagnetic materials are either cubic, with positive or negative anisotropy coefficients, or hexagonal, and these are all covered by the general formulæ obtained for the relative energies and widths of different types of boundary. Estimates of absolute values, such as are made for nickel, iron and cobalt, and could be made similarly for materials for which the basic experimental data are available, are much more uncertain.

In §2 the method of approach is indicated ; §3 deals with the energies and §4 with the widths of the domain boundaries neglecting the effect of magnetostriction. This is considered in §5, and in §6 the theoretical results for nickel, iron and cobalt are collected together.

A survey of the background to the subject of this paper is given by Stoner (1948, 1950 ; see in particular 1950, §3). Reference may also be made to a review article by Kittel (1949).

§2. Method.

In an unstrained ferromagnetic material in zero applied field each domain is magnetized along one of the crystallographically and energetically equivalent easiest directions. In domains in cobalt the magnetization vector, $\mathbf{I}_0$, can only lie along the hexagonal axis and thus only 180° boundaries (*i. e.* boundaries in which $\mathbf{I}_0$ rotates through 180°) can occur. In iron the domains can be magnetized along any one of the six equivalent cube edges, of type [100], and 90° and 180° boundaries are possible. Domains in nickel can be magnetized along a cube diagonal, of type [111], giving rise to 70·53°, 109·47° and 180° boundaries.

Néel (1944) emphasizes the importance of the condition that I_n, the normal component of $\mathbf{I}_0$, should have the same value not only on each side of the boundary, but also in it. This corresponds to the absence of free poles (*i. e.* a zero value of div $\mathbf{I}$) in the transition region. The presence of internal free poles would in general correspond to a free energy very much greater than that for some other arrangement satisfying the condition of zero divergence. It is convenient to specify the direction of magnetization at any point in the boundary by (θ, ϕ), where θ is the angle between $\mathbf{I}_0$ and the normal to the boundary, and ϕ the angle between the projection of $\mathbf{I}_0$ on the boundary plane and some selected zero direction in this plane. In particular the initial and final directions of $\mathbf{I}_0$ in the adjacent domains may be denoted by (θ, ϕ_1) and (θ, ϕ_2), constancy of I_n being equivalent to constancy of θ.

The free energy per unit volume of the boundary may be expressed in the form

$$\mathrm{F}=\mathrm{F}_a+\mathrm{F}_e, \qquad \ldots\ldots\ldots \quad (2.1),$$

where F_a is anisotropy and F_e exchange energy. The field energy is zero since the applied field and div $\mathbf{I}$ are both zero (*cf.* Stoner 1950, equations (3.14), (3.15)). The energy and effective width of the domain

boundary are determined from the condition that F, integrated over the range in which ϕ changes from ϕ_1 to ϕ_2, shall be a minimum. The anisotropy energy, F_a, may be expressed in the form

$$F_a = F_c + F_m, \quad \ldots\ldots\ldots \quad (2.2)$$

or

$$\beta f_a = \beta f_c + \beta' f_m, \quad \ldots\ldots\ldots \quad (2.3)$$

where F_c is magneto-crystalline and F_m magneto-elastic anisotropy energy; f_a, f_c and f_m are expressions for reduced energies adjusted, by subtracting appropriate constant terms, to make each zero for $\mathbf{I}_0$ along (θ, ϕ_1) and (θ, ϕ_2); β, β' stand for the appropriate magneto-crystalline and magneto-elastic anisotropy energy density coefficients respectively. The effect of the term F_m will not be considered until § 5.

General expressions for boundary energy and width.

It is convenient to consider the boundary to be in the yz plane with its normal along Ox and to take Oy as the zero direction for measurement of ϕ. If $\delta\psi$ is the angle between the spins in adjacent layers $\delta\psi = \sin\theta\,\delta\phi$, and the exchange energy, which is proportional to $1-\cos\delta\psi$, may be written (Néel 1944, p. 7; *cf.* Stoner 1950, equation (3.1))

$$F_c = \alpha a^2 \sin^2\theta (d\phi/dx)^2, \quad \ldots\ldots\ldots \quad (2.4)$$

where α is proportional to the exchange energy for parallel spins, and a is a lattice constant. With the Weiss treatment of ferromagnetism α would be proportional to $\frac{1}{2}N_w I_0^2$, N_w being the molecular field coefficient.

The energy, γ, per unit area of the boundary is then given by

$$\gamma = \int \{\alpha a^2 \sin^2\theta (d\phi/dx)^2 + \beta f_a\}\, dx. \quad \ldots\ldots\ldots \quad (2.5)$$

It follows from a simple variational treatment that, for γ to have a minimum value,

$$\beta f_a = \alpha a^2 \sin^2\theta (d\phi/dx)^2, \quad \ldots\ldots\ldots \quad (2.6)$$

i. e. the exchange and anisotropy contributions to the energy are equal (see Néel 1944, pp. 6–8; *cf.* Becker and Döring 1939, p. 191; Stoner 1950, equations (3.1)–(3.6)). Equation (2.6) may be written

$$(dx/d\phi) = b_0 \sin\theta f_a^{-\frac{1}{2}}, \quad \ldots\ldots\ldots \quad (2.7)$$

giving, by substitution in (2.5),

$$\gamma/\gamma_0 = 2 \sin\theta \int_{\phi_1}^{\phi_2} f_a^{\frac{1}{2}}\, d\phi, \quad \ldots\ldots\ldots \quad (2.8)$$

where b_0 is a unit of length normal to the boundary, and γ_0 a unit for the energy per unit area of the boundary (*cf.* Stoner 1950, equation (3.7)) given by

$$b_0 = (\alpha a^2/\beta)^{\frac{1}{2}}; \quad \gamma_0 = (\alpha a^2 \beta)^{\frac{1}{2}}. \quad \ldots\ldots\ldots \quad (2.9)$$

Equations (2.8) and (2.7) will be used to calculate domain boundary energies and widths.

Magneto-crystalline anisotropy energy.

For a cubic crystal the magneto-crystalline energy, F_c, apart from constant terms, may be represented, with sufficient approximation, by (*cf.* Stoner 1950, equation (2.1))

$$F_c = K_4(\alpha_2^2\alpha_3^2 + \alpha_3^2\alpha_1^2 + \alpha_1^2\alpha_2^2), \quad . \quad . \quad . \quad . \quad . \quad . \quad (2.10)$$

where α_1, α_2, α_3 are the direction cosines of $\mathbf{I}_0$ relative to the cube edges of the crystal. The reduced energy f_c is a function of θ and ϕ and may be written

$$\beta f_c(\theta, \phi) = (F_c)_{\theta,\phi} - (F_c)_{\min}, \quad . \quad . \quad . \quad . \quad . \quad (2.11)$$

where $(F_c)_{\theta,\phi}$ is the value of F_c corresponding to $\mathbf{I}_0$ along the direction (θ, ϕ); $(F_c)_{\min}$ that corresponding to $\mathbf{I}_0$ along an easy direction; and for cubic crystals, $\beta = |K_4|$. For iron K_4 is positive and thus

$$(F_c)_{\min} = 0. \quad . \quad . \quad . \quad . \quad . \quad . \quad . \quad . \quad (2.12)$$

Fig. 2.1.

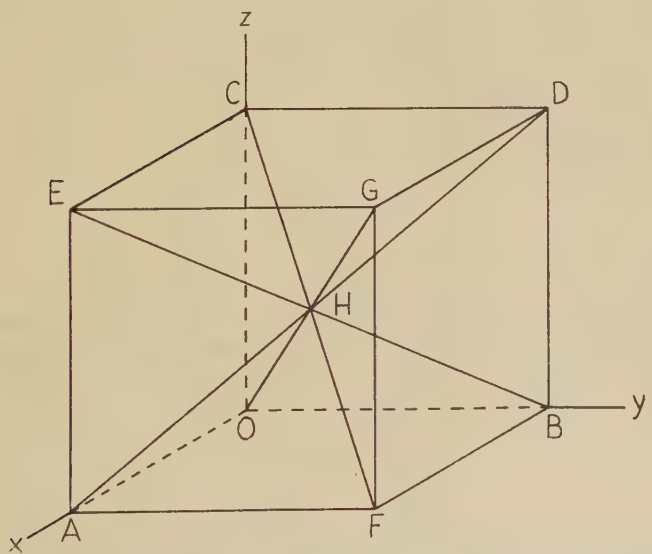

Cubic crystal, showing easy directions in iron (edges) and in nickel (diagonals).

For nickel K_4 is negative giving

$$(F_c)_{\min} = K_4/3 = -\beta/3. \quad . \quad . \quad . \quad . \quad . \quad . \quad (2.13)$$

The form of the function f_c can be determined for boundary planes of all possible orientations, and in the most general case a very complicated expression is obtained, but only certain boundaries satisfy the condition imposed upon I_n. All 90° boundaries in iron are similar to those in which $\mathbf{I}_0$ rotates from [100] (*i. e.* OA in fig. 2.1) to [010] (OB); and [11*l*] or [$\bar{1}\bar{1}l$] (*i. e.* any direction in the plane OCGF) are the only directions which make equal angles with these cube edges. In nickel all 109·47°

boundaries are similar to those in which $\mathbf{I}_0$ rotates from $[\bar{1}11]$ (HD) to $[1\bar{1}1]$ (HE) and, again, only $[11l]$ or $[\bar{1}\bar{1}l]$ make equal angles with these cube diagonals. All 70·53° boundaries in nickel are similar to those in which $\mathbf{I}_0$ rotates from $[1\bar{1}1]$ (HE) to $[1\bar{1}\bar{1}]$ (HA); and $[hk0]$ (*i. e.* any direction in the plane parallel to OAFB drawn through H) are the only directions making equal angles with these initial and final easy directions. All 180° boundaries in iron are similar to those formed by a rotation of $\mathbf{I}_0$ from $[001]$ to $[00\bar{1}]$ and in nickel from $[111]$ to $[\bar{1}\bar{1}\bar{1}]$, the normals to the boundaries thus lying in the (001) and (111) planes respectively. Thus, for 90° boundaries in iron possible boundary planes are parallel to the $\{11l\}$ planes ($\{11l\}$ being understood, in the usual crystallographic notation, to mean any plane of the type $(11l)$); for 109·47° boundaries in nickel to the $\{11l\}$ planes; and for 70·53° boundaries in nickel to the $\{hk0\}$ planes. It is convenient to consider $\{001\}$ to be $\{11l\}$ planes with $l=\infty$; the parameters h, k and l can each take any value between $-\infty$ and $+\infty$. The $\{001\}$, $\{110\}$ and $\{111\}$ planes are particular examples of the $\{11l\}$ planes; $\{100\}$ and $\{110\}$ of either the $\{11l\}$ or $\{hk0\}$ planes. In these cases f_c assumes particularly simple forms and it is then possible to derive analytical expressions for the boundary energies and widths. The normals to all 180° boundaries in iron and nickel lie in the $\{001\}$ and $\{111\}$ planes respectively.

For hexagonal cobalt, the magneto-crystalline energy may be represented, with sufficient approximation, by

$$\mathrm{F}_c=\beta f_c(\theta,\phi)=\mathrm{K}_2'\sin^2\phi, \quad . \quad . \quad . \quad . \quad . \quad . \quad (2.14)$$

where $\beta=\mathrm{K}_2'$. The angle θ is equal to 90° and hence ϕ is the angle between $\mathbf{I}_0$ and the hexagonal axis. This relation also holds, if the natural magneto-crystalline effect can be neglected, for materials of positive or negative isotropic magnetostriction under tension or compression respectively.

Magneto-crystalline anisotropy energy of cubic crystals as a function of θ and ϕ.

If the normal to the boundary is the $[11l]$ direction it is possible to determine the direction cosines of $\mathbf{I}_0$ with respect to the axes $[11l]$, $[\bar{1}10]$, $[\bar{l}\bar{l}2]$. A simple transformation then gives the direction cosines with respect to the [100], [010], [001] axes defined by the cube edges, and it follows from (2.10) that

$$\begin{aligned}\mathrm{F}_c=\frac{\mathrm{K}_4}{4(l^2+2)^2}\,[&4(2l^2+1)+4(l^2+1)(l^2-4)\sin^2\theta-(3l^2+4)(l^2-4)\sin^4\theta\\&-4(l^2-1)\{6+(l^2-4)\sin^2\theta\}\sin^2\theta\sin^2\phi\\&+4(l^2+3)(l^2-1)\sin^4\theta\sin^4\phi\\&-2^{5/2}\,l\cos\theta\sin\theta\sin\phi\{2(l^2-1)\\&-(5l^2+4)\sin^2\theta+2(l^2+5)\sin^2\theta\sin^2\phi\}]. \quad . \quad . \quad . \quad (2.15)\end{aligned}$$

This relation holds for $\{11l\}$ boundary planes in any crystal whose magneto-crystalline energy may be represented by (2.10). In particular, $l=\infty$, 0, 1 correspond to boundary planes whose normals are [001], [110], [111] respectively. The energy expression is now in a convenient form for use in calculating boundary energies and widths.

§ 3. Boundary Energies.

The energy of a domain boundary when magneto-crystalline anisotropy and exchange energy alone are considered, given by replacing f_a by f_c in (2.8), is

$$\gamma/\gamma_0=2\sin\theta\int_{\phi_1}^{\phi_2} f_c^{\frac{1}{2}}\,d\phi. \qquad . \quad . \quad . \quad . \quad . \quad . \quad (3.1)$$

Nickel. For a boundary plane in nickel whose normal is $[11l]$ the values of θ and ϕ_3, ϕ_4 corresponding to $\mathbf{I}_0$ along the $[\bar{1}11]$, $[1\bar{1}1]$ directions respectively, can be determined in terms of l:

$$\theta=\cos^{-1} l/\{3(l^2+2)\}^{\frac{1}{2}}, \qquad 0<\theta<\pi\,; \quad . \quad . \quad . \quad . \quad . \quad . \quad (3.2)$$

$$\left.\begin{aligned}&\phi_3=\cos^{-1}\{(l^2+2)/(l^2+3)\}^{\frac{1}{2}}, \qquad 0<\phi_3<\pi/2\,;\\ &\phi_4=\pi-\phi_3.\end{aligned}\right\} \quad . \quad . \quad . \quad (3.3)$$

The domain boundaries in nickel which are of particular importance are now considered, and the results are summarized in Table 3.1. A [001], 70·53° boundary is understood to mean a 70·53° boundary the normal to whose plane lies in the direction [001], about which $\mathbf{I}_0$ rotates from the initial to the final easy direction. The values of θ, ϕ_3 and ϕ_4 are obtained by substituting the appropriate value of l in (3.2) and (3.3), ϕ_1 and ϕ_2 are found from ϕ_3 and ϕ_4, and $f_c^{\frac{1}{2}}$ is then determined by substitution in (2.15) and using (2.11) and (2.13). The relative energies, (γ/γ_0), of the boundaries are then calculated using (3.1).

The [001], 109·47° boundary is effectively two successive [001], 70·53° boundaries since $\mathbf{I}_0$ must rotate through $[\bar{1}\bar{1}1]$ (*i. e.* HC in fig. 2.1) in passing from $[\bar{1}11]$ (HD) to $[1\bar{1}1]$ (HE). Its energy is, therefore, twice that of the [001], 70·53° boundaries. It is impossible to have [111], 70·53° boundaries since the angles between [111] and any two easy directions containing an angle of 70·53° (*e. g.* HD and HC in fig. 2.1) are not equal.

180° *Boundaries.* All 180° boundaries are similar to those formed by a rotation of $\mathbf{I}_0$ from [111] to $[\bar{1}\bar{1}\bar{1}]$. A new system of axes $Ox'y'z'$ which has directions [111], $[\bar{1}10]$, $[\bar{1}\bar{1}2]$ (corresponding to $l=1$ in the $[11l]$, $[\bar{1}10]$, $[\bar{l}\bar{l}2]$ axes of § 2) with respect to the system, $Oxyz$, formed by the cube edges of the crystal, may be set up. A particular boundary may be specified by ω if $\mathbf{I}_0$ rotates through OP, which lies in the $y'z'$ plane, and where ω is the angle between OP and Oy' (see fig. 3.1). The boundary

thus formed is in the plane whose normal is $[3^{\frac{1}{2}}\sin\omega-\cos\omega, -3^{\frac{1}{2}}\sin\omega-\cos\omega, 2\cos\omega]$. The angle ω can have any value and, in particular, when $\omega+30°=n60°$, where n is any integer, $\mathbf{I}_0$ rotates through an easy direction intermediate between [111] and $[\bar{1}\bar{1}\bar{1}]$. It is thus convenient to write *

$$\lambda=\omega+30°, \quad . \quad . \quad . \quad . \quad . \quad . \quad . \quad . \quad . \quad (3.4)$$

and the normal to the boundary plane as $[\sin\lambda-3^{\frac{1}{2}}\cos\lambda, -2\sin\lambda, \sin\lambda+3^{\frac{1}{2}}\cos\lambda]$. The angle λ is that between the projections of $\mathbf{I}_0$ and the easy direction $[\bar{1}1\bar{1}]$ on the (111) plane.

TABLE 3.1.

Reduced energies of 70·53° and 109·47° domain boundaries in nickel.
θ, angle between $\mathbf{I}_0$ and Ox, the normal to the boundary.
ϕ_1, ϕ_2, angles between projection of $\mathbf{I}_0$ on yz plane and Oy, corresponding to initial and final easy directions respectively.
f_c, reduced magneto-crystalline energy.
γ, boundary energy per unit area.
$\gamma_0=(\alpha a^2\beta)^{\frac{1}{2}}$ (see (2.9)).
$\eta=\cos^{-1}(2/3)^{\frac{1}{2}}(=35·26°)$: 2η=angle between [111] and $[\bar{1}11]$.

Type of boundary	Easy directions; initial, final.	θ	ϕ_1, ϕ_2.	$3^{\frac{5}{2}}2f_c^{\frac{1}{2}}$	$3^{\frac{3}{2}}(\gamma/\gamma_0)$	(γ/γ_0)
[001], 70·53°	$[\bar{1}11]$, $[\bar{1}\bar{1}1]$.	$\frac{1}{2}\pi-\eta$	0, $\pi/2$.	$2^2 3^{3/2}\sin\phi\cos\phi$	$2^{3/2}/3$	0·5443
[001], 109·47°	$[\bar{1}11]$, $[1\bar{1}1]$.	$\frac{1}{2}\pi-\eta$	0, π.	$2^2 3^{3/2}\sin\phi\cos\phi$	$2^{5/2}/3$	1·0887
[110], 70·53°	$[\bar{1}1\bar{1}]$, $[\bar{1}11]$.	$\frac{1}{2}\pi$	$-\eta$, η.	$3^2(1-3\sin^2\phi)$	$2^{\frac{1}{2}}-\eta$	0·4611
[110], 109·47°	$[\bar{1}11]$, $[1\bar{1}1]$.	$\frac{1}{2}\pi$	η, $\pi-\eta$.	$3^2(3\sin^2\phi-1)$	$2^{\frac{1}{2}}+\pi/2-\eta$	1·3680
[111], 109·47°	$[\bar{1}11]$, $[1\bar{1}1]$.	2η	$\pi/6$, $5\pi/6$.	$2^7 3^2(1-\sin 3\phi)^{\frac{1}{2}}$	$2^{15}3^2/3^4$	1·2903

The magneto-crystalline energy may be represented by

$$F_c=(K_4/12)\{4\cos^4\phi+3\sin^4\phi+2^{5/2}\cos\phi\sin^3\phi\sin\omega(3-4\sin^2\omega)\}, \quad (3.5)$$

* This angle, following the usage of Néel (1944), is denoted by λ. It is not to be confused with a magnetostriction coefficient, which is always written in this paper with a directional suffix, *e.g.*, λ_{100}.

by putting $l=1$ and replacing θ by ϕ and ϕ by ω in (2.15). The magnetization vector, $\mathbf{I}_0$, must rotate in the plane of the boundary and $\sin\theta$ in (3.1) is, therefore, equal to unity. From (2.11), (2.13), (3.1) and (3.5) it follows that

$$\gamma/\gamma_0=3^{-\frac{1}{2}}\int_0^{\pi}(1+\rho\sin\phi\cos\phi+7\cos^2\phi)^{\frac{1}{2}}\sin\phi\,d\phi, \quad . \quad . \quad (3.6)$$

where

$$\left.\begin{aligned}\rho&=-2^{5/2}\sin 3\omega\\&=2^{5/2}\cos 3\lambda\end{aligned}\right\};\ -2^{5/2}\leqslant\rho\leqslant+2^{5/2}. \quad . \quad . \quad . \quad (3.7)$$

Fig. 3.1.

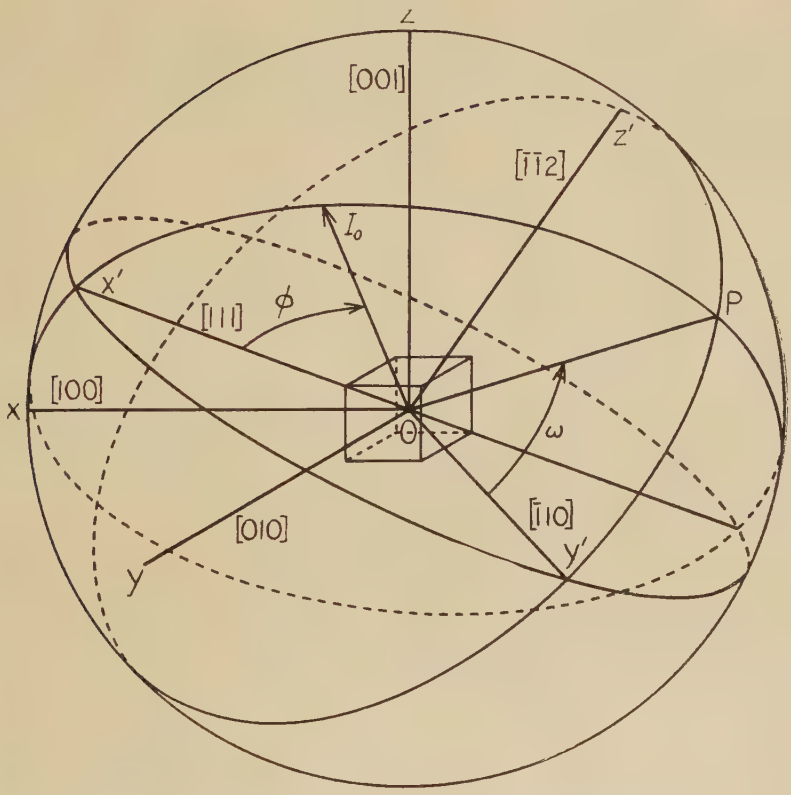

Coordinate axes used in describing 180° boundaries in nickel.
OP, direction in $y'z'$ plane through which $\mathbf{I}_0$ rotates.
ω, angle between OP and Oy'.
ϕ, angle between $\mathbf{I}_0$ and Ox'.

It is possible, without any difficulty, to evaluate the integral analytically when $\rho=\pm 2^{5/2}$ since $(\sin^2\phi\pm 2^{5/2}\sin\phi\cos\phi+8\cos^2\phi)$ is a perfect square. Similarly when $\rho=0$ the integral can be evaluated analytically in terms of an inverse trigonometric hyperbolic function. For a general value of ρ the integration is slightly more troublesome.

It is possible to make the mixed term of (3.6) equal to zero by writing

$$\phi=\chi+\kappa, \quad . \quad . \quad . \quad . \quad . \quad . \quad . \quad . \quad (3.8)$$

where χ is a new variable and κ is a function of ρ only, and choosing κ such that

$$\tan 2\kappa=\rho/7. \quad . \quad . \quad . \quad . \quad . \quad . \quad . \quad . \quad (3.9)$$

Then

$$\gamma/\gamma_0=3^{-\frac{1}{2}}(7\sec 2\kappa)^{\frac{1}{2}}\left\{\int_{-\kappa}^{\pi-\kappa}(r^2-\sin^2\chi)^{\frac{1}{2}}\sin\kappa\cos\chi\,d\chi\right.$$
$$\left.+\int_{-\kappa}^{\pi-\kappa}(r^2-\sin^2\chi)^{\frac{1}{2}}\cos\kappa\sin\chi\,d\chi\right\}. \quad (3.10)$$

The first integral is evaluated by substituting $u=(\sin\chi)/r$ and the second by substituting $v=(\cos\chi)/s$ and, after some manipulation, the energy of a boundary whose normal is $[\sin\lambda-3^{\frac{1}{2}}\cos\lambda,\ -2\sin\lambda,\ \sin\lambda+3^{\frac{1}{2}}\cos\lambda]$ may be written

$$\gamma/\gamma_0=3^{-\frac{1}{2}}\{2^{3/2}+(7\sec 2\kappa)^{\frac{1}{2}}(r^3t\sin^{-1}t+s^3p\sinh^{-1}p)\}, \quad . \quad . \quad (3.11)$$

where

$$\left.\begin{aligned}14r^2&=9\cos 2\kappa+7\\14s^2&=9\cos 2\kappa-7\end{aligned}\right\};\ s^2=r^2-1;\quad \left.\begin{aligned}t&=(\sin\kappa)/r\\p&=(\cos\kappa)/s.\end{aligned}\right\} \quad . \quad . \quad (3.12)$$

When $\lambda=0°, 120°, 240°$, $\rho=2^{5/2}$; $\lambda=60°, 180°, 300°$, $\rho=-2^{5/2}$, and these six particular cases correspond to boundary planes of the (110) type and to a rotation of $\mathbf{I}_0$ through an easy direction intermediate between [111] and $[\bar{1}\bar{1}\bar{1}]$. Thus the energy of these boundaries is equal to the sum of the energies of [110], 70·53° and [110], 109·47° boundaries (*cf.* Table 3.1) and by substitution in (3.11)

$$\gamma/\gamma_0=3^{-\frac{1}{2}}(2^{3/2}+\pi/2-2\eta)=1\cdot 8292. \quad . \quad . \quad . \quad . \quad . \quad (3.13)$$

This is the minimum value for the energy of 180° boundaries in nickel. When $\lambda=30°$, $\rho=0$, the normal to the boundary is $[\bar{1}\bar{1}2]$ and the energy as given by (3.11) is a maximum,

$$\gamma/\gamma_0=3^{-\frac{1}{2}}\{2^{3/2}+7^{-\frac{1}{2}}\sinh^{-1}(7^{\frac{1}{2}})\}=2\cdot 0040. \quad . \quad . \quad . \quad (3.14)$$

Iron. For a boundary plane whose normal is $[11l]$ the values of θ and ϕ_3, ϕ_4 corresponding to $\mathbf{I}_0$ along the [100], [010] directions are given by

$$\theta=\cos^{-1}(l^2+2)^{-\frac{1}{2}}, \quad 0<\theta<\pi; \quad . \quad . \quad . \quad . \quad (3.15)$$

$$\left.\begin{aligned}\phi_3&=\cos^{-1}-\{(l^2+2)/2(l^2+1)\}^{\frac{1}{2}},\ \pi<\phi_3<3\pi/2;\\\phi_4&=\cos^{-1}\{(l^2+2)/2(l^2+1)\}^{\frac{1}{2}},\ 3\pi/2<\phi_4<2\pi.\end{aligned}\right\} \quad . \quad . \quad (3.16)$$

The domain boundary energies may be calculated in a way similar to that used for nickel, using (3.15), (3.16) and (2.12) instead of (3.2), (3.3) and (2.13). The results are summarized in Table 3.2.

TABLE 3.2.

Reduced energies of 90° domain boundaries in iron.
In all cases the initial and final easy directions are [100] and [010] respectively. (See Table 3.1 for symbols.)

Type of boundary	θ	ϕ_1, ϕ_2.	$4f_c^{\frac{1}{2}}$	γ/γ_0	γ/γ_0
[001], 90°	$\pi/2$	$-3\pi/4$, $-\pi/4$.	$2(1-2\sin^2\phi)$	1	1·0000
[110], 90°	$\pi/4$	π, 0.	$\sin\phi(8-3\sin^2\phi)^{\frac{1}{2}}$	$1+2^{-3}3^{-\frac{1}{2}}5\sinh^{-1}(3/5)^{\frac{1}{2}}$	1·7274
[111], 90°	$\pi/2-\eta$	$-5\pi/6$, $-\pi/6$.	$2^3 3^{-3/2}(1+\sin 3\phi)^{\frac{1}{2}}$	$2^5/3^3$	1·1852

Fig. 3.2.

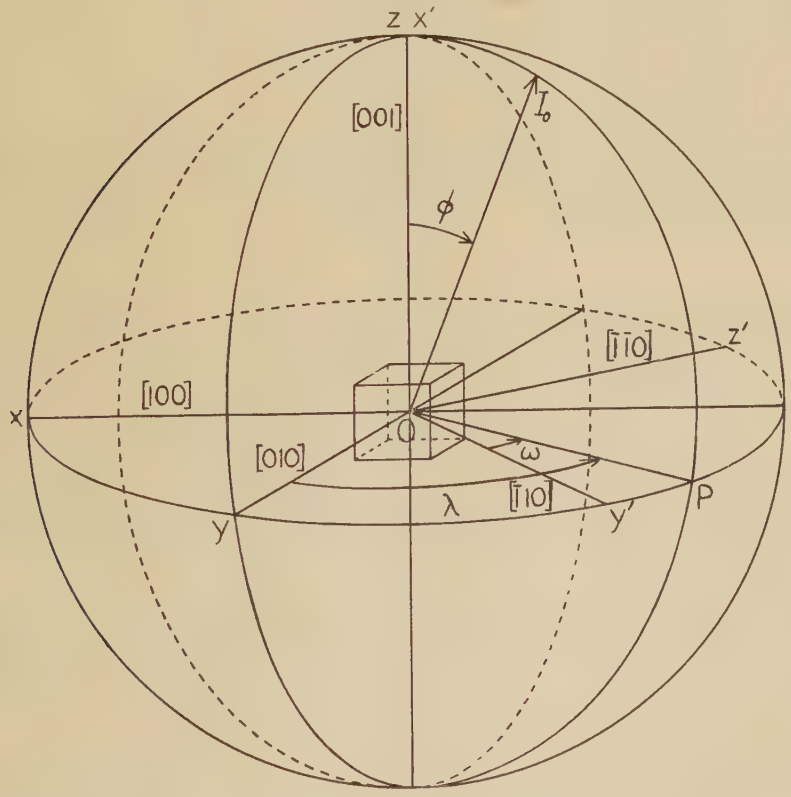

Coordinate axes used in describing 180° boundaries in iron.
OP, direction in xy ($y'z'$) plane through which $\mathbf{I}_0$ rotates.
ω, angle between OP and Oy'.
λ, angle between OP and Oy.
ϕ, angle between $\mathbf{I}_0$ and Oz (Ox').

180° *Boundaries.* A rotation of $\mathbf{I}_0$ from [001] to [00$\bar{1}$] through OP, which is in the xy plane (see fig. 3.2) is considered by substituting $l=\infty$ and replacing θ by ϕ and ϕ by ω in (2.15). By writing

$$\lambda=\omega+45^\circ \quad . \quad . \quad . \quad . \quad . \quad . \quad . \quad . \quad (3.17)$$

(*cf.* equation (3.4)) the magneto-crystalline anisotropy energy may be expressed by

$$f_c=\sin^2\phi-\mu\sin^4\phi, \quad . \quad . \quad . \quad . \quad . \quad . \quad (3.18)$$

where

$$\left.\begin{aligned}\mu&=(7-\cos 4\omega)/8,\\ &=(7+\cos 4\lambda)/8 \quad (cf.\ \text{Néel 1944, p. 11}).\end{aligned}\right\} \quad . \quad . \quad . \quad (3.19)$$

The angle λ is that between [010] and the projection of $\mathbf{I}_0$ on the (001) plane.

The normal to the boundary specified by λ is $[-\cos\lambda, -\sin\lambda, 0]$. By substitution in (3.1) it follows that

$$\gamma/\gamma_0=2\{1+(1-\mu)\mu^{-\frac{1}{2}}\sinh^{-1}(\mu/1-\mu)^{\frac{1}{2}}\} \quad . \quad . \quad . \quad . \quad (3.20)$$

When $\lambda=n\pi/2$, where n is any integer, $\mu=1$, and the boundary can be considered to be the sum of two [001], 90° type boundaries. Its energy as calculated from (3.20) is twice that of a [001], 90° boundary and is given by

$$\gamma/\gamma_0=2. \quad . \quad . \quad . \quad . \quad . \quad . \quad . \quad . \quad (3.21)$$

This is the minimum value for the energy of 180° boundaries in iron. If $\lambda=n\pi/2+45^\circ$, corresponding to $\mu=3/4$, the energy is a maximum and equal to

$$\gamma/\gamma_0=2+3^{-\frac{1}{2}}\sinh^{-1}(3^{\frac{1}{2}})=2{\cdot}7603 \quad . \quad . \quad . \quad . \quad (3.22)$$

for boundaries in the {110} planes.

The relative energies of domain boundaries in iron have already been calculated by Néel (1944), whose method is essentially the same as that employed above.

Cobalt. Only 180° boundaries occur in hexagonal cobalt and F_c is zero along the easy directions. Thus, from (2.14),

$$f_c=\sin^2\phi, \quad . \quad . \quad . \quad . \quad . \quad . \quad . \quad . \quad (3.23)$$

giving, from (3.1), writing $\sin\theta=1$,

$$\begin{aligned}\gamma/\gamma_0&=2\int_0^{\pi}\sin\phi\,d\phi\\ &=4. \quad . \quad . \quad . \quad . \quad . \quad . \quad . \quad . \quad . \quad (3.24)\end{aligned}$$

The energies of all boundaries in cobalt are the same.

§ 4. Boundary Widths.

If exchange and magneto-crystalline anisotropy energy alone are considered the distance x, measured normal to the boundary, can be obtained as a function of ϕ, the angle between the projection of $\mathbf{I}_0$ on the boundary plane and the zero direction, by replacing f_a by f_c in equation (2.7), giving

$$(dx/d\phi)=b_0 \sin\theta f_c^{-1}. \quad . \quad . \quad . \quad . \quad . \quad . \quad . \quad . \quad (4.1)$$

This section will be devoted to a consideration of the variation of x with ϕ for the various boundaries considered in § 3, and of the resultant " boundary widths ".

Fig. 4.1.

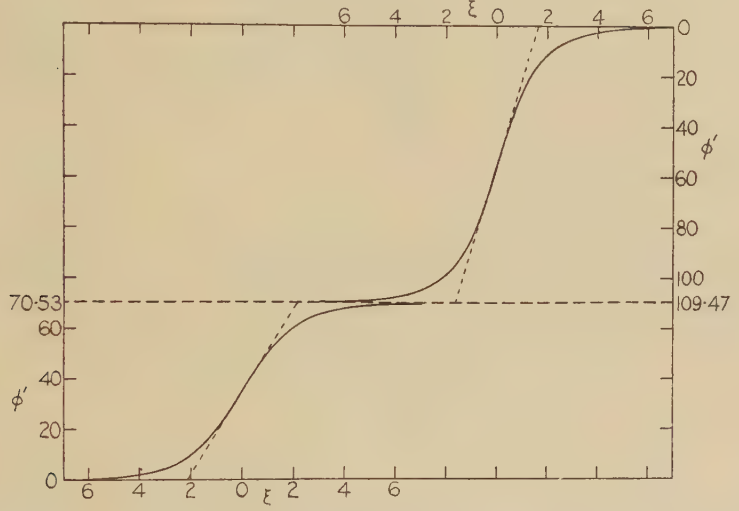

Variation with distance normal to the boundary plane of the angle, ϕ', through which $\mathbf{I}_0$ has rotated, for [110], 70·53° and [1$\bar{1}$0], 109·47° domain boundaries in nickel.

The broken line is an asymptote common to the two curves. $\xi=x/b_0$. x, distance normal to boundary.

For $\phi\to\phi_1$ or ϕ_2, $f_c\to 0$, $|x|\to\infty$, and if the boundary is to satisfy the minimum energy condition it has no sharply defined width, as is shown in figs. 4.1, 4.2 and 4.3. It will be convenient to introduce a non-dimensional parameter (*cf.* Stoner 1950, equation (3.8)),

$$\xi=x/b_0, \quad . \quad . \quad . \quad . \quad . \quad . \quad . \quad . \quad . \quad . \quad (4.2)$$

for measurement of length normal to the boundary. All ϕ, ξ curves for 70·53° and 109·47° nickel, 90° iron and 180° cobalt boundaries are symmetrical about their points of inflexion which lie at $\phi=(\phi_1+\phi_2)/2$. For such boundaries the effective width, b, may be conveniently taken as

$$(b/b_0)=(\phi_2-\phi_1)(d\xi/d\phi)_{\text{inflexion}}, \quad . \quad . \quad . \quad . \quad . \quad . \quad (4.3)$$

where the notation is self-explanatory. All ϕ, ξ curves for 180° boundaries in nickel and iron are of the form indicated in figs. 4.2 and 4.3 respectively, and the effective width, b, may be taken as

$$(b/b_0)=(\xi_c-\xi_a)+\phi_a(d\xi/d\phi)_a+(\pi-\phi_c)(d\xi/d\phi)_c, \quad . \quad . \quad . \quad (4.4)$$

Fig. 4.2.

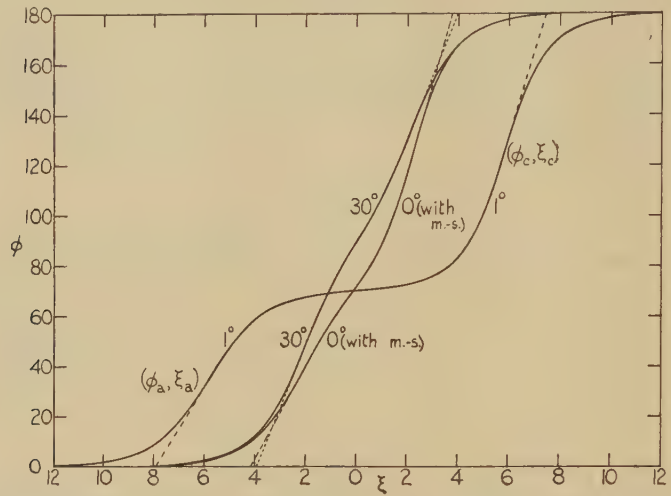

Variation with ξ of ϕ for 180° boundaries in nickel. The numbers on the curves indicate the values of λ; the curve marked 0° (with m.-s.) is that for $\lambda=0°$ when magnetostriction is taken into account (see § 5).

$\xi=x/b_0$. x, distance normal to boundary.

ϕ, angle between $\mathbf{I}_0$ and [111].

Fig. 4.3.

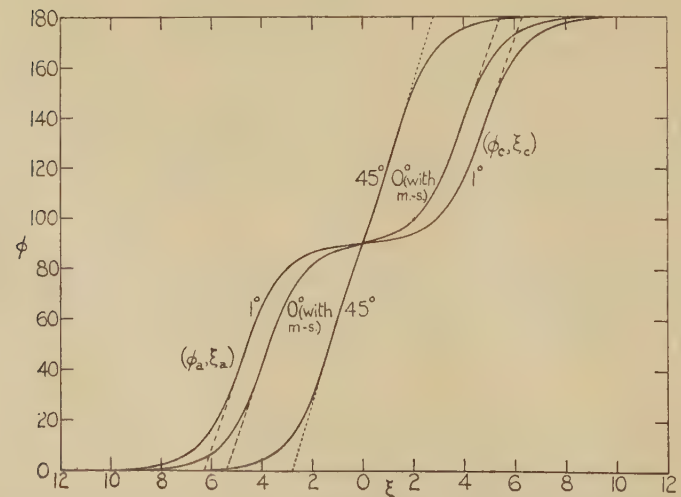

Variation with ξ of ϕ for 180° boundaries in iron. The numbers on the curves indicate the values of λ; the curve marked 0° (with m.-s.) is that for $\lambda=0°$ when magnetostriction is taken into account (see § 5).

$\xi=x/b_0$. x, distance normal to boundary. ϕ, angle between $\mathbf{I}_0$ and [001].

where (ϕ_a, ξ_a), (ϕ_c, ξ_c) (see figs. 4.2 and 4.3) are the first and third points of inflexion. It will be noted that all 180° boundaries in iron, and 180° boundaries in nickel when $\lambda = n60° + 30°$ (where λ is defined as the angle between the projections of $\mathbf{I}_0$ and the easy direction $[\bar{1}1\bar{1}]$ on the (111) plane (see (3.4)), are symmetrical about $\phi = \pi/2$. The expressions (4.1) and (4.2) are used to find ξ as a function of ϕ, the constant of integration being omitted, and (4.3), (4.4) are used to determine the boundary widths. The results for 70·53° and 109·47° boundaries in nickel are summarized in Table 4.1 and those for 90° boundaries in iron in Table 4.2. The values of θ, ϕ_1 and ϕ_2 and $f_c^{\frac{1}{2}}$ are given in Tables 3.1 and 3.2 and are not repeated here.

TABLE 4.1.

Reduced widths of 70·53° and 109·47° domain boundaries in nickel.
$\xi = x/b_0$.
x, distance normal to boundary.
b, effective boundary width.
b_0, unit for measurement of x and b ; $b_0 = (\alpha a^2/\beta)^{\frac{1}{2}}$ (see (2.9)).
$\eta = \cos^{-1}(2/3)^{\frac{1}{2}} (= 35·26°)$.

Type of boundary	$(2/3)^{\frac{1}{2}}\xi$	$(2/3)^{\frac{1}{2}}(b/b_0)$	(b/b_0)
[001], 70·53°	$ln \lvert \tan \phi \rvert$	π	3·8476
[001], 109·47°		∞	∞
[110], 70·53°	$2 \tanh^{-1} (2^{\frac{1}{2}} \tan \phi)$	$2^{5·2}\eta$	4·2642
[110], 109·47°	$-2 \coth^{-1} (2^{\frac{1}{2}} \tan \phi)$	$2^{\frac{1}{2}}(\pi - 2\eta)$	3·3093
[111], 109·47°	$ln \lvert \tan (\pi/8 - 3\phi/4) \rvert$	π	3·8476

TABLE 4.2.

Reduced widths of 90° domain boundaries in iron.
(See Table 4.1 for symbols.)

Type of boundary	ξ	(b/b_0)	(b/b_0)
[001], 90°	$ln \lvert \tan (\phi + \pi/4) \rvert$	π	3·1416
[110], 90°	$-\sinh^{-1} \{(8/5)^{\frac{1}{2}} \cot \phi\}$	$(8/5)^{\frac{1}{2}}\pi$	3·9738
[111], 90°	$-ln \lvert \tan (3\pi/8 - 3\phi/4) \rvert$	π	3·1416

It may be noted, in connection with the expressions for ξ in the Tables, that the inverse hyperbolic functions may be expressed as logarithmic functions as follows :

$$\left.\begin{aligned} \sinh^{-1} x &= ln\{x + (x^2+1)^{\frac{1}{2}}\} ; \\ 2 \tanh^{-1} x &= ln\{(1+x)/(1-x)\}, \ x^2 < 1 ; \\ 2 \coth^{-1} x &= ln\{(x+1)/(x-1)\}, \ x^2 > 1 ; \\ 2 \tanh^{-1} (\tan \phi) &= ln \lvert \tan (\phi + \pi/4) \rvert . \end{aligned}\right\} \quad . \quad . \quad (4.5)$$

Values of these functions are tabulated by Comrie (1949).

If the magnetostriction term, f_m, is not introduced, the [001], 109·47° boundary in nickel can only be regarded as two successive 70·53° boundaries, and as these would necessarily have an infinite distance between them, the resultant boundary width would be infinite. This case will be considered in § 5.

In fig. 4.1 the ϕ, ξ curves for [110], 70·53° and [110], 109·47° boundaries in nickel have been plotted. All ϕ, ξ curves for 70·53° and 109·47° nickel and 90° iron boundaries are similar to these.

180° *Boundaries in nickel.* The parameter ξ is expressed as a function of ϕ by using (4.1), (4.2), (3.5), (2.11) and (2.13) and may be written

$$\xi = 3^{\frac{1}{2}}2\int(1+\rho\cot\phi+8\cot^2\phi)^{-\frac{1}{2}}\operatorname{cosec}^2\phi\,d\phi \quad . \quad . \quad . \quad . \quad . \quad (4.6)$$

$$\left.\begin{aligned} &= -(3/2)^{\frac{1}{2}}\sinh^{-1}\{(16\cot\phi+\rho)/(32-\rho^2)^{\frac{1}{2}}\} \\ &= -(3/2)^{\frac{1}{2}}\sinh^{-1}\{\operatorname{cosec}3\lambda(2^{3/2}\cot\phi+\cos 3\lambda)\}. \end{aligned}\right\} \quad . \quad . \quad (4.7)$$

The ϕ, ξ curves corresponding to $\lambda=1°$ and 30°, where λ is the angle between the projections of $\mathbf{I}_0$ and the easy direction $[\bar{1}1\bar{1}]$ on the (111) plane, are plotted in fig. 4.2. The curve for $\lambda=30°$ is a limiting case; and as λ approaches 0° the central portion broadens and becomes more nearly parallel to the ξ axis until, when $\lambda=0°$, the boundary width is infinite and the wall can be regarded as two infinitely distant walls of the form shown in fig. 4.1. When

$$\left.\begin{aligned} &\lambda = 0°, (b/b_0) = \infty\,; \\ &\lambda = 1°, (b/b_0) = 15{\cdot}4029\,; \\ &\lambda = 30°, (b/b_0) = 2(3/2)^{\frac{1}{2}}\{\sinh^{-1}(6^{\frac{1}{2}})+(7/2)^{\frac{1}{2}}\sin^{-1}(2/7^{\frac{1}{2}})\} \\ &\qquad\qquad = 7{\cdot}9161. \end{aligned}\right\} \quad . \quad (4.8)$$

180° *Boundaries in iron.* For iron ξ may be written, by using (4.1), (4.2) and (3.18), in the form

$$\xi = \int(\sin^2\phi-\mu\sin^4\phi)^{-\frac{1}{2}}\,d\phi \quad . \quad . \quad . \quad . \quad . \quad . \quad . \quad . \quad . \quad . \quad . \quad (4.9)$$

$$= -\sinh^{-1}\{(\cot\phi)/(1-\mu)^{\frac{1}{2}}\} = -\sinh^{-1}(2\operatorname{cosec}2\lambda\cot\phi). \quad (4.10)$$

Curves, similar to those for 180° nickel boundaries, are plotted in fig. 4.3, that for $\lambda=45°$ (λ being the angle between the projection of $\mathbf{I}_0$ on the (001) plane and the easy direction [010]), corresponding to a normal in the direction $[\bar{1}\bar{1}0]$, being a limiting case. In the other limiting case $\lambda=0°$ and the boundary can be considered to be two infinitely distant boundaries of the [001], 90° type. When

$$\left.\begin{aligned} &\lambda = 0°, \quad (b/b_0) = \infty\,; \\ &\lambda = 1°, \quad (b/b_0) = 12{\cdot}6258\,; \\ &\lambda = 22{\cdot}5°, \quad (b/b_0) = 2\{\sinh^{-1}(6^{\frac{1}{2}})+(7/2)^{\frac{1}{2}}\sin^{-1}(2/7^{\frac{1}{2}})\} \\ &\qquad\qquad = 6{\cdot}4635\,; \\ &\lambda = 45°, \quad (b/b_0) = 2\{\sinh^{-1}(2^{\frac{1}{2}})+3^{\frac{1}{2}}\sin^{-1}(2/3)^{\frac{1}{2}}\} \\ &\qquad\qquad = 5{\cdot}6018. \end{aligned}\right\} \quad . \quad (4.11)$$

Boundaries in cobalt. For cobalt ξ may be written, by using (4.1), (4.2) and (3.23), in the form

$$\xi=\int \operatorname{cosec}\phi\, d\phi \quad . \quad . \quad . \quad . \quad . \quad . \quad . \quad . \quad . \quad (4.12)$$

$$=ln\,|\tan(\phi/2)|\,. \quad . \quad . \quad . \quad . \quad . \quad . \quad . \quad . \quad . \quad (4.13)$$

This curve is similar to those for 70·53° and 109·47° nickel and 90° iron boundaries. The reduced boundary width, b/b_0, is equal to π and is the same for all the boundaries.

§ 5. Effect of Magnetostriction.

The introduction of a magneto-elastic anisotropy energy term, F_m, has important consequences. This section will be devoted to a consideration of its effect on 180° boundaries, and particularly to those which have been considered in §§3 and 4 to be the sums of two infinitely distant boundaries. They no longer have infinite " boundary widths " since the effective result of the introduction of this term is an attraction between neighbouring 109·47° and 70·53° nickel boundaries and between adjacent 90° boundaries in iron (see Stoner 1950, § 3 (i); Kittel 1949, pp. 563–4).

The strain tensor and the energy term $\beta' f_m$. The magneto-elastic energy, F_m, of a cubic crystal is the sum of magnetostrictive and elastic parts and may be written (Becker and Döring 1939, p. 146)

$$\left.\begin{aligned} F_m=\{&-3C_2\lambda_{100}(\alpha_1^2A_{11}+\alpha_2^2A_{22}+\alpha_3^2A_{33})\\ &-3C_3\lambda_{111}2(\alpha_1\alpha_2A_{12}+\alpha_2\alpha_3A_{23}+\alpha_3\alpha_1A_{31})\}\\ &+\{\tfrac{1}{2}C_1(A_{11}+A_{22}+A_{33})^2+C_2(A_{11}^2+A_{22}^2+A_{33}^2)\\ &+2C_3(A_{12}^2+A_{23}^2+A_{31}^2)\}, \end{aligned}\right\} \quad . \quad (5.1)$$

where the A_{ik} are components of the strain tensor, and λ_{100}, λ_{111} are magnetostriction coefficients. Comparison of (5.1) with Bitter (1937, p. 172, equation (138)) shows that the constants C_1, C_2, C_3 are given in terms of the elastic coefficients c_{11}, c_{12}, c_{44} by

$$C_1=c_{12}\,; \qquad C_2=(c_{11}-c_{12})/2\,; \qquad C_3=c_{44}. \quad . \quad . \quad . \quad (5.2)$$

The stable configuration of the crystal may be determined by minimizing F_m with respect to the A_{ik}. It follows that

$$A_{ik}=(3/2)\lambda_{111}\alpha_i\alpha_k, \qquad A_{ii}=(3/2)\lambda_{100}\{\alpha_i^2-C_1/(3C_1+2C_2)\}, \quad . \quad (5.3)$$

$$i\neq k;$$

from which it is evident that the components, A_{ik}, of the strain tensor are the same for domains magnetized in opposite directions. It may be shown further (*cf.* Lifshitz 1944, pp. 338–9) that they remain constant throughout the 180° boundary, *i. e.* the deformation of the material of

the boundary is effectively the same as that in the adjacent domains. The A_{ik} are found by substitution in (5.3) of the direction cosines corresponding to the easy directions in the domains.

The excess magneto-elastic energy of the boundary, $\beta' f_m$, with respect to the domains can now be calculated by substitution in (5.1) of the appropriate values of $[\alpha_1\alpha_2\alpha_3]$, corresponding to the directions of $\mathbf{I}_0$ in the boundary and in the domains. (See Lifshitz 1944, p. 339; Kittel 1949, p. 564.)

Nickel. The directions of magnetization in adjacent domains are [111] and $[\bar{1}\bar{1}\bar{1}]$ (*cf.* §§ 3 and 4) and the strain tensor has components

$$A_{12}=A_{23}=A_{31}=\lambda_{111}/2\,; \qquad A_{11}=A_{22}=A_{33}=C_2\lambda_{100}/(3C_1+2C_2). \quad (5.4)$$

For a rotation of $\mathbf{I}_0$ through OP (see fig. 3.1) the values of α_1, α_2 and α_3 in the boundary are

$$\left.\begin{aligned}\alpha_1&=6^{-\frac{1}{2}}\{2^{\frac{1}{2}}\cos\phi-(3^{\frac{1}{2}}\sin\lambda+\cos\lambda)\sin\phi\},\\ \alpha_2&=6^{-\frac{1}{2}}\{2^{\frac{1}{2}}\cos\phi+2\cos\lambda\sin\phi\},\\ \alpha_3&=6^{-\frac{1}{2}}\{2^{\frac{1}{2}}\cos\phi+(3^{\frac{1}{2}}\sin\lambda-\cos\lambda)\sin\phi\},\end{aligned}\right\} \quad . \; . \; . \quad (5.5)$$

giving, for the excess magneto-elastic energy, an expression,

$$\beta' f_m=(9/2)C_3\lambda_{111}{}^2\sin^2\phi, \quad . \; . \; . \; . \; . \; . \quad (5.6)$$

which is independent of the angle λ. The reduced anisotropy energy may be written, from (2.3), (2.11), (2.13), (3.5), (3.7) and (5.6), in the form

$$f_a=\{(1+\tau)/12\}\{1+\rho'\sin\phi\cos\phi+\sigma\cos^2\phi\}\sin^2\phi, \quad . \; . \quad (5.7)$$

where

$$\tau=(54C_3\lambda_{111}{}^2)/|K_4|\,; \qquad \rho'=\rho/(1+\tau)\,; \qquad \sigma=7/(1+\tau). \quad . \quad (5.8)$$

Substitution in (2.8), with $\sin\theta$ equal to unity, and comparison with (3.6) gives

$$\left.\begin{aligned}\gamma/\gamma_0&=\{(1+\tau)/3\}^{\frac{1}{2}}\int_0^{\pi}(1+\rho'\sin\phi\cos\phi+\sigma\cos^2\phi)^{\frac{1}{2}}\sin\phi\,d\phi,\\ &=\{(1+\tau)/3\}^{\frac{1}{2}}\{(\sigma+1)^{\frac{1}{2}}+(\sigma\sec 2\kappa)^{\frac{1}{2}}(r_1^3t_1\sin^{-1}t_1\\ &\qquad\qquad +s_1^3p_1\sinh^{-1}p_1)\},\end{aligned}\right\} \quad . \; . \quad (5.9)$$

where

$$\left.\begin{aligned}2\sigma r_1^2&=(\sigma+2)\cos 2\kappa+\sigma\\ 2\sigma s_1^2&=(\sigma+2)\cos 2\kappa-\sigma\end{aligned}\right\}\,; \quad s_1^2=r_1^2-1\,; \quad \left.\begin{aligned}t_1&=(\sin\kappa)/r_1\\ p_1&=(\cos\kappa)/s_1,\end{aligned}\right\} \quad (5.10)$$

and $\tan 2\kappa=\rho'/\sigma=\rho/7$.

The elastic coefficients of single nickel crystals have been measured by Bozorth *et al.* (1949). Values of the magnetostriction coefficients are given by Becker and Döring (1939, pp. 277–80), and of the magneto-crystalline anisotropy coefficient, K_4, by Stoner (1950, § 2). The constants required are

$$\left.\begin{aligned} c_{11}&=2{\cdot}50\times10^{12}\text{ erg cm.}^{-3}, & \lambda_{100}&=-46\times10^{-6},\\ c_{12}&=1{\cdot}60\times10^{12}\text{ erg cm.}^{-3}, & \lambda_{111}&=-25\times10^{-6},\\ c_{44}&=1{\cdot}185\times10^{12}\text{ erg cm.}^{-3}, & K_4&=-0{\cdot}50\times10^{5}\text{ erg cm.}^{-3}, \end{aligned}\right\} \quad . \quad . \quad . \quad . \quad . \quad . \quad . \quad . \quad . \quad . \quad (5.11)$$

and the value of τ calculated from them is 0·80.

When

$$\rho=\pm2^{5/2},\quad \gamma/\gamma_0=3^{-1/2}[(8+\tau)^{1/2}+\{(9+\tau)/9\}\sin^{-1}(9+\tau)^{-1/2}+(2^{3/2}\tau/9)\sinh^{-1}(8/\tau)^{1/2}],$$

$$=2{\cdot}19\,; \quad . \quad . \quad . \quad . \quad . \quad . \quad . \quad . \quad . \quad . \quad . \quad . \quad . \quad . \quad . \quad (5.12)$$

$$\rho=0,\qquad \gamma/\gamma_0=\{(1+\tau)/3\}^{1/2}\{(\sigma+1)^{1/2}+\sigma^{-1/2}\sinh^{-1}(\sigma^{1/2})\},$$

$$=2{\cdot}27. \quad . \quad . \quad . \quad . \quad . \quad . \quad . \quad . \quad . \quad . \quad . \quad . \quad . \quad . \quad . \quad (5.13)$$

These energies are greater than those calculated in § 3 where the effect of magnetostriction is neglected.

The parameter ξ may now be expressed as a function of ϕ, using (5.7), by

$$\xi=-2\{3/(8+\tau)\}^{1/2}\sinh^{-1}[\{2(8+\tau)\cot\phi+\rho\}/\{4(8+\tau)(1+\tau)-\rho^2\}^{1/2}].$$

$$. \quad . \quad . \quad . \quad . \quad . \quad . \quad . \quad . \quad . \quad . \quad (5.14)$$

When

$$\left.\begin{aligned} \rho&=\pm2^{5/2}, & b/b_0&=7{\cdot}91\,;\\ \rho&=0, & b/b_0&=4{\cdot}45. \end{aligned}\right\} \quad . \quad . \quad . \quad . \quad (5.15)$$

The boundary width no longer approaches infinity as ρ approaches $\pm2^{5/2}$ and the introduction of a magneto-elastic energy term produces effectively an attraction between [110], 70·53° and [110], 109·47° boundaries.

Iron. The directions of $\mathbf{I}_0$ in adjacent domains are [001] and [00$\bar{1}$] (*cf.* §§ 3 and 4) and the strain tensor has components (*cf.* Lifshitz 1944, pp. 338–9; Kittel 1949, p. 564)

$$A_{12}=A_{23}=A_{31}=0\,;\ A_{11}=A_{22}=-3\lambda_{100}C_1/2(3C_1+2C_2)\,;$$

$$A_{33}=3\lambda_{100}(C_1+C_2)/(3C_1+2C_2). \quad . \quad . \quad . \quad . \quad . \quad (5.16)$$

For a rotation through OP (see fig. 3.2) the direction of $\mathbf{I}_0$ in the boundary is $[-\sin\lambda\sin\phi,\ \cos\lambda\sin\phi,\ \cos\phi]$ and, hence,

$$\beta' f_m=(9/2)C_2\lambda_{100}^2\sin^2\phi, \quad . \quad . \quad . \quad . \quad . \quad (5.17)$$

which is independent of the angle λ. The reduced anisotropy energy may be written in the form

$$f_a=(1+\tau')\,(\sin^2\phi-\mu'\sin^4\phi), \qquad (5.18)$$

where

$$\tau'=(9C_2\lambda_{100}{}^2)/2K_4\,;\ \mu'=\mu/(1+\tau'). \qquad (5.19)$$

It follows that

$$\gamma/\gamma_0=2(1+\tau')^{\frac{1}{2}}[1+(1-\mu')\mu'^{-\frac{1}{2}}\sinh^{-1}\{\mu'/(1-\mu')\}^{\frac{1}{2}}], \qquad (5.20)$$

and that

$$\left.\begin{aligned}\xi&=-(1+\tau')^{-\frac{1}{2}}\sinh^{-1}\{(1-\mu')^{-\frac{1}{2}}\cot\phi\}\ ;\\ b/b_0&=2(1+\tau')^{-\frac{1}{2}}[\sinh^{-1}\{(2\mu'-1)/(1-\mu')\}^{\frac{1}{2}}+2\mu'^{\frac{1}{2}}\sin^{-1}(2\mu')^{-\frac{1}{2}}].\end{aligned}\right\} \qquad (5.21)$$

The constants c_{11}, c_{12}, c_{44} are given by Kittel (1949, p. 556), λ_{100}, λ_{111} by Becker and Döring (1939, p. 280), and K_4 by Stoner (1950, § 2) as follows :

$$\left.\begin{aligned}c_{11}&=2{\cdot}41\times10^{12}\text{erg cm}^{-3}, &\lambda_{100}&=19{\cdot}5\times10^{-6},\\ c_{12}&=1{\cdot}46\times10^{12}\text{erg cm}^{-3}, &\lambda_{111}&=-18{\cdot}8\times10^{-6},\\ c_{44}&=1{\cdot}12\times10^{12}\text{erg cm}^{-3}, &K_4&=4{\cdot}7\times10^{5}\text{ erg cm}^{-3}.\end{aligned}\right\} \qquad (5.22)$$

The value of C_2 obtained from these is $0{\cdot}48\times10^{12}$ erg cm^{-3} giving a value of

$$\tau'=0{\cdot}0017.$$

When

$$\left.\begin{aligned}\lambda&=0,\\ \mu&=1,\end{aligned}\right\}\ \gamma/\gamma_0=2\{(1+\tau')^{\frac{1}{2}}+\tau'\sinh^{-1}(\tau'^{-\frac{1}{2}})\}$$

$$=2{\cdot}02, \qquad (5.23)$$

$$b/b_0=2(1+\tau')^{-\frac{1}{2}}[\sinh^{-1}\{(1-\tau')/\tau'\}^{\frac{1}{2}}+2(1+\tau')^{-\frac{1}{2}}\sin^{-1}\{(1+\tau')/2\}^{\frac{1}{2}}]$$

$$=10{\cdot}87\ ; \qquad (5.24)$$

$$\left.\begin{aligned}\lambda&=45^\circ,\\ \mu&=3/4,\end{aligned}\right\}\ \gamma/\gamma_0=2[(1+\tau')^{\frac{1}{2}}+\{(1+4\tau')/3^{\frac{1}{2}}2\}\sinh^{-1}\{3/(1+4\tau')\}^{\frac{1}{2}}]$$

$$=2{\cdot}77, \qquad (5.25)$$

$$b/b_0=2(1+\tau')^{-\frac{1}{2}}[\sinh^{-1}\{(2-4\tau')/(1+4\tau')\}^{\frac{1}{2}}+\{3^{\frac{1}{2}}/(1+\tau')\}\sin^{-1}\{2(1+\tau')/3\}]$$

$$=5{\cdot}59. \qquad (5.26)$$

Thus the inclusion of a term representing the magneto-elastic energy of the crystal has little effect on the value of the domain boundary energy (*e.g.* 2·02 as compared with 2·00 for a [001], 180° boundary ; for other values see Table 6.1), but results, as in the case of nickel, in an important modification of the results obtained, in § 4, for the boundary widths.

In this section the numerical values of τ and τ' are given to two significant figures ; those of γ/γ_0 and b/b_0 are given to three figures. The accuracy of these values is, however, determined by the accuracy with which the constants concerned (given in (5.11), (5.22)) have been measured.

Cobalt. The effect of magnetostriction in cobalt is not important since only 180° boundaries are possible and none of these has an infinite width even if magneto-elastic energy is neglected. Moreover, the introduction of this further term would have very little effect on the boundary energy since the magnetostriction coefficients of cobalt are smaller than those for iron, and the magneto-crystalline anisotropy coefficient, β, is much greater (by a factor of about 10) than that for iron.

§ 6. Collected Results and Conclusion.

In conclusion, it is appropriate to tabulate the results obtained. This is done in Tables 6.1 and 6.2, in which " with m.-s." is to be understood to mean " with magnetostriction taken into account ". In cobalt the hexagonal axis lies in the domain boundaries.

Table 6.1.

Reduced energies, γ/γ_0, of domain boundaries in ferromagnetics.
γ, boundary energy per unit area.
For estimated values of γ_0 see text.

Type of boundary		Direction of normal to boundary			
		[001]	[110]	[111]	[$\bar{1}\bar{1}$2]
Ni	70·53°	0·5443	0·4611	—	—
	109·47°	1·0887	1·3680	1·2903	
	180°	—	1·8292	—	2·0040
	180° (with m.-s.)	—	2·19	—	2·27
Fe	90°	1·0000	1·7274	1·1852	
	180°	2·0000	2·7603	—	
	180° (with m.-s.)	2·02	2·77	—	
Co	180°		4·0000		

For 180° boundaries in both nickel and iron the angle λ is that between the projections of $\mathbf{I}_0$ and an easy direction on a plane whose normal is the initial direction of $\mathbf{I}_0$ (see § 3). In Table 6.2 the values of b/b_0 for $\lambda=1°$ are included in brackets below the infinite values for $\lambda=0°$.

TABLE 6.2.

Reduced widths, b/b_0, of domain boundaries in ferromagnetics. b, effective boundary width.
For estimated values of b_0 see text.

Type of boundary		Direction of normal to boundary			
		[001]	[110]	[111]	[$\bar{1}\bar{1}$2]
Ni	70·53°	3·8476	4·2642	—	
	109·47°	∞	3·3093	3·8476	
	180°	—	∞ (15·4029)	—	7·9161
	180° (with m.-s.)	—	7·91	—	4·45
Fe	90°	3·1416	3·9738	3·1416	
	180°	∞ (12·6258)	5·6018		
	180° (with m.-s.)	10·87	5·59		
Co	180°		3·1416		

The effect of introducing a magneto-elastic energy term is most important in nickel, less important in iron, and of least importance in cobalt. Values of γ_0 and b_0 are given by Stoner (1950, table 3.2), who also discusses the uncertainty of these estimates due to uncertainties in the detailed treatment of exchange interaction effects. For nickel, iron and cobalt γ_0, measured in erg cm^{-2}, is 0·14, 0·62 and 2·05; b_0, measured in 10^{-8} cm, is 260, 130 and 50. (Néel (1944) obtains for iron values of 0·7 and 165 for γ_0 and b_0 respectively; Kittel (1949), using the method employed by Lifshitz (1944), in which the exchange energy is calculated from the coefficient of $T^{3/2}$ in Bloch's law of approach to saturation at low temperatures, obtains corresponding values of 0·9 and 230.) Thus the energies, γ erg cm^{-2}, of 180° boundaries in nickel, iron and cobalt (taking $\lambda=0°$ for nickel and iron, and without neglecting magnetostriction) are 0·31, 1·25 and 8·20; the widths, b, in 10^{-8} cm are 2060, 1410 and 160 respectively. These comparisons have a bearing on the character and relative ease of production of powder patterns and on the sizes of domains in the three ferromagnetics (see Stoner 1950). For nickel, iron and cobalt, the boundary widths, at room temperature, are, in general, small compared with the linear dimensions of the domains. If the boundary widths are of the same order of magnitude as the domain size the ferromagnetic can no longer be regarded as being magnetized along some easy direction over most of its volume. This effect may be important in many alloys, and also in the ferromagnetic elements themselves at higher temperatures.

I am indebted to Professor E. C. Stoner, F.R.S., for suggesting the problem and for his guidance and constant encouragement; to Dr. P. Rhodes for helpful discussions and constructive criticism; and to the Department of Scientific and Industrial Research for a grant.

References.

Becker, R., and Döring, W., 1939, *Ferromagnetismus*. (Berlin : Springer). (Photo-lithoprint Reproduction, 1943, Ann Arbor, Michigan : Edwards Brothers).

Bitter, F., 1937, *Introduction to Ferromagnetism*. (New York : McGraw-Hill).

Bloch, F., 1932, *Z. Phys.*, **74**, 295.

Bozorth, R. M., Mason, W. P., McSkimin, H. J., and Walker, J. G., 1949, *Phys. Rev.*, **75**, 1954.

Comrie, L. J., 1949, *Chambers's Six-Figure Mathematical Tables, Vol. 2, Natural Values*. (London and Edinburgh : Chambers).

Kittel, C., 1949, *Rev. Mod. Phys.*, **21**, 541.

Landau, L., and Lifshitz, E., 1935, *Phys. Z. Sowjet.*, **8**, 153.

Lifshitz, E., 1944, *J. Phys. U.S.S.R.*, **8**, 337.

Néel, L., 1944, *Cahiers de Phys.*, **25**, 1.

Stoner, E. C., 1948, *Phys. Soc. Rep. Progr. Phys.*, **11**, 43 ; 1950, *Ibid.*, **13**, 83.

LXXII. *The Statistical Analysis of Electrical Noise.*

By D. K. C. MacDonald,
Clarendon Laboratory, Oxford *.

[Received May 19, 1950.]

Abstract.

Fundamental criticism is made of two recent papers by Meltzer on electrical noise on general and particular grounds. Correction of the errors in the analysis also provides an opportunity for a discussion of the fundamental relation between a stochastic equation and the corresponding frequency spectrum of a fluctuating variable. An example taken from the field of classical Brownian movement clarifies the concept of the observable velocity of a particle.

Two recent papers by Meltzer (1949, 1950) in this Journal on electrical current fluctuations (noise) present much cause for criticism. The first, (A), implies that a proof has been given of a fundamental physical identity between thermal and shot noise. But in brief the paper simply reiterates the well-known fact that any purely random phenomenon, which may be idealized as a Markoff process, obeys a certain rather simple statistical law. Membership of the same statistical class, however, is remote from an essential physical identity of two phenomena, and the suggestion that a serious proof of this has been given is at least rather misleading. The second paper, (B), however, takes up the problem of current noise in metallic resistors and uses analysis which is invalid in fundamental, but elementary, respects; the ensuing results and comparison with the experimental work of Bernamont are consequently fallacious.

We first consider the specific errors of the second paper and then take the opportunity of a more general discussion (relevant to both papers) of the statistics and frequency spectrum of fluctuations. An example taken from the field of classical Brownian movement clarifies the concept of the observable velocity of a particle.

It is simplest in considering (B) to present afresh in correct form Meltzer's analysis, adhering as far as possible to his notation. Consider some cross-section of a conductor and let us observe the charge crossing this during a set of time intervals of (arbitrary) length, τ †. Let n be the total number of charges e_i, of magnitude e, crossing in any particular member of the set. This number will of course not be constant, because

* Communicated by the Author.

† We prefer to use τ in place of Meltzer's t.

of the very presence of fluctuations, but will vary from interval. Let n_1 be the number crossing in the "positive" direction and n_2 in the "negative" direction, and let the respective probabilities be p and q. Thus denoting the *mean* values of the three statistical variables n, n_1 and n_2 by N, N_1 and N_2 we have:

$$N_1=pN\ ;\ N_2=qN$$

and the mean current, I, is given by:

$$I=(p-q)\frac{eN}{\tau}. \quad . \quad . \quad . \quad . \quad . \quad . \quad . \quad . \quad . \quad (1)$$

Then, following Meltzer, we set:

$$Q=\sum_{i=1}^{n} e_i=(n_1-n_2)e \quad . \quad . \quad . \quad . \quad . \quad . \quad . \quad . \quad . \quad . \quad . \quad (2)$$

$$\therefore\ \overline{Q}=(\bar{n}_1-\bar{n}_2)e=Ne(p-q)=I\tau$$

and

$$Q^2=\sum_i e_i^2+\sum_{i\neq j} e_i e_j \quad . \quad . \quad . \quad . \quad . \quad . \quad . \quad . \quad . \quad . \quad (3)$$

$$\therefore\ \overline{Q^2}=\bar{n}_1e^2+\bar{n}_2e^2+\overline{n_1(n_1-1)}e^2+\overline{n_2(n_2-1)}e^2-2\overline{n_1n_2}e^2 \quad . \quad . \quad (4)$$

$$=(N_1+N_2)e^2+(\overline{n_1^2}-N_1)e^2+(\overline{n_2^2}-N_2)e^2-2\overline{n_1n_2}e^2.$$

Now let

$$n_1=N_1+\delta_1\ ;\ n_2=N_2+\delta_2$$

$$\therefore\ \overline{n_1^2}=N_1^2+\overline{\delta_1^2}\ ;\ \overline{n_2^2}=N_2^2+\overline{\delta_2^2}\ ;\ \overline{n_1n_2}=N_1N_2+\overline{\delta_1\delta_2}$$

and

$$\overline{Q^2}=Ne^2+(N_1-N_2)^2e^2+(\overline{\delta_1^2}+\overline{\delta_2^2}-2\overline{\delta_1\delta_2}-(N_1+N_2))e^2 \quad . \quad (5\,a)$$

$$=Ne^2+N^2(p-q)^2e^2+(\overline{\Delta^2}-N)e^2, \quad . \quad . \quad . \quad . \quad . \quad . \quad . \quad (5\,b)$$

if we set $\Delta\equiv\delta_1-\delta_2$.

This should be compared with Meltzer (B), equation (5). Meltzer has throughout made no distinction between average and mean square values, etc., of the relevant statistical variables, which appears a rather serious error in a paper intended to deal with fluctuations.

The achievement of further real progress depends now very naturally on the assumption of some *physical* model for the system considered. The only assumption of a general nature that we can essay *here* is that of an overall equilibrium distribution:

$$\overline{\Delta^2}=N \quad . \quad . \quad . \quad . \quad . \quad . \quad . \quad . \quad . \quad (6\,a)$$

or more specifically to assume:

$$\overline{\delta_1^2}=N_1\ ;\ \overline{\delta_2^2}=N_2\ ;\ \overline{\delta_1\delta_2}=0 \quad . \quad . \quad . \quad . \quad . \quad . \quad . \quad (6\,b)$$

both yielding:

$$\overline{Q^2}=Ne^2+N^2(p-q)^2e^2 \quad . \quad . \quad . \quad . \quad . \quad . \quad . \quad . \quad . \quad (7)$$

and using (1):

$$\overline{Q^2}=Ne^2+I^2\tau^2. \qquad (8)$$

Using finally Einstein's classic result (Einstein (1906)) that for a resistor, R, in thermal equilibrium at temperature T, the effective fluctuation in charge ($\overline{\Sigma e_i^2}$ after equation (3)) is given by $(2kT/R)\tau$, we may write:

$$\overline{Q^2}=\left(\frac{2kT}{R}\right)\tau+I^2\tau^2. \qquad (9)$$

This is of course just Meltzer's starting point, (B) equation (1), from which no amount of algebra by itself can possibly derive any essentially new expression for the fluctuation involved. By the very fact of writing down this equation, Meltzer has implicitly assumed a complete knowledge of the statistics of the fluctuation in the presence of the term in τ, representative of a purely random component, and the term in τ^2, representative of a pure "d.c." contribution. The simple addition of the two terms embodies immediately the assumption that these are entirely independent—or physically, to sum up, that the passage of a direct current I *has had no effect whatsoever on the fluctuations to be observed.*

In particular, then, all equations subsequent to (5) in Meltzer (B) are spurious and consequently the suggested comparison with the experiments of Bernamont (1937) is invalid.

Let us remark that it may prove possible to set up a phenomenological theory of current noise in thin metallic films and semiconductors proceeding from (our) equations (5) by making appropriate assumptions about the last term (in either form) in any particular physical model. In any case, however, great care will be necessary in formulating and interpreting an analysis of this type since the current observed at the terminals of a resistance, say, is composed of the contributions of *all* electrons in the body and a fluctuating current may well be induced by motion of remote charge without electrons actually crossing locally a specific cross-section of the body. It is in this sense that a rigid interpretation of N may be entirely misleading and, in particular, Meltzer's "equivalent shot-effect current" defined by $I_0=kT/Re$ in (A) has no very direct physical significance.

A general feature which perhaps is not sufficiently widely appreciated is the complete, immediate equivalence of a statistical equation such as (9) above to the statement of the current fluctuations in terms of a frequency spectrum. If we are provided with the auto-correlation function $\overline{y(t).y(t+\tau)}^t$ of a stationary statistical variable, $y(t)$, then it should now be well known that the theorem of Wiener and Khintchine provides an immediate transformation to the corresponding (power) frequency spectrum. In addition, however, as we have shown (MacDonald (1949)) a knowledge of the average mean-square deviation of a variable over any arbitrary time-interval τ also leads directly to the frequency spectrum:

this concept is sometimes more natural than the auto-correlation function which deals with the *instantaneous* values of the variable concerned. Thus equation (9) is in fact precisely equivalent to writing :

$$\overline{\mathrm{I}_f^2} = \frac{4}{\mathrm{R}} k\mathrm{T}\Delta f + \mathrm{I}^2 \,.\, \delta(f) \quad . \quad . \quad . \quad . \quad . \quad . \quad (10)$$

(where $\delta(f)$ is a Dirac function " at " zero frequency, representative of the *direct current*, I, such that $\int_0^\infty \delta(f)df = 1$).

An interesting application of these ideas arises in the original extended equations of Brownian movement due to Langevin (1908) and others (*e.g.* Fürth (1920)).

If x be the displacement of a free Brownian particle, of mass m, in a medium of viscous resistance λ at temperature θ, then in time τ :

$$\overline{\delta x^2} = \frac{2k\theta}{\lambda}\{\tau - \mathrm{T}(1-\epsilon^{-\tau/\mathrm{T}})\}, \quad \text{where} \quad \mathrm{T} = m/\lambda, \quad . \quad . \quad . \quad (11)$$

thus the mean square deviation of the velocity averaged over the interval τ is

$$\overline{\delta v_\tau^2} \equiv \frac{\overline{\delta x^2}}{\tau^2} = \frac{2k\theta}{\lambda}\left\{\frac{1}{\tau} - \frac{\mathrm{T}}{\tau^2}(1-\epsilon^{-\tau/\mathrm{T}})\right\}. \quad . \quad . \quad . \quad . \quad (12)$$

We can then immediately, as pointed out above, derive the frequency spectrum of the true " instantaneous " velocity :

$$\overline{\delta v_f^2} = \frac{4k\theta}{\lambda}\left\{\frac{df}{1+(2\pi f\mathrm{T})^2}\right\}. \quad . \quad . \quad . \quad . \quad . \quad . \quad (13)$$

By integration over all f from 0 to ∞, we have

$$\overline{\delta v^2} = \frac{4k\theta}{2\pi\lambda\mathrm{T}} \cdot \frac{\pi}{2} = \frac{k\theta}{m} \quad . \quad . \quad . \quad . \quad . \quad . \quad . \quad (14)$$

in agreement with the classical equipartition formula of Einstein, while (13), on the other hand, shows immediately that, unless our measuring instruments respond to, or resolve, events of natural frequency considerably greater than $1/\mathrm{T}$, we shall not in fact observe the " true " Brownian movement velocity as given by (14) (*cf.* Ramsay (1892), Exner (1900), Svedberg (1906)). If, however, the limiting resolution time of our instrument is, say, T_1 then (13) enables us to *determine* the value of $\overline{\delta v_{\mathrm{obs}}^2}$ which should in fact be observed. Thus :

$$\overline{\delta v_{\mathrm{obs}}^2} = \frac{4k\theta}{\lambda}\int_0^{1/\mathrm{T}_1} \frac{df}{(1+(2\pi f\mathrm{T})^2)}$$

$$= \frac{2k\theta}{\pi m}\left(\arctan\frac{2\pi\mathrm{T}}{\mathrm{T}_1}\right), \quad . \quad . \quad . \quad . \quad . \quad . \quad . \quad (15\,a)$$

or, if $\mathrm{T} \ll \mathrm{T}_1$,

$$\overline{\delta v_{\mathrm{obs}}^2} \approx \frac{4k\theta}{m}\left(\frac{\mathrm{T}}{\mathrm{T}_1}\right). \quad . \quad . \quad . \quad . \quad . \quad . \quad . \quad . \quad (15\,b)$$

In examining the early literature to find measurements for comparison with equations (15), I was unable to find entirely satisfactory data, generally because no very precise record of T_1 was kept. However, those of F. M. Exner (*loc. cit.*) enable a good comparison to be made. Since $T=m/\lambda$ and $\lambda=6\pi\eta a$, for a small spherical particle, of radius a, observed in a medium of viscosity η, we have:

$$\overline{\delta v^2_{\text{obs}}} \approx \frac{4k\theta}{6\pi\eta a T_1} \quad . \quad . \quad . \quad . \quad . \quad . \quad . \quad . \quad . \quad (16)$$

It appears that Exner followed visually the track of the particle continuously, in so far as he was able. It therefore appears reasonable to take $T_1 \sim 0{\cdot}1$ second, with an upper limit certainly of 1 second.

Now,

$$a = 3{\cdot}5 \times 10^{-5} \text{ cm.}$$
$$\eta \approx 10^{-2} \text{ poises.}$$
$$\theta = 293^\circ \text{ K. } (20^\circ \text{ C.}).$$

Whence $\sqrt{(\overline{\delta v^2_{\text{obs}}})} \approx 5 \times 10^{-4}$ cm./sec. (with a lower limit of $1{\cdot}6 \times 10^{-4}$ cm./sec.). The velocity observed by Exner at this temperature was in fact $3{\cdot}2 \times 10^{-4}$ cm./sec., and the agreement is thus very satisfactory.

This analysis appears also of interest because it has been stated in the past that the velocity of a Brownian particle as observed visually has only a subjective significance.

I should like to thank Professor M. H. L. Pryce and Mr. D. F. Gibbs for helpful discussion.

References.

Bernamont, J., 1937, *Ann. de. Phys.*, **7**, 71.
Einstein, A., 1906, *Ann. Phys., Lpz.*, **19**, 371.
Exner, F. M., 1900, *Ann. Phys., Lpz.*, **2**, 843.
Fürth, R., 1920, *Zs. f. Phys.*, **2**, 244.
Langevin, P., 1908, *Comptes Rendues*, **146**, 530.
MacDonald, D. K. C., 1949, *Phil. Mag.*, **40**, 561.
Meltzer, B., 1949, *Phil. Mag.*, **40**, 1224; 1950, *Ibid.*, **41**, 393.
Ramsay, W., 1892, *Chem. News*, **65**, 90.
Svedberg, Th., 1906, *Zs. f. Elektrochem.*, **12**, 853, 909.

LXXIII. *The Origin of Single Cosmic Ray Protons.*

By S. Lattimore,
Imperial College of Science and Technology, London *.

[Received June 2, 1950.]

Abstract.

The frequency of production, and the angular and energy distributions of single cosmic ray protons produced in photographic emulsions exposed at 3650 m. are given. It is shown that, after corrections for protons emitted from stars have been made, the results agree with those given in a previous paper (Lattimore 1949).

The rates of production of fast protons in paraffin wax, carbon, aluminium, and lead are deduced from measurements of the number of protons observed to cross 100μ C.2 emulsions surrounded completely by these materials. From the results for paraffin wax and carbon, the rate of production in hydrogen is also deduced.

Introduction.

In a previous paper (Lattimore 1949) it has been shown that the number of proton tracks observed crossing 100μ C.2 emulsion is several times greater than the number to be expected if these tracks were due solely to protons from cosmic ray stars in the surrounding material. From the number of such tracks, and the number of protons observed to end in the emulsion, it was deduced that 62 protons were produced c.c./day in emulsion at 3650 m., and that their energy of production was 30 MeV. or more. In the calculation of the number of protons crossing the emulsion, star protons of energies greater than 30 MeV. were ignored. The number of such star protons was therefore included in the value of 63/c./c./day.

It must be emphasized that at the time of these previous experiments, emulsions sensitive to tracks of minimum or near minimum ionization were not available. The C.2 emulsion was not of sufficient sensitivity for protons with energies of 30 MeV. or greater to give recognizable tracks. Now, however, emulsions sensitive to minimum ionization tracks are available, and it is possible to study the actual beginnings of the single proton tracks. The present paper is concerned with the origin of these single protons and their angular and energy distributions. The relative numbers of protons produced in various materials is also given.

* Communicated by Sir George Thomson, F.R.S.

Part A.

1. *Frequency of Production.*

Ilford G.5. 200μ emulsion on glass were used. The emulsion was searched twice, using a $\times 95$ oil immersion objective. A total of 89 fast protons, other than those produced by stars, were observed to start within the emulsion. Of these, 74 occurred singly. Five cases were observed where two fast protons were produced together. Of these, two occur near the surface, and may be coincidences. One case was observed of what may be a proton of energy greater than 100 MeV. either producing a proton of 60 MeV. and vanishing itself, or losing considerable energy in passing through a nucleus, without producing visible tracks. Two cases were found where a fast proton apparently produces a second proton, and escapes itself. The value of 25 ± 2/c.c./day is obtained for the rate of production in emulsion of these fast protons at 3650 m. In addition to these protons, we now observe many fast protons emitted from stars. These were not observed in the C.2 emulsions, in general, because of the low sensitivity. In Table I. is shown the number of protons of energy greater than 30 MeV. associated with stars.

Table I.

Star Size	Mean No. of Protons of Energy greater than 30 MeV. per star	No. of Protons of Energy greater than 30 MeV. produced/c.c./day
2, 3, or 4 prongs	1·1	20·5
4 prongs	1·26	7·5

This gives a total of 28 protons of energy greater than 30 MeV. produced/c.c./day in emulsion at 3650 m. from stars.

Considering, therefore, both the protons produced singly, or in processes other than normal star production, and those protons of energy greater than 30 MeV. produced in stars, we find a total rate of production of 53/c.c./day in emulsion at 3650 m. These are protons actually observed to start in the emulsion.

2. *Angular and Energy Distribution.*

The angles between the projection of the proton tracks on the surface of the emulsion and the vertical were measured by means of a protractor attached to one of the eyepieces of the microscope. The angles of dip were also measured, by means of a graduated fine focusing adjustment. This was calibrated by measuring the thickness of the emulsion, which was assumed to be 200 microns. The lengths of the projections of the tracks on the surface of the emulsion were measured, and the number of grains along the tracks. From these four measurements we could calculate the true angle between the proton and the vertical, and also true grain density. Not all of the tracks found were suitable for measurement, either because of shear in the emulsion, or because they dipped too steeply for us to perform a reliable grain count.

A grain density-energy curve for protons was constructed by measuring grain densities along ρ mesons which stopped in the emulsion, and using

Energy in MeV.

the relation $dN/dR = e^2 f(\beta)$, where dN/dR is the grain density, "e" the charge of the particle, and $f(\beta)$ some function of the velocity of the particle.

Fig. 1 *a*.

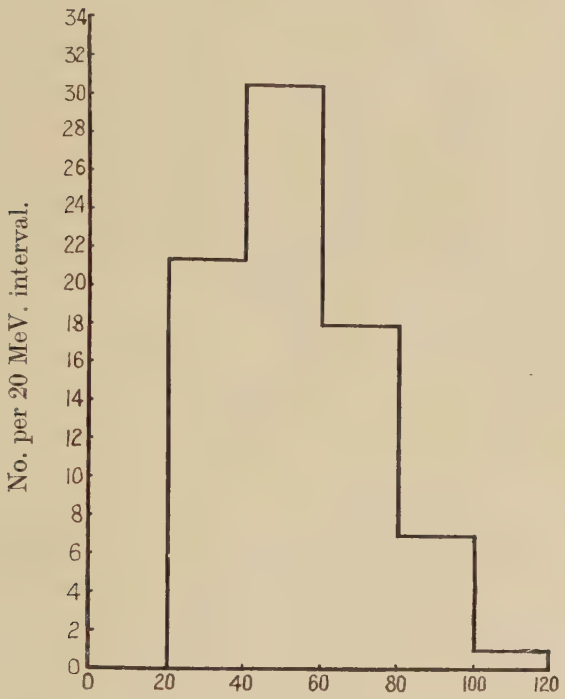

Fig 1 *b*.

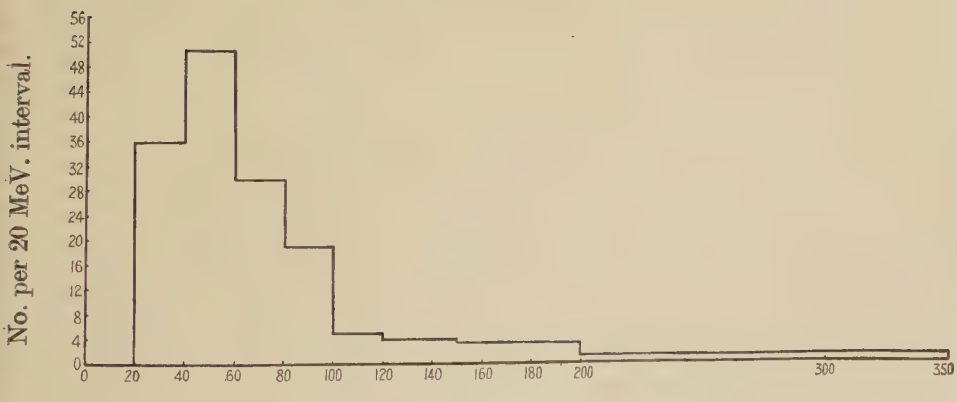

Energy in MeV.

The energy distribution of those protons produced other than in stars is shown in fig. 1*a*. It has a maximum between 40 and 60 MeV., and falls to zero at 120 MeV. The energy distribution for both protons from stars and protons produced singly is shown in fig. 1*b*.

The distribution shown in fig. 1*a* falls to zero at an energy of 20 MeV. Single protons are produced with energies below 20 MeV. (see previous paper), but most of these have very low energies (5 MeV.) and it is probable that these are true single prong stars. The cut-off at 20 MeV. is therefore somewhat arbitrary.

Fig 2*a*.

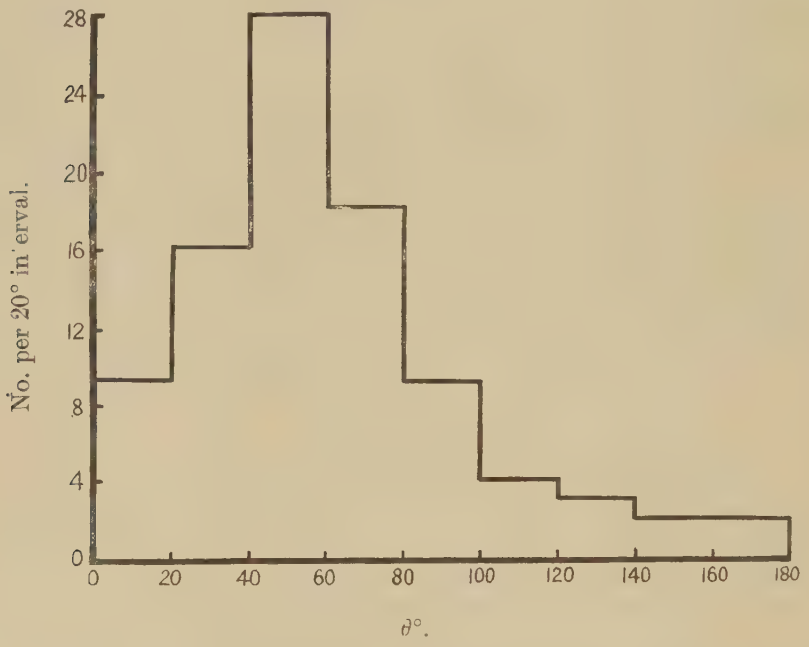

In fig. 2*a* is shown the angular distribution of the single protons, of energy greater than 20 MeV., at production, and in fig. 2*b*, the angular distribution of all fast protons produced, *i. e.* both those produced in stars and those in other processes. In these figures θ is the angle between the track and the vertical.

3. *Comparison with Previous Results.*

In a previous paper (Lattimore 1949) it was deduced that 62 fast protons were produced c.c.$^{-1}$ day in emulsion at 3650 m. This value was deduced from the number of proton tracks observed to cross the emulsion, and from an estimate of the sensitivity of the emulsion used. It is clearly difficult to assess this latter quantity with any accuracy, and it is probable that the sensitivity was underestimated in these earlier experiments.

In fig. 3 is shown the angular distribution of all fast protons produced. $N(\theta)$ represents the number of protons emitted unit solid angle at an angle of θ° or $(180-\theta)^\circ$ to the vertical. The full line is the distribution obtained in the previous paper (fig 4*b*). The agreement is reasonably good, although the statistics are poor.

Fig. 2*b*.

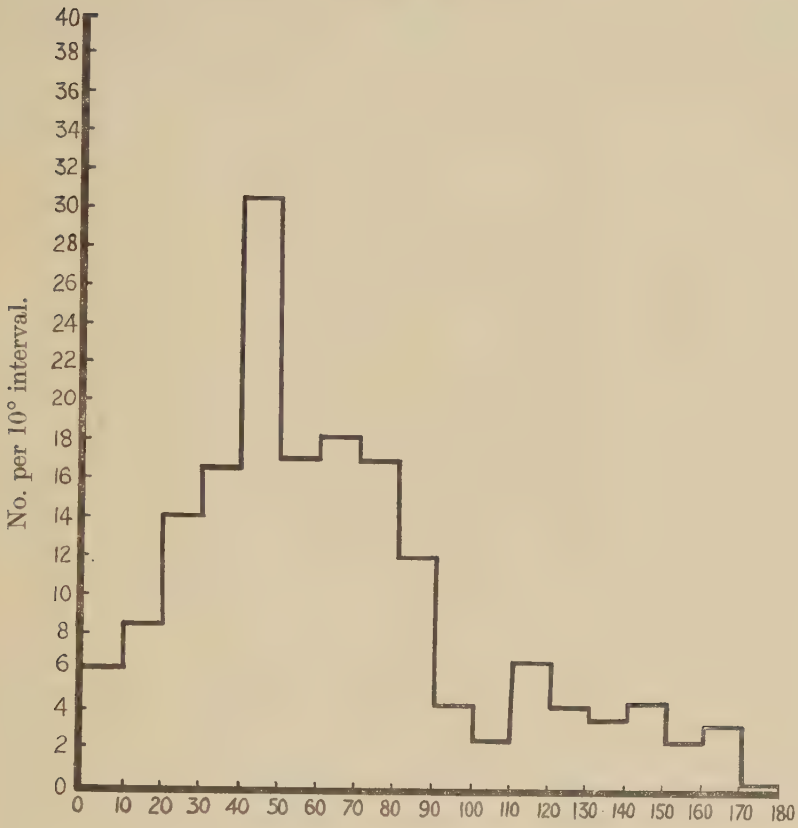

PART B.

Variation of Frequency of Production with Material.

For this part of the experiment, it was necessary to revert to the original method of counting, single protons which crossed the emulsion, and which were therefore produced in the surrounding material. 100μ C.2 emulsions on film were used and these were surrounded on all sides by the various materials and exposed horizontally, emulsion uppermost, at 3650 m. C.2 emulsions were used in preference to G.5 because the latter records all ionizing particles, including fast mesons and electrons. It was found that the number of protons crossing the emulsion was independent of the surrounding material, in agreement with results of Perkins (1947) and Morand and Cuër (1949).

In Table II. are shown the number of protons observed to cross the emulsion with the different surrounding materials. Also shown are the calculated rate of production in the various materials. For the calculation of the rate of production, it is necessary to know the sensitivity of the

emulsion, by which we mean the energy of the fastest proton that can be observed to cross the emulsion (see previous paper). This was taken as 35 MeV., a value which brings the rate of production given in our previous paper (Lattimore 1949) into agreement with the rates found in emulsion in the present experiment. We can then find the rates of

Fig. 3.

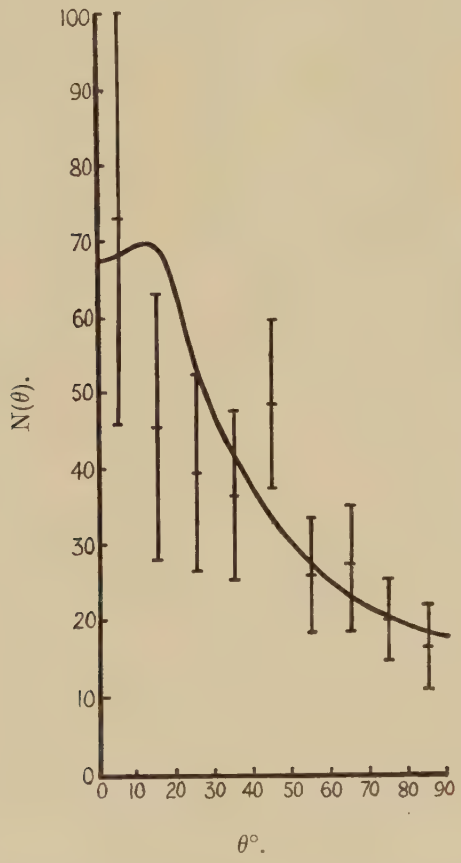

production in the various materials by using the formula given in the previous paper. The ranges were calculated from the equation

$$dE/dx = 4{\cdot}15\rho(Z/A)\mu_e/\beta^2\left[\log\frac{\beta^2}{(1-\beta^2)I}-\beta^2\right]$$

(Bethe 1937), where ρ, Z, and A are respectively the density, atomic number and atomic weight of the stopping material, μ_e the mass of the electron, β the velocity of a proton of energy E, and x the range of the proton in gms./cm.^{2}. I is the ionization potential of the stopping material (see Table II.). This equation was integrated graphically. Since the

calculated absolute values for the rate of production depend upon the value taken for the sensitivity of the emulsion used, they are perhaps open to doubt, but the relative values should be approximately correct.

Table II.

Material	No. crossing emulsion Arbitrary units	I(eV)	No. produced/gm/day
Pb.	38·7±2	1150	6·5±0·5
Al.	37·4±2	175	9·65±0·7
C.	40·4±2	81	15·1±1·1
CH.	42·7±2		18·6±1·4
H.		13·5	39·6±12

Discussion of Errors. The principal error involved, other than purely statistical errors, is introduced by taking the emulsion thickness as 200 μ. The thickness was unfortunately not measured before development. Measurements on two further batches give errors of 6 per cent and 8 per cent in the thickness. Any error will affect the angular distributions only slightly by altering the angle of dip, but affects the number of single tracks produced/c.c./day directly.

Conclusions.

This work has confirmed our earlier conclusions given in the previous paper, that protons are produced singly, and that they are mainly directed downwards.

It would seem reasonable to suppose that these protons are produced by the same primaries as produce stars, since the number both of stars and single tracks vary in the same way under ice (Harding *et al.* 1949) and under air (Lattimore unpublished). It follows that any theory of single proton production must take account of star production also. Attempts are being made to produce such a theory, and any results will be published later.

References.

Harding, 1949, *Phil. Mag.*, **40**, 530.
Lattimore, 1949, *Phil. Mag.*, **40**, 394.
Livingstone and Bethe, 1937, *Rev. Mod. Phys.*, **9**, 245.
Morand and Cüer, 1949, *Cosmic Radiation* (London: Butterworths).
Perkins, 1947, *Nature, Lond.*, **160**, 707.

LXXIV. *The Control of a Wilson Cloud Chamber by means of an Internal Counter.*

By A. L. Hodson, A. Loria* and N. V. Ryder†.
The Physical Laboratories, The University, Manchester ‡.

[Received June 8, 1950.]

[Plates XXV.–XXVIII.]

Abstract.

A technique is described for controlling a Wilson cloud chamber by an internal counter whose cathode consists of a hexagonal array of rods and whose sensitive volume is not separated from the main cloud chamber volume by any wall and in fact forms part of the usable chamber volume. The counter has no stopping power beyond that of the gas unless the incident particle chances to hit one of the rods. Events in which heavily ionizing particles are produced in the cloud chamber and events in which low energy particles traverse the chamber can thus be photographed. Discrimination between single fast particles or events of high ionization can be made at will. Altogether 26 slow particles (excluding electrons) have been photographed—corresponding to a vertical intensity of $9{\cdot}3\times10^{-5}$ slow particles cm.$^{-2}$ min.$^{-1}$ sterad.$^{-1}$ at sea level. Details of a proposed arrangement for photographing nuclear stars in the gas of the chamber are given. The technique is applicable to the study of the discharge phenomena of counters and some preliminary photographs of these phenomena are presented. The counter is quite stable and the technique of operation is not unduly difficult.

§ 1. Introduction.

In many cloud chamber experiments it would be an advantage if the chamber could be triggered on the occurrence of a heavily ionizing event. A proportional counter operated within the chamber offers a means of detecting such events, but for the observations of processes involving or caused by very low energy particles the absorption in the wall of the counter is an important factor. The possibility of employing a counter in which this absorption was reduced to a minimum by means of a cathode assembly consisting of rods was investigated by Hodson and Page in 1948 with a view to detecting and photographing nuclear stars occurring in the gas of a cloud chamber||. The idea of using a cathode of this form

* Now at the Università di Padova, Italy.
† On leave from Victoria University College, New Zealand.
‡ Communicated by Professor P. Ms. Blackett, F.R.S.
|| After this initial work, attention was drawn to a proposal of Cohen to use a cloud chamber as an ionization chamber for this purpose (Cohen 1948). The success of this method has since been reported (Cohen 1949a, b).

was obtained from the work of McCusker (1942) who had used such an arrangement for Geiger-Müller counters in glass envelopes. After experimenting with various rod assemblies McCusker showed that a hexagonal arrangement of rods was the most satisfactory. Hodson and Loria (1949) succeeded in controlling a Wilson cloud chamber by an internal counter having a cathode of this type but whose sensitive volume was not separated from the main chamber volume by any envelope and in fact formed part of the usable chamber volume.

This paper gives details and progress of this technique, together with some preliminary results obtained.

§2. Experimental Details.

(a) *Constructional details of the counter* :

The counter at present employed is 25 cm. in length and 4 cm. in diameter and is illustrated in Pl. XXV. .The cathode rods are of steel, 2 mm. in diameter, supported at each end by a brass framework, the whole

Fig. 1.

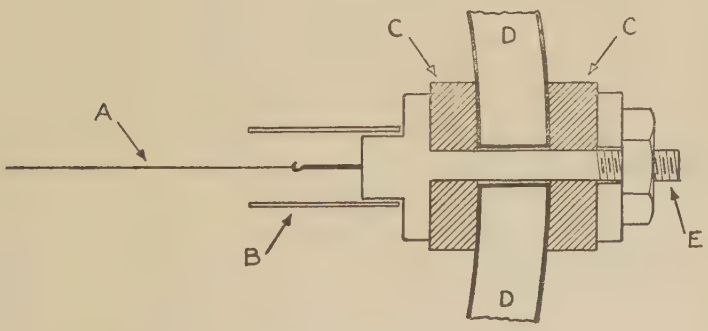

Diagram of wire mounting.

A. Anode wire.
B. Shield·
C. Rubber gasket.
D. Glass cylinder.
E. Threaded support.

cathode assembly being chromium plated. It is mounted across the middle of a cloud chamber of 28 cm. diameter and 9 cm. depth. The anode wire is attached to two metal supports (for details see fig. 1) passing through holes in the glass cylinder of the chamber, the holes then being sealed with small rubber gaskets. The compressibility of the gaskets also provides a useful means for the final tensioning of the wire. Both tungsten and platinum wires (diameter 0·1 mm. and 0·17 mm.) have been used successfully, but, for reasons to be given later, platinum wires are preferable. In future applications it is proposed to use cathode rods of smaller diameter with surfaces blackened to reduce the amount of light scattered.

(b) *Chamber filling* :

In normal cloud chamber operation advantage is taken of the readiness with which electrons produced by ionizing particles attach themselves to oxygen molecules in the gas to form heavy negative ions. In counters, however, the production of gas multiplication depends on the electrons remaining freely mobile, and electron attachment must be avoided. For this reason precautions must be taken to exclude oxygen and water vapour. The cloud chamber is therefore filled with commercial argon (stated to be of 99·8 per cent purity and oxygen-free) and saturated with absolute ethyl alcohol vapour—a mixture which gives good cloud chamber tracks and at the same time is a satisfactory filling for the counter. As it is not possible to evacuate the chamber, the air initially present is removed by partial extraction with argon : argon is admitted to a pressure of 1·5 atmospheres and the pressure is then released to one atmosphere. This procedure is repeated at least ten times and the chamber then finally filled with argon to the required pressure of about 118 cm.Hg in the compressed position.

If there is no appreciable negative ion formation the electrons produced along the path of an ionizing particle are rapidly swept away by the general clearing field applied across the chamber. The tracks observed when the cloud chamber is expanded thus arise from positive-ion condensation only.

It is found that if no further precautions are taken the pulse size of the counter decreases steadily over a period of several days after the cloud chamber has been filled—presumably due to the slow release of oxygen and water vapour from the walls and velvet background of the chamber and to the slow diffusion of air into the chamber through the rubber diaphragm. The increasing amount of electron attachment which thus occurs results in an undesirable doubling of the tracks, showing that condensation is now occurring on both positive and negative ions. (A similar difficulty has been experienced by Cohen (1949 b) with his combination cloud- and ion-chamber). The *status quo* can be restored temporarily by reflushing the chamber with argon and for the present purposes it has proved sufficient to do this once a week. However, a method of continuously removing oxygen and water vapour is essential for a permanent and reproducible pulse size in the counter, and we are now investigating various possible methods.

(c) *Operation of the counter* :

The counter will operate satisfactorily either in the proportional region or in the Geiger region. With the pressures used (118 cm. of mercury) and a wire diameter of 0·17 mm., suitable proportional operation is achieved over the range 1950–2300 volts, while the threshold potential for the Geiger region is about 2500 volts.

The cathode rods of the counter are earthed and the anode wire is connected to a positive high voltage supply through a 2 megohm resistance.

It will be seen later that the most suitable method for detecting particles inside a cloud chamber is to operate in the proportional region, using a fairly low gas multiplication and high external (valve) amplification. In this mode of operation the negative pulses obtained from the wire are amplified by a high gain linear amplifier (gain variable between 500 and $3 \cdot 10^5$) incorporating a biased diode discriminator at the output stage, which, in conjunction with the gain setting, determines the minimum size of pulse that will be accepted.

Particular care is necessary to avoid spurious pulses at the input stage of the amplifier. Any appreciable leakage from high voltage points associated with the anode wire will give rise to spurious pulses, but by mounting the anode wire directly on the glass cylinder of the chamber so that the leakage path is made as long as possible and by using polystyrene supports for all high voltage components, leakage is readily reduced to a negligible level. A silicone varnish (trade name " Aquatect ") has proved very effective in reducing residual leakage across the surface of the glass cylinder. These initial precautions being taken, the counter has been operated continuously for many weeks without any trouble due to spurious pulses.

For these initial investigations the counter has been operated in coincidence with two Geiger counters placed above the chamber in a vertical telescope arrangement. The output pulse from a threefold Rossi coincidence circuit is used to expand the cloud chamber, and within a few microseconds (*q. v.*) of a coincidence being detected the high voltage on the wire is removed electronically. The voltage is thus removed before the positive ions along the path of the incident particle have had time to move any appreciable distance and the track is therefore visible and undistorted even within the sensitive volume of the counter (Photograph (*a*), Pl. XXVI.). The small " bead " of ionization observed on the wire near to the track of the incident particle consists of the positive ions formed by the gas multiplication which occurs near the wire during the discharge of the counter. By using high values of the amplifier gain and quenching rapidly it is, in fact, possible to remove the voltage on the wire before the process of gas multiplication has reached completion—the " bead " observed is then correspondingly smaller and may even be too small to be visible on the cloud chamber photograph. However, it is often desirable to know which particle discharged the counter and this is possible if a track can be associated with a " bead " on the wire. For this reason the removal of the anode voltage is usually delayed by approximately 20 microseconds ; this allows the discharge to develop until it is quenched by a space-charge reduction of the field near the wire (Stever 1942), and a " bead " of reasonable size is observed.

The columns of ionization marked W in Photographs (*a*) and (*b*), Pl. XXVI., and also visible in the subsequent photographs arise as a result of surface irregularities of the wire. If the wire is not smooth or if particles of dust adhere to it an " electric wind " or corona phenomenon produces

continuous streams of positive ions moving away from the wire and occurring at the same points in successive photographs. This phenomenon does not interfere directly with the normal operation of the counter but the streamers are rather undesirable from the point of view of clear cloud chamber pictures. Fortunately it is possible to avoid most of them by cleaning the wire carefully. The initial cleaning consists merely of washing the wire with alcohol with a fine brush. Platinum wires are preferable to tungsten as they have a smoother surface and may be safely glowed in air after closing the chamber as the final stage of the cleaning process. The "electric winds" have been investigated in some detail

Fig. 2.

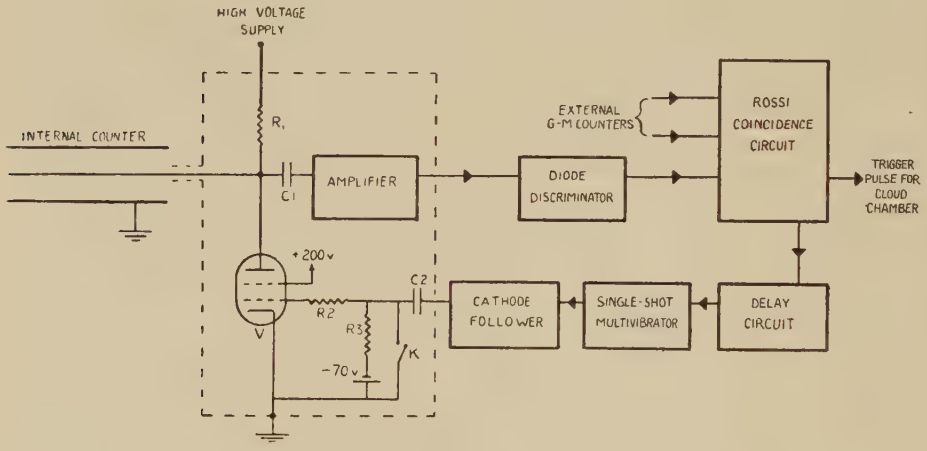

Schematic circuit diagram.

R_1	2 m.Ω.	2 watt.
R_2	30 k.Ω.	½ watt.
R_3	1 m.Ω.	1 watt.
C_1	100$\mu\mu$F.	High voltage.
C_2	0·5 μF.	
Valve V.	CV73 (M.A.P.).	

and the exact mechanism of their production will be discussed in a subsequent paper. They are more pronounced at higher voltages on the wire.

The general circuit arrangement used for removing the anode voltage of the counter after a coincidence has been detected is shown diagrammatically in fig. 2. The valve V is normally biased beyond anode current cut-off so that the full positive potential is applied to the wire of the counter. When a coincidence is detected a pulse, delayed by about 20 microseconds, triggers a single-shot multivibrator. This produces a square positive pulse ($\sim$1/3 second long) which is applied to the grid of the valve V. Valve V then becomes fully conducting and the anode

voltage of the counter is rapidly removed. A few milliseconds after the cloud chamber is triggered the control mechanism of the chamber closes a relay contact K and maintains the grid of valve V at earth potential until the cleaning cycles of the chamber have been completed. The anode voltage of the counter is therefore approximately zero during this period (fig. 3) and the production of fresh ionization by discharges of the counter and by the "electric wind" phenomenon during the cleaning expansions is thereby avoided.

Operation of the counter in the manner described above, *i. e.* in the proportional region with removal of the anode voltage a few microseconds

Fig. 3.

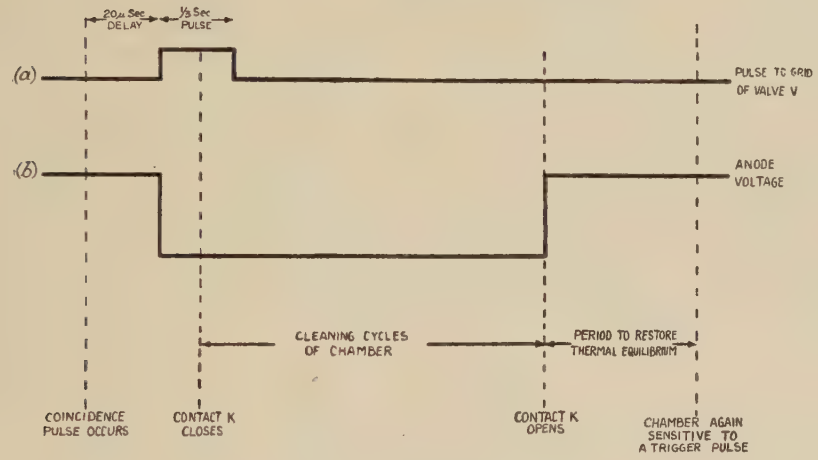

Sequence of operations.

after triggering the cloud chamber, will hereafter be referred to simply as "the normal mode of operation". Other modes of operation will be described in § 3.

§ 3. The Discharge Phenomena of Proportional and Geiger-Muller Counters.

The technique of operating an open counter in the gas of a cloud chamber is one that is obviously applicable to the study of discharge phenomena in counters. When a counter is operated in the Geiger region the discharge is known to spread along the wire from the point where the particle passed through the counter (Stever 1942). Several determinations of the velocity of this discharge spread have been made and various mechanisms for this process have been suggested. Corson and Wilson (1948) have published a useful review of this work and it has been discussed more recently by Balakrishnan and Craggs (1950). Of special

interest also is the transition between the proportional region of a counter and the Geiger region. The present technique is being applied to the study of these problems and an account of this work will be published separately. However, a few photographs will be given here to indicate the possibilities of the method.

If the counter is operated in the proportional region and the cloud chamber is triggered without removing the voltage from the anode wire the positive ions formed near the wire in the discharge of the counter move outwards towards the cathode until condensation begins. Instead of forming a " bead " near the wire as in Photograph A, the positive ions now appear as a " ring " of ions in Photograph (*b*) (Pl. XXVI.). Photographs (*a*) and (*b*) demonstrate directly the extreme localization of the discharge in the proportional region.

Photograph (*c*) (Pl. XXVI.) was taken a ta rather higher anode voltage than Photographs (*a*) and (*b*) and is typical of photographs obtained in the transitional region between the proportional and the Geiger regions. It was obtained by removing the anode voltage about 20 microseconds after triggering the chamber and may be compared with Photograph (*a*). At the higher voltage it is seen that the discharge spreads along the wire in a series of quite characteristic and fairly regularly spaced " jumps ", and the positive ion space charge consists of a number of " beads " along the wire. It has been observed that as the anode voltage is further increased the discharge becomes progressively more continuous along the length of the wire.

From the previous description of the normal mode of operation it is clear that the anode voltage is removed only when expansion of the chamber is about to take place. But bursts of ionization are being produced continually in the counter and although the initial radial movement of the " bead " is very rapid the time for the complete collection of the positive ions on the cathode rods is several milliseconds, owing to the high gas pressure used in the chamber. There is thus a probability that besides the selected particle and its associated " bead " of ionization there will be present tracks and " rings " of ionization due to events which occurred within a certain interval before the principal track. Examples of this may be seen on Photographs (*e*) and (*f*), Pl. XXVII. At low voltages, where the discharge is very localized, the " rings " so formed are narrow and not very intense. At voltages sufficiently high to produce spreading of the discharge along the wire the effect of a previous count becomes more noticeable, due to the formation of extended " ring " systems (*e. g.* Photograph (*d*), Pl. XXVI.) or even continuous " cylinders " of positive ions (*e. g.* Photograph (*c*), Pl. XXVI.). These are undesirable in photographs intended to show interesting particle events in a cloud chamber, and from this point of view the most suitable operating region of the counter for particle detection is the proportional region. By keeping the gas multiplication fairly low any single " rings " present do not seriously obscure any part of the cloud chamber.

§ 4. Discussion of Results.

We now describe a series of photographs which demonstrate the potentialities of the internal counter technique for detecting particles inside a cloud chamber. The internal counter was used in the normal mode of operation, with the threefold telescope arrangement described in §2 and with the discriminator biased towards events of high total ionization.

The photographs may be divided into three types :

Type (*a*). Photographs showing the internal counter being triggered by single heavily ionizing particles.

Type (*b*). Photographs of local showers and air showers in which two or more fast particles of minimum ionization traverse the internal counter simultaneously.

Type (*c*). Photographs of single fast particles which produce slow knock-on electrons in the gas or in the cathode rods of the counter.

Type (a). Slow Particles.

Photographs (*e*) and (*f*), Pl. XXVII., show slow particles, probably protons, triggering the internal counter. The slow particle in (*f*) appears to originate in a nuclear star in the glass cylinder of the cloud chamber.

Photograph (*g*), Pl. XXVII., shows an event which is almost certainly the decay of a μ-meson in the glass cylinder at the bottom of the chamber. The decay electron re-enters the chamber, travels upwards at a rather steep angle, unfortunately misses the counter and passes out of the illuminated region of the chamber. Both tracks project back to a point in the cylinder.

Photograph (*h*), Pl. XXVII., shows a slow particle which stops within the sensitive volume of the counter. It is out of the illuminated region at the top of the chamber. From the observed scattering in the gas the particle is very probably a slow meson. No decay electron is visible in the chamber and unfortunately the end of the track is obscured by the large bead of ionization near the wire. For a given quenching delay, the size of the bead round the wire increases with the amount of initial ionization in the counter. As the operating conditions of the counter which affect the size of the bead (in particular the anode voltage and the gas purity) are not necessarily the same in all the photographs, too strict a comparison of bead sizes is not justified. However, this bead is appreciably larger than any obtained under the same conditions. Mutual repulsion of the positive ions in the dense space charge before condensation occurs is more likely to be the cause of the unusually large diameter of the bead, rather than their motion under the influence of the applied field in the few microseconds before it is removed. The spherical nature of the bead supports this view.

In Photograph (*i*), Pl. XXVIII., a slow electron is seen to discharge the counter. This shows that it is possible to trigger a cloud chamber by events which involve electrons or β-particles having energies too low for detection by conventional techniques.

Altogether 26 slow particles (excluding electrons) of ionization greater than about three times minimum have been photographed in a total sensitive time of 727 hours—corresponding to a vertical intensity of about $9{\cdot}3\times10^{-5}$ cm.$^{-2}$ min.$^{-1}$ sterad.$^{-1}$, that is, about 0·01 per cent of the total vertical cosmic ray flux at sea level. In three cases there are definite indications that the heavily ionizing particles are mesons (*e. g.* Photographs (*g*) and (*h*), Pl. XXVII.). In the remaining cases, however, the particles cannot be identified with certainty. On account of the material above the internal counter (chamber wall, external counters, etc.), the slow mesons observed would have incident momenta in the range $(9{\cdot}2\text{–}10{\cdot}1)\times10^{7}$ eV./c., while the protons would lie within the range $(4{\cdot}3\text{–}6{\cdot}0)\times10^{8}$ eV./c.

It is difficult to compare the above rate with the results of other workers obtained under different experimental conditions, but Montgomery (1949) in discussing the rather indefinite evidence available has suggested a value of the order 6×10^{-4} cm.$^{-2}$ min.$^{-1}$ for the omnidirectional intensity of slow particles at sea level. Anderson and Neddermeyer (1936) and Widhalm (1940) have shown that the heavily ionizing particles are much less concentrated about the vertical direction than is the total ionizing component, so the unidirectional intensity is probably of the order 10^{-4} particles cm.$^{-2}$ min.$^{-1}$ sterad.$^{-1}$, a value which is in satisfactory agreement with our observed rate.

Rossi, Sands and Sard (1947) have measured the slow meson intensity at sea level in the momentum range $(6-12)\times10^{7}$ eV./c. and obtained a value $5{\cdot}4\times10^{-5}$ slow mesons cm.$^{-2}$ min.$^{-1}$ gm.$^{-1}$ (range in air). This corresponds to an omnidirectional intensity of $14{\cdot}0\times10^{-5}$ cm.$^{-2}$ min.$^{-1}$ in our momentum range. The unidirectional intensity in this momentum range is therefore probably of the order 5×10^{-5} slow mesons cm.$^{-2}$ min.$^{-1}$ sterad.$^{-1}$, since the angular distribution of slow mesons is likely to be such that there is a general concentration about the vertical. (On the other hand, the angular distribution of slow protons may be expected to be much more isotropic, since many are secondary particles emitted from nuclear evaporations in local material (Anderson and Neddermeyer, 1936). Rochester and Bound (1940) measured the number of slow protons in the range $(3{\cdot}9\text{–}5{\cdot}5)\times10^{8}$ eV./c., and from their results Rossi (1948) has deduced a rate of $(3\pm1)\times10^{-5}$ slow protons cm.$^{-2}$ min.$^{-1}$ sterad.$^{-1}$. These results for the intensities of slow mesons and slow protons taken together give a total slow particle rate which is again in fair agreement with the present results for comparable momentum ranges. It seems reasonable to suppose that the numbers of slow mesons and slow protons observed with the present experimental arrangement are of a similar order.

Type (b) Showers.

The internal counter obviously cannot distinguish between one slow particle having an ionization three times minimum (say) and three

simultaneous particles of minimum ionization. The threefold telescope arrangement is therefore sensitive to showers, either incident from the air or locally produced. Examples of events of this type are shown in Photographs (*j*) and (*k*) of Pl. XXVIII. It will be noticed that when particles pass simultaneously through the sensitive volume of the counter, each produces a local discharge near the wire. A particle traversing the counter some short time before the cloud chamber was triggered would be associated with a " ring " of positive ions, more or less expanded (*e. g.* Photograph (*f*), Pl. XXVII.), while a particle arriving after the counter voltage was removed would produce no discharge. This ability to determine whether two or more particles are contemporary decreases the effective resolving time of the chamber and could be employed with advantage in certain experiments. A preliminary estimate of the time interval required for the positive ions to move outwards from a " bead " to a recognizable " ring " gives the effective resolving time of the order 100 microseconds, whereas the resolving time of a normal chamber of this size is of the order 1/50 second.

Type (*c*). *Knock-on electrons.*

Photograph (*l*) of Pl. XXVIII. is typical of many photographs obtained with the experimental arrangement described : a fast cosmic ray particle produces a slow knock-on electron in the gas. The ionization of the fast particle alone would not have given a sufficiently large pulse to pass the discriminator, and it is clearly the slow electron which contributed most to the large pulse obtained. Slow knock-on electrons in the gas or cathode rods of the counter occur fairly frequently, and must be responsible for many of the large pulses obtained from the normal enclosed type of proportional counter. (This conclusion was previously reached by Cook (1949) in some recent work using proportional counters). In experiments using conventional proportional counters there is often an undesirable uncertainty in knowing exactly what events triggered the counter. This is avoided in the present technique.

§ 5. The Internal Counter Technique for Detecting Nuclear Disintegrations.

The internal counter need not, of course, be operated in coincidence with an arrangement of external Geiger counters as in the present work. For example the cloud chamber may be triggered by single pulses from the internal counter alone. With the discriminator set to record only events of high ionization a short run on these lines produced photographs mainly of contamination α-particles. This arrangement would undoubtedly be also sensitive to nuclear disintegrations occurring in the gas of the cloud chamber. A rough calculation based on photographic plate evidence (George and Jason 1949) gives the rate of nuclear stars in the gas of the cloud chamber as four per day. A comparison of this with the measured α-particle rate of the counter, gives an expected yield of only

one star photograph per 500 photographs of contamination α-particles. (Cohen has reported a similar difficulty with his combination cloud- and ion-chamber). To bias the counter towards events of higher ionization than that of a contamination α-particle would of course mean that many stars would not be recorded, especially those whose origins lay outside the sensitive volume of the counter.

However, an arrangement consisting of two or more open counters operated in coincidence inside a cloud chamber would be sensitive to stars but not to contamination α-particles provided the counters were separated by a distance greater than the range of such α-particles in the gas ($\sim$5 cms.). At the same time there would be no necessity to bias towards events of very high total ionization. It is hoped to employ this arrangement in the near future.

§ 6. Conclusions.

The technique of controlling a Wilson cloud chamber by an internal counter of the type described has the following features :

(*a*) The counter may be used in the proportional region and set to record either single particles of minimum ionization or heavily ionizing events.

(*b*) Unless a particle happens to hit one of the cathode rods the counter has no stopping power beyond that of the gas filling. Slow particles traversing the cloud chamber and events producing slow particles within it can therefore be photographed.

(*c*) The counter may be operated in such a way as to obtain tracks throughout the sensitive volume of the counter, and thus the useful volume of the cloud chamber is not reduced. This is an important feature, especially since it is proposed to put two or more of these counters inside a cloud chamber to detect nuclear disintegrations in the gas.

(*d*) It is possible to observe the exact event which triggered the counter.

(*e*) The technique is one which is readily applicable to the study of the discharge phenomena in counters.

(*f*) The internal counter affords a means of testing the contemporary nature of particles which pass through it, and the effective resolving time of the cloud chamber is thereby greatly reduced.

(*g*) The technique is not difficult and, given the few elementary precautions described, the counter is quite stable.

§ 7. Acknowledgments.

We wish to thank Professor P. M. S. Blackett, F.R.S., for the interest he has taken in this work and for allowing us to make use of the excellent facilities of his laboratory. We are also grateful to Dr. J. G. Wilson for his continued interest and for helpful comments, and to Dr. Nora Page for assistance in some of the initial work. One of us (A. L.) wishes to

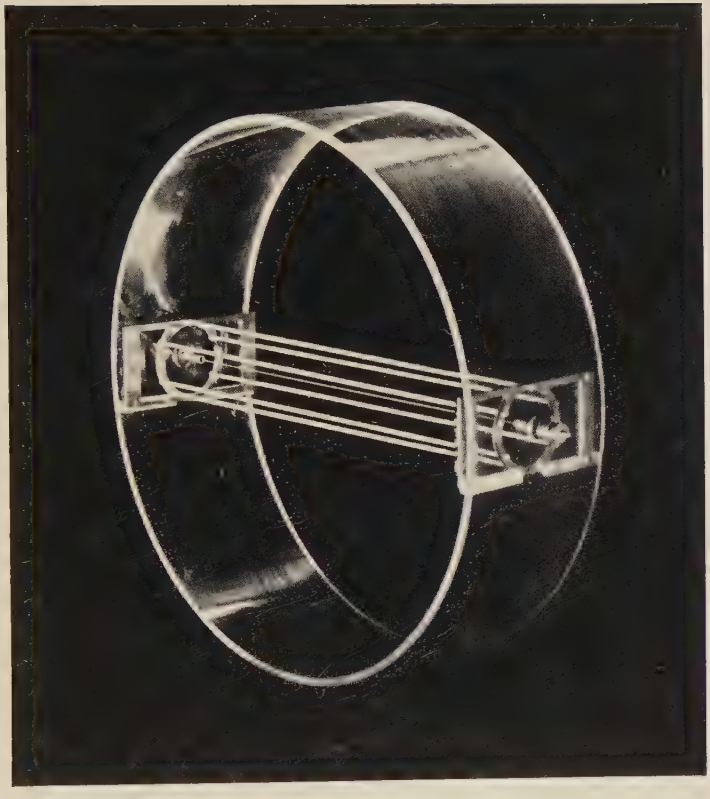

To face page 836

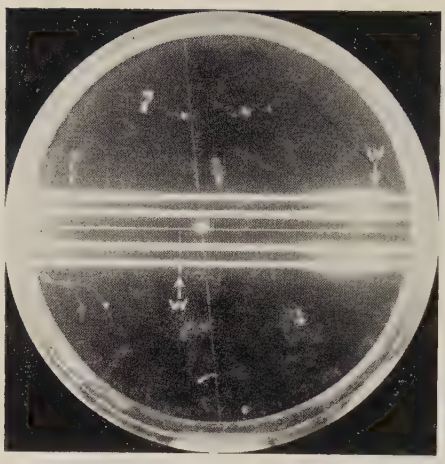

(*a*)

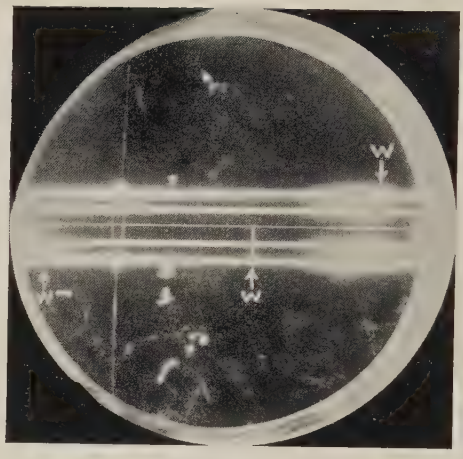

(*b*)

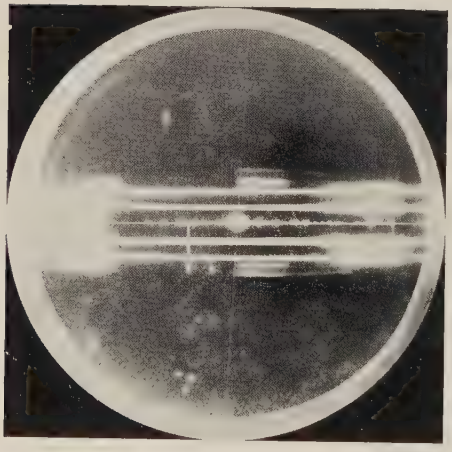

(*c*)

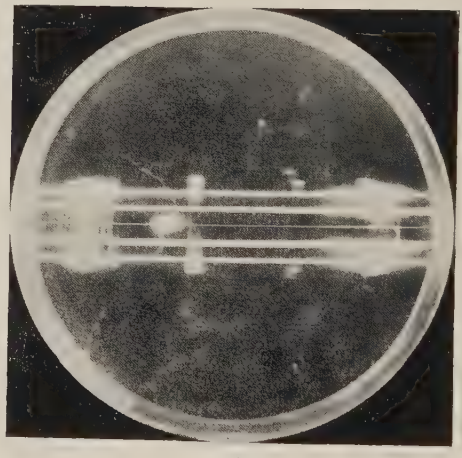

(*d*)

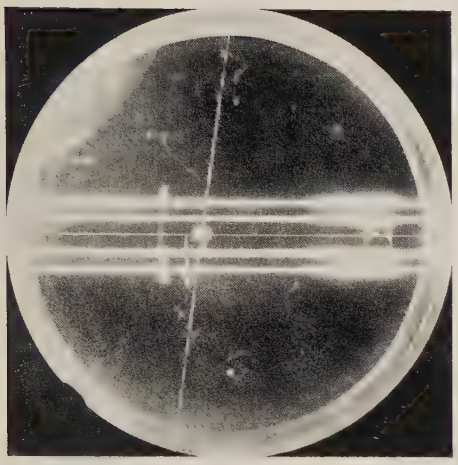

(*e*)

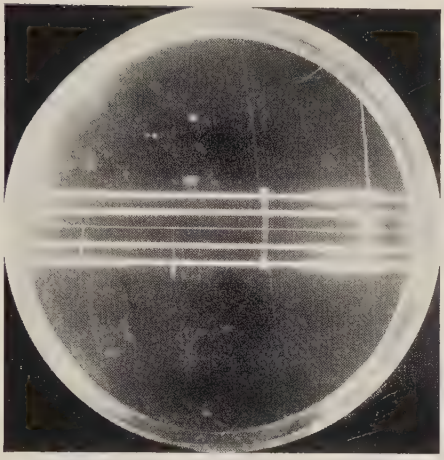

(*f*)

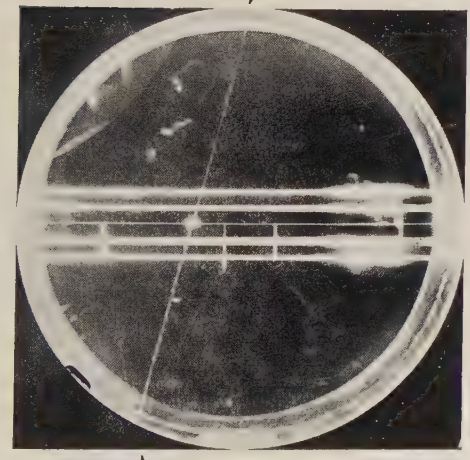

(*g*)

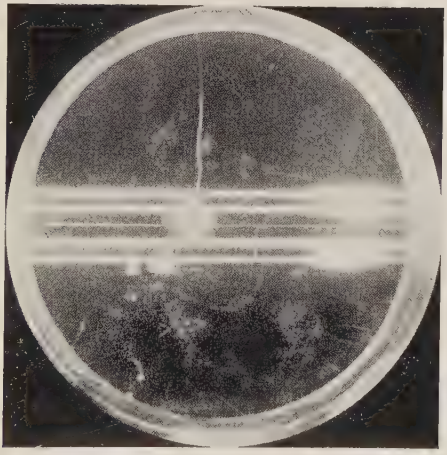

(*h*)

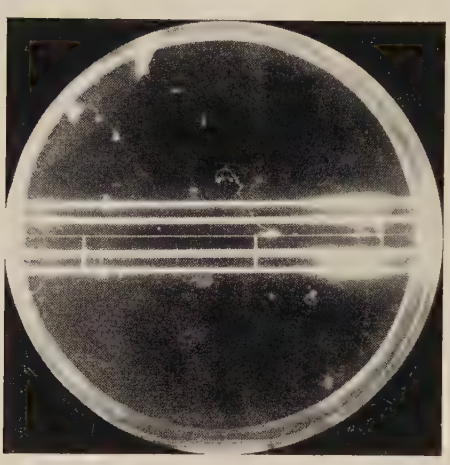

(*i*)

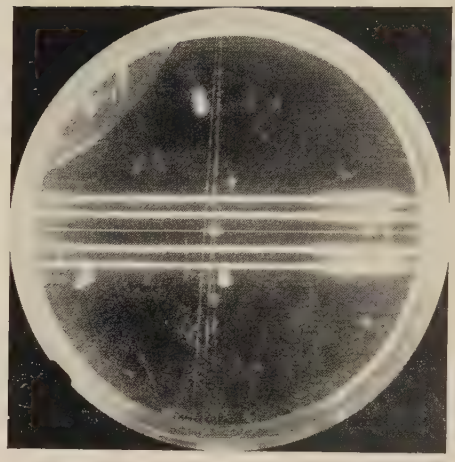

(*j*)

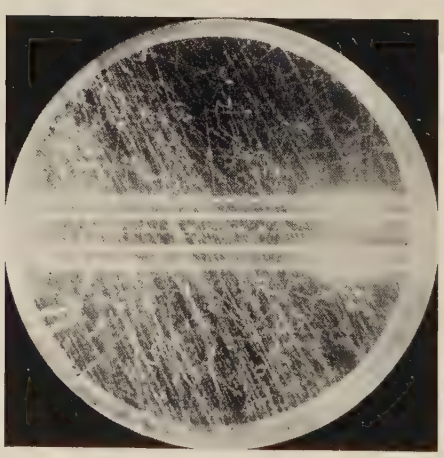

(*k*)

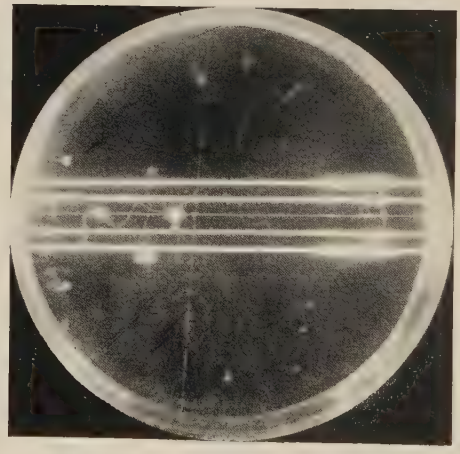

(*l*)

thank the University of Manchester for the award of the John Harling Fellowship, and one of us (N. V. R.) is indebted to the Nuffield Foundation for the award of a Dominion Travelling Fellowship.

References.

Adams, R. V., Anderson, C. D., Lloyd, P. E., and Saxena, R. C., 1948, *Rev. Mod. Phys.*, **20**, 334.

Anderson, C. D., and Neddermeyer, S. H., 1936, *Phys. Rev.*, **50**, 263.

Balakrishnan, C., and Craggs, J. D., 1950, *Proc. Phys. Soc.* A, **63**, 358.

Cohen, M. J., 1948, *Phys. Rev.*, **74**, 1244; 1949*a*, *Ibid.*, **75**, 1329; 1949*b*, *Biennial Report* (July 1947–June 1949), Palmer Physical Laboratory, Princeton University.

Cook, J. R., 1949, unpublished.

Corson, D. R., and Wilson, R. R., 1948, *Rev. Sci. Inst.*, **19**, 207.

George, E. P., and Jason, A. C., 1949, *Proc. Phys. Soc.*, A, **62**, 243.

Hodson, A. L., and Loria, A., 1949. *Report to the Como Conference on Cosmic Rays.*

McCusker, C. B. A., 1944, *J. Sci. Inst.*, **21**, 120.

Montgomery, D. J. X., 1949, *Cosmic Ray Physics* (Princeton: University Press), p. 288.

Rochester, G. D., and Bound, M., 1940, *Nature, Lond.*, **146**, 745.

Rossi, B., 1948, *Rev. Mod. Phys.*, **20**, 537.

Rossi, B., Sands, M., and Sard, R., 1947, *Phys. Rev.*, **72**, 120.

Stever, H. G., 1942, *Phys. Rev.*, **61**, 38.

Widhalm, A., 1940, *Zeits. f. Phys.*, **115**, 481.

LXXV. *The Nature of the Neutral Particle Emitted in the Decay of the π-Meson.*

By C. O'Ceallaigh*.
The H.H. Wills Physical Laboratory, University of Bristol†.

[Received July 3, 1950.]

[Plate XXIX.]

Summary.

In order that momentum and energy be conserved in the process of π–μ-decay at rest, it is necessary to assume the emission of a single additional non-ionizing particle in a direction opposite to the initial line of motion of the μ-meson. There exists strong experimental evidence for the conclusion that the neutral particle has small or negligible rest-mass. Hence, we may suppose that it is either (*a*), some light neutral particle possibly identical with the neutrino of β-decay, or, (*b*), a photon.

Some 250 suitable cases of π–μ-decay in Ilford G5 Nuclear Research plates have been examined with a view to testing the hypothesis (*b*). A careful search has been made in the requisite direction, for associated pairs of electrons. In a total scan-length of 38 cms. no such case was observed. Statistical analysis shows that, if indeed a photon were emitted, the probability that it would fail to produce a pair under the conditions of the experiment was 4×10^{-3}.

Since this result would appear to exclude the possibility of photon emission, it is inferred that the π-meson normally decays in accordance with (*a*).

It is shown that the present experiment has much in common with those devised to demonstrate the existence of the neutrino of β-decay.

§ 1. The Decay of π-Mesons.

In the μ-decay of π-mesons as observed in photographic emulsions, it is known that the distribution in range of the μ-particles is consistent with the assumption that they are always emitted with constant kinetic energy, the departures of the individual values of the range from the mean being due to "straggling". It follows from this result that the disintegration is a two-body process, momentum, energy and charge being conserved by the emission of a single neutral particle, which leaves no recognizable trace in its passage through the emulsion.

* On leave of absence from University College, Cork.
† Communicated by Professor C. F. Powell, F.R.S.

A study of many examples of the process as it ordinarily occurs in the plates has shown that the spatial distribution of the trajectories of the μ-meson is isotropic with respect to the final direction of motion of the disintegrating π-meson (Lattes *et al.*, 1947, Bradner 1949). Taken in conjunction with the constancy in the range of the μ-meson, this result proves that the π-mesons are commonly moving with very small velocities at the instant of decay. If it were otherwise, the range of the μ-mesons would vary widely according to their direction of emission with respect to the line of motion of the parent π-particles. The neutral particle formed in the decay will therefore be projected in a direction opposite to the initial line of motion of the μ-meson.

Mass of the Neutral Particle.

By application of the conservation laws it may be shown that the rest-mass (n_0) of the neutral particle bears a ratio (P) to that of the μ-meson given by

$$P=n_0/m_\mu=\sqrt{(Q^2-2QB_\mu+1)} \quad . \quad . \quad . \quad . \quad . \quad . \quad (1)$$

where $Q=m_\pi/m_\mu$, and $B\mu$ is the value of $(1-\beta^2)^{-1/2}$ proper to the μ-meson at the instant of its formation. The following Table calculated from (1) gives, for certain pairs of values of Q and B_μ, some real values of the mass of the neutral particle expressed in terms of the mass of the electron, m_e.

Table I. n_0/m_e.

Q \ Bμ	1·036	1·037	1·038	1·039	1·040
1·325	21·2	18·3	14·7	10·0	—
1·321	18·7	15·3	10·8	1·2	—
1·317	15·8	11·6	4·2	—	—
1·315	14·2	9·2	—	—	—
1·313	12·3	6·0	—	—	—
1·312	11·3	3·4	—	—	—
1·311	10·1	—	—	—	—

The most recent measurements (Berkeley Group 1950) give $m_\pi=276\pm6m_e$; $m_\mu=210\pm4m_e$; $Q=1{\cdot}315$. They are in good agreement with those found for cosmic-ray mesons in this laboratory (Franzinetti 1950). The observed range of the μ-meson in Ilford G5 emulsion is 595 ± 10 microns. Using the established range-energy relationship (Fowler 1950), and setting $m_\mu=210\,m_e$, we find $B_\mu=1{\cdot}038$.

It will be clear from Table I. that an exact determination of n_0/m_e in the region $n_0 \to 0$ requires very precise knowledge of the values both of Q and of $B\mu$. Nevertheless, the accuracy of the experimental measurements seems to be such that we may conclude with confidence that the neutral particle has a mass not greater than a few electron masses. Since there is no certain evidence for the existence of neutral particles with a mass of this order, it appears preferable to suppose that it has negligible rest mass. This assumption is consistent with all present experimental information and will be made in what follows.

In order to conserve momentum the neutral particle, if of negligible rest-mass, must have energy $=30{\cdot}1$ MeV. Such a particle might be (*a*) the neutrino of β-decay, (*b*) some light neutral particle other than the neutrino or (*c*) a photon.

If it is the neutrino of β-decay, its interaction with matter would appear to be negligible (Nahmias 1935, Ellis and Wooster 1927), and thus it would be expected to escape detection in the photographic emulsion. Evidence based on the shape of the β-ray spectrum of tritium indicates that its rest-mass is probably less than $1/30\ m_e$ (Nielsen 1949).

If the neutral particle is analogous to the neutrino, but not identical with it, it is impossible to state, a priori, in what manner it will interact with matter, save in respect of its energy loss by ionization which will be negligible.

On the other hand, if the particle is a photon, its interaction with matter, though small, will not be negligible. For a photon of 30 MeV., the most important interaction will lead to the creation of electron pairs. Later, it will be shown that the cross-section for the production of a single Compton electron is only 1/7 that for pair production. For this reason we shall be justified in disregarding such of these as may be produced under the conditions of the experiment. It has been the aim of the present investigation to detect pairs of electrons, if they exist, by scanning under high power in a direction opposite to that of the initial path of the μ-meson. The observations would appear to exclude the hypothesis that the neutral radiation emitted in the decay of the μ-meson consists of photons, and strong evidence is thus provided for the existence of some form of "neutrino". That this is identical with the neutrino of β-decay is not certain, but the two particles will be shown to have several properties in common.

§ 2. Experimental Method.

(a) *Geometry of Problem.*

The search for electron pairs associated with π-decay was carried out in the batch of Ilford G5 electron-sensitive plates referred to in previous communications from this laboratory (Camerini *et al.*, 1950). About 400 cases of π-μ-decay were examined. On each of these, measurements were made of the position in the emulsion of the origin of the μ-meson and of its apparent angle of dip using the first 25μ of track. Tracks of which the dip was greater than 15° were then rejected.

The emulsion of these plates was 400μ thick before processing, and after processing, 160μ. It has been shown (Fowler 1950) that for regions of the plates more than 1 cm. from the edges, this shrinkage takes place only in a direction at right angles to the plane of the emulsion and is a uniform linear transformation in this coordinate. We define the shrinkage factor t_u/t_p=S=400/160 for the plates concerned. Here, and subsequently, the subscripts u and p will refer respectively to the unprocessed and processed emulsions.

Fig. 1 represents a vertical section of the emulsion. The path of the neutral particle through the unprocessed emulsion will be OE=t, O being the origin of the μ-meson, and E the point at which the particle leaves the emulsion. The angle of dip, ϑ=arc tan PQ/25, PQ being measured

Fig. 1.

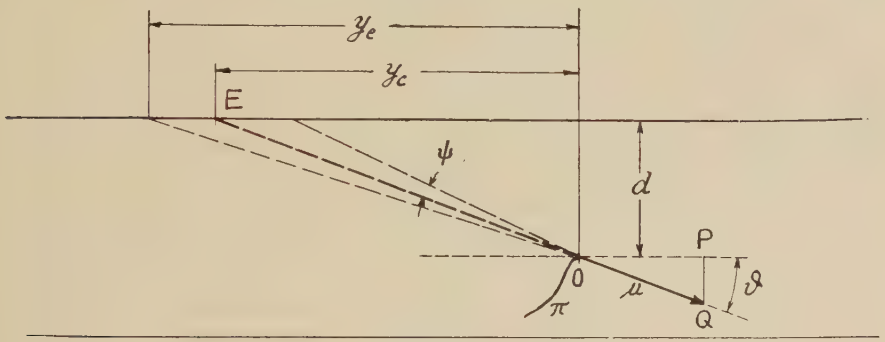

in microns. We have the following relationships valid for processed and unprocessed emulsions:

$$\tan \vartheta_u = S \tan \vartheta_p \quad . . . . . (2)$$

$$y = d_u \cot \vartheta_u = d_p \cot \vartheta_p \quad . . . . . (3)$$

$$t_u = y(1 + \tan^2 \vartheta_u)^{1/2} \quad . . . . . (4)$$

In the actual experiment the most convenient distance to measure is y. For each track, ten measurements of dip were made by means of an eyepiece scale, and the graduated focusing drum of the focusing scale of the instrument. The distance d_p was measured for the same setting of the instrument. From these data, the value of y was computed using equation (3). The path-length thus estimated is less than the actual path t_u in the unprocessed emulsion, but it may be seen from (4) that the defect of y from t_u is small for the values of ϑ included in the measurements, and further, it may be allowed for.

(b) *Method of scanning and allowance for multiple scattering.*

The scanning of the plate was carried out under magnifying power objective×45, with binocular eyepieces×8. A hair-line in one eyepiece was set so that its direction was parallel to the y-axis of motion of the microscope stage. The plate was then rotated until the hair-line appeared

to lie evenly along the mean-line of the grains in the first 25μ of the μ-meson track. The field of view extended to 100μ on either side of the hair-line.

The path followed by the neutral particle will be tangent to the μ-meson track at the point of origin. In general, because of multiple scattering, the directions of the mean-line and of the tangent will not coincide. The angle between these directions will be normally distributed about the direction of the mean-line and the variance of the distribution may be computed from the momentum of the scattered particle and the composition of the emulsion (Rossi and Greisen 1941). Calculation shows negligible probability that the projection of the tangent lies outside a sector of angle 2° on either side of the mean-line, with centre on the origin of the μ-meson. For values of $y \leqslant 2500\mu$ it may be seen that the whole of this sector lies within the 200μ strip defined by the field of view. For longer scans, 1 cm. $> y \geqslant 0{\cdot}25$ cm., two additional $200\,\mu$ strips were scanned on either side of the central strip.

The estimate of y is, in similar manner, uncertain because of the effect of multiple scattering. Referring to fig. 1 it will be clear that this estimate, say y_c, depends on a measurement of the dip of the projection on a vertical plane, of the *chord* of the first $25\,\mu$ of μ-meson track. A correct estimate, say y_t, would be based on the dip of the *tangent* at the origin. It may be shown that the angle between chord and tangent has a normal distribution about the direction of the chord, and has variance $\langle\psi^2\rangle = \frac{1}{3}\langle\phi^2\rangle$ (Rossi and Greisen 1941). $\langle\phi^2\rangle$ is the mean square value of the projection of the angle between the tangents at the end-points of the segment. The value of $(\langle\psi^2\rangle)^{1/2}$ for the conditions of the experiment was calculated to be 1·8°.

For any individual track, y_t may be greater or less than the observable y_c. For tracks of sensible dip, because of the small half-width of the distribution of ψ, this difference is small or negligible. It is otherwise for tracks of small dip, and especially for "flat" tracks ($\vartheta_p \simeq 0$), and must be taken into account. This was done by finding the distribution function for y in terms of d, and ϑ (fig. 1) assuming normal distribution of ψ. The mean value $\langle y\rangle$, of y was obtained for this by graphical integration. For tracks of measurable dip the scan was continued to $y_e > y_c$ (fig. 1) such that the mean value of y, computed as above, was equal to y_c. For "flat" tracks, which by their nature make large contribution to the length scanned, it was found possible to express $\langle y\rangle$ in terms of a closed expression involving the tabulated functions $\mathrm{E}rf(x)$ and $\mathrm{E}i(x)$.

§ 3. Experimental Results.

The total number of π-μ decay events selected as suitable was 253. The sum of all the effective scan-lengths Σy_c computed as above was 36 cms. The corresponding true path-length in the emulsion Σt_u was 38 cms. 35 pairs of particles, probably electron pairs, were observed to have their points of origin within the scan strip-width (but not necessarily within the sector). The total area of the scan was

1·32 cm². This yields a density of 26 pairs per cm². of these plates. Other workers in this laboratory (Carlson *et al.*, 1950) report a density of 24 pairs/cm². The agreement is satisfactory. Neither figure has been corrected for failure to observe the small proportion of very steeply dipping pairs which are bound to escape detection.

For 24 cms. of this scan length each field was scanned twice and for the remaining 12 cms. the field was scanned once only. The corresponding areas of scan were calculated to be, respectively, 1·0 cm². and 0·32 cm². The number of pairs observed in the first series was 28 and, in the second series, 7. It may be concluded from these figures that there was no significant reduction in the efficiency of detecting pairs introduced by the change to single scanning. The apparent disproportion between scan-length and scan-area arises from the facts that the ratio scan-area/scan-length increases with the cube of the scan-length, and that the incidence of long scans was slightly smaller in the second series.

Theoretical Cross-Sections.

It has been shown (Heitler 1944) that, for high energies, both electrons of a pair are emitted in the forward direction. The solid angle Ω into which the electrons are emitted is of the order $\Omega \sim m_e c^2/T$, where T is the total energy of the pair. For 30 MeV. photons $\Omega \sim 1/60$.

The cross-section for pair-production σ_{pair} by 30 MeV. photons $= 7\bar{Z}^2 \times 5{\cdot}71 \times 10^{-28}$ cm², and for Compton Effect

$$\sigma_{Comp} = 3 \times 10^{-2} \bar{Z} \times 6{\cdot}57 \times 10^{-25} \text{ cm}^2.$$

From data supplied by the manufacturers of the G5 plates we may calculate $\bar{Z}^2 = 451$, $\bar{Z} = 13{\cdot}1$. The number of atoms per c.c. of emulsion $= 8{\cdot}37 \times 10^{22}$. We obtain from this $\sigma_{pair}/\sigma_{Comp} = 7$, and a probability of pair production per cm. path in the emulsion $= 0{\cdot}152$. Hence, if the neutral particle is a photon, we should expect to observe, on the average, 5·77 electron pairs " associated " with the cases of π–μ-decay examined.

The criteria of " association " are somewhat complicated by the multiple scattering of the μ-meson, but for present purposes, may be formulated with sufficient accuracy as follows :

(1) The origin of such a pair must be found within a solid angle containing OE (fig. 1) of such magnitude as to allow, in any individual case, for uncertainty as to the direction of the tangent at the origin of the μ-meson track. The projection on the surface of the emulsion of this solid angle is the sector already referred to.

(2) The pair must lie within a small calculable solid angle with OE as axis since the electrons are projected in the forward direction.

(3) It must be a pair of electrons of energy 30 MeV. to within the experimental error of measurement.

36 pairs were examined in respect of these criteria. All, save one, were rejected because of violation of (1) and (2). One pair remains which satisfied (1) and (2) but did not satisfy (3). This event will be fully

described in the appendix to this paper where it will be shown that it is most unlikely to be a pair of electrons. It has not been found possible to furnish a precise identification of its nature.

It is extremely improbable that any "associated" pairs escaped detection. Firstly, such pairs, if produced, would be more favourably situated for observation than the background pairs. Their dip will be small on account of the exclusion of steeply dipping μ-mesons. Furthermore, even if their points of origin were undetected in one field, their direction would be such that they would be readily observed as converging pairs of tracks in the succeeding two or three fields. Secondly, as has already been stated, the superficial density of background pairs is in satisfactory agreement with that found by other workers using plates chosen from the same series.

There remains to be considered a statistical possibility namely that the neutral particles are indeed photons, but that they failed to be materialized in a scan-distance in which 5–6 pairs were to be expected. Each scan-length y_j microns corresponding to the jth π–μ event, constitutes a "trial" in which the probability of producing a pair is $1{\cdot}52\times10^{-5}y_j$. The probability of failure in this trial is $(1-1{\cdot}5\times10^{-5}y_j)$ and the probability of failure in all n trials $P_F=\prod_{j=1}^{n}(1-1{\cdot}5\times10^{-5}y_j)$. A sufficient approximation to P_F will be Poisson's Function of Rare Statistical Frequency applicable to the case where all trials have equal probability. This yields $P_F=\epsilon^{-\mu}=\epsilon^{-5{\cdot}77}=4\times10^{-3}$. Rejecting this supposition on the grounds of its extreme improbability, we may conclude with reasonable confidence that the neutral particle, whatever be its nature, is not a photon.

§ 4. Interpretation of Results.

(a) *Spin of the π and μ-mesons.*

Further support for the reasonableness of this conclusion appears from considerations of spin conservation. Experiment has shown that the μ-meson decays into an electron and more than one neutral particle. (Leighton *et al.* 1949, Davies *et al.* 1949). Evidence based on the average energy of the electron spectrum favours the emission of two neutral particles, presumably identical. The results of these workers would appear to be confirmed by a more extended series of measurements on which the writer is at present engaged. Counter experiments (Hincks and Pontecorvo, 1949, 1950 ; Piccioni, 1949) appear to exclude the possibility that these are photons. Taken in conjunction with the results of the present work, these findings indicate that the decay chain π-μ-e takes place as follows :

$$\pi \rightarrow \mu + \nu_1$$

$$\mu \rightarrow e + 2\nu_2.$$

Whether the spin of ν_2 is integral of half-integral, it follows that that of the μ-meson is half-integral. This result is consistent with evidence based on the distribution curve of burst frequency (Christy and Kusaka, 1941).

If ν_1 has spin integral or zero, it follows that the π-meson has half-integral spin. This is in contradiction to the role of the π-meson in the theory of nuclear force fields which envisages interactions of the type $p \rightarrow n + \pi^+$; $n \rightarrow p + \pi^-$, an assumption supported by experimental evidence for the creation of π-mesons by nucleon–nucleon collisions *. We infer that ν_1 is a fermion (a particle of spin $\frac{1}{2}$), a conclusion not contradicted by the results of the present experiment.

Similarly, we may conclude that if the competing decay process $\pi \rightarrow e + \nu_3$ exists, it is likely to lead to the production of monoergic electrons unless an odd number >1 of neutral particles is emitted. The theoretical cross-section for this process is of the order 1/100 that for the chain π-μ-e (Ruderman and Finkelstein 1949).

(b) *Existence of the Neutrino.*

It appears that the characteristics of the decay of π-mesons may have a close bearing on this problem. It would be tempting to identify, ν_1, ν_2 and ν_3 with the neutrino of β-decay. In common with this particle, it would seem that they are fermions of negligible rest-mass. However, the present state of theory is such that perhaps it would be unwise to press the analogy between π-decay and the β-decay of radioactive elements.

It is a necessary consequence of the assumed properties of the " neutrino ", that such particles have a very weak interaction with matter. Attempts have therefore been made to prove the existence of the particles indirectly. It has commonly been considered that satisfactory evidence would consist in a demonstration that the conservation of momentum, as well as that of energy, requires the assumption of the emission of a neutral particle in the β-decay of a nucleus, or in the process of K-capture.

Several such experiments have been described involving the β-ray spectra of Cl^{38} (Crane and Halpern 1938, 1939) Kr^{88} (Jacobsen and Kofoed-Hansen, 1945) and on the formation of Li^7 by K-capture from Be^7 (Allen 1942), the magnitude of the recoil momentum has been shown to be consistent with the neutrino hypothesis. These experiments, though brilliantly conceived, are attended by great difficulties, because the disparity between the masses of the electron and the nucleus has the consequence that the energy of recoil of the latter is very small.

The present experiment has points of similarity with that of Allen in which the recoil momentum of the Li^7 was shown to be due entirely to the emission of the neutrino. The recoil energy was only about 50 eV. and was measured electrostatically. The present method is similar in principle, but the μ-recoil has energy 4·1 MeV., is visible in the emulsion and its momentum is measured by use of the well established range-energy relationship. If subsequent developments should establish the fact that of the neutral particle is identical with the β-decay neutrino, the

* *Note added in proof*—Additional direct experimental evidence for the conclusion that the π-meson is not a fermion comes from the recent work of Panofsky, Aanodt and York (*Phys. Rev.*, **78**, 825, 1950) on the γ-radiation associated with the absorption of π^--mesons in hydrogen under high pressure. This would appear to demonstrate the occurrence of the reaction $\pi^- + p \rightarrow n + \gamma$.

present experiment could be regarded as supplementing and confirming the β-ray experiments. In view, however, of the anomalous nature of the particle apparently associated with a case of π-μ-e decay, already referred to, and described in detail in the Appendix, it would seem at present unwarranted to conclude that the neutral particles emitted in meson decay are to be identified with the "neutrino" postulated by Fermi and by Pauli in order to explain the observed phenomena of β-decay.

APPENDIX.

In the course of the search for electron pairs which could be attributed to γ-rays liberated by the decay of π-mesons, an event was observed of which photo-micrographs are reproduced in Pl. XXIX. Although no definite conclusion can be drawn from it, it displays a number of remarkable features, and it was therefore found desirable to describe it in detail :

Fig. 2.

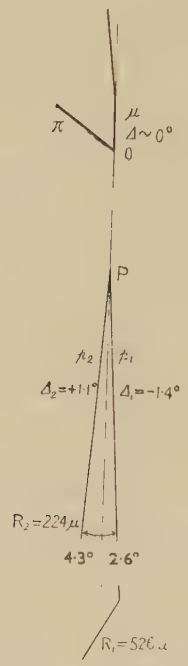

1500 μ from the point of arrest, O, of a π-particle in the emulsion, and in the line of motion of the μ-meson produced by the decay of the π-particle, and which subsequently decayed itself into an electron of 36 MeV., a pair of particles p_1 and p_2 appear to originate at a point P. OP is indistinguishable from the initial line of motion of the μ-meson. Further, OP is inclined to the plane containing the initial directions of motion of the two particles p_1 and p_2 at an angle less than 1°. These relationships, the angles of dip (Δ), positive if towards glass, of tracks p_1 and p_2 and the lengths (R) of the tracks are shown in fig. 2.

Although the ranges of the two particles in the emulsion are relatively short, it has been found possible to make a determination of the scattering parameter $\bar{\alpha}$ (Fowler 1950), for the tracks are heavily scattered and short "cell-lengths" of 20 μ can therefore be employed. The values of $\bar{\alpha}$ thus obtained are :—for p_1, $\bar{\alpha}_{100\mu}=1{\cdot}63\pm0{\cdot}25$; and for p_2, $\bar{\alpha}_{100\mu}=1{\cdot}6\pm0{\cdot}35$. The grain-density in the two tracks are $16{\cdot}3\pm3{\cdot}0$ and 20 ± 4 grains per 50 μ, respectively, values which may be compared with those due to particles with minimum ionization recorded in the same plates ; namely, 11·5 grains per 50 μ. The uncertainties quoted are standard deviations.

If the tracks are due to particles with the elementary electronic charge, the observed values of the scattering parameter correspond to particles of kinetic energy $\sim$ 10 MeV., and in view of the considerable limits of error due to statistical fluctuations, it would therefore be reasonable, from the point of view of the kinetic energy of the particles, to attribute them to electrons produced by a 30 MeV. γ-ray. Other features of the observations, however, make it very difficult to accept this explanation.

Firstly, the grain-density in the tracks is exceptionally high if they are due to particles moving at relativistic velocities, as would be the case, over most of the trajectory, if the particles were electrons. Here again, the statistical fluctuations, due to the relatively restricted lengths of the trajectories is rather large, and the evidence is not decisive. Observations, however, on more than 1000 tracks, of length >3000 μ, of which the grain density has the minimum value, have been made in this laboratory in connection with other investigations. These observations were analyzed to determine the frequency with which the grain-density in the tracks of particles of high energy, measured over a length of 500 μ, gave an apparent grain-density of 16 or greater. In no case was a value observed as high as the mean for the two tracks under discussion.

A second feature of the event is that the two trajectories both appear to terminate in the emulsion without any indication of an increase in the specific ionization due to a gradual reduction in velocity. Such an effect might be explained as due to the annihilation of a positive electron, and to a concomitant large angle deviation in the track of an electron. Since both of the particles cannot be positive electrons, the apparent endings of the tracks have been scrutinized. They occur in the middle of the emulsion where there are no abnormalities of any obvious kind.

A third feature of the observations is the angle between the pair, viz. 9·5°. This angle is very large if the pair is attributed to the materialization of a 30 MeV. γ-ray, but not impossibly so. Because of the occurrence of these three unusual features in the same event, it is reasonable to reject the view that it is due to a pair of electrons. In this case, we have to account for a phenomenon in the line of motion of a neutral particle emitted in the decay of a π-meson with exceptional features not previously observed.

The values of grain-density and scattering constant $\bar{\alpha}$ correspond to masses of the order 30 m_e for both tracks, but, as is well known, statistical fluctuations may lead to serious error in an estimate of mass based on observations on a single relatively short track.

If we accept the evidence of the grain-density and scattering of the track as not being seriously in error, it appears to be very difficult to account for the phenomena in terms of charged particles of which the existence is established. It is also difficult to find a consistent explanation of the observations in terms of known particles which have, by chance, passed through the emulsion during development. Two protons, for example, originating in a nuclear explosion during development would produce thin tracks but they should show evidence of an increase in grain-density towards the end of their range, a feature which is not observed. It appears best, however, to defer an attempt to identify the event until a second observation of the same kind allows us to exclude the possibility that it is to be attributed to a rare but trivial occurrence.

Acknowledgments.

The writer wishes to thank Professor C. F. Powell, F.R.S. for suggesting the experiment, for extending to him the hospitality of his laboratory and for his continued interest and encouragement. It is a pleasure to record his thanks to his wife who assisted in the experiment and is responsible for most of the dip measurements, to Mr. R. J. M. Gold who gave assistance with the graphical integrations, to the various members of the laboratory research group, particularly Mr. U. Camerini and Mr. J. H. Davies for many helpful discussions, to Miss P. Dyer and Mr. R. Gattiker for preparing the Plate, and, finally to the team of microscope observers. He also wishes to thank the Governing Body of University College, Cork, for leave of absence and a grant towards maintenance.

References.

Allen, 1942, *Phys. Rev.*, **61**, 692.
Bradner, 1949, *U.C.R.L.*, 486.
Camerini, Fowler, Lock and Muirhead, 1950, *Phil. Mag.*, **41**, 413.
Carlson, Hooper and King, 1950, Private Communication
Christy and Kusaka, 1941, *Phys. Rev.*, **59**, 414.
Crane and Halpern, 1938, *Phys. Rev.*, **53**, 789.
Davies, Lock and Muirhead, 1949, *Phil Mag.*, **40**, 1250.
Ellis and Wooster, 1927, *Proc. Roy. Soc.* A, **117**, 109.
Fowler, 1950, *Phil. Mag.*, **41**, 169.
Franzinetti, 1950, *Phil. Mag.*, **41**, 86.
Heitler, W., *Quantum Theory of Radiation.* Oxford, 1944.
Hincks and Pontecorvo, 1948, *Phys. Rev.*, **75**, 257 ; 1949, *Phys. Rev.*, **75**, 698 ; 1950, *Can. Journ. Res.*, **28**, 29.
Jacobsen and Kofoed-Hansen, 1935, *K.D.V.S.*, **23**, No. 12.
Lattes, Occhialini and Powell, 1947, *Nature*, **160**, 453.
Leighton, Anderson and Seriff, 1949, *Phys. Rev.*, **75**, 1432.
Nahmias, 1935, *Proc. Camb. Phil. Soc.*, **31**, 99.
Nielsen, C. E., 1949, quoted Gamow and Critchfield, *Atomic Nuclei.* Oxford, 1949 : Appendix III.
Piccioni, 1948, *Phys. Rev.*, **74**, 1754.
Rossi and Greisen, 1941, *Rev. Mod. Phys.*, **13**, 240.
Ruderman and Finkelstein, 1949, *Phys. Rev.*, **76**, 1458.
Sard and Althaus, 1948, *Phys. Rev.*, **73**, 1251 ; **74**, 1364.
Smith, Barkas, Bishop, Bradner and Gardner, 1950, Berkeley group, *Phys. Rev.*, **78**, 86.

To face page 848

LXXVI. CORRESPONDENCE

An Estimate for the Position of the Lowest Dipole-level of a Nucleus.

By B. F. Touschek,
Department of Natural Philosophy, The University, Glasgow *.

[Received June 20, 1950.]
* Communicated by the Author.

The completeness property of the set of nuclear eigenfunctions can be used to obtain an inequality for the position of the lowest dipole level of a nucleus, *i.e.* for the lowest level that can be reached from the groundstate by a dipole transition.

Feenberg (1935) has applied sum rules to obtain a lower limit for the energy of a hypothetical excited state of He^4. His method can be adapted to apply to any nuclear system, though the actual evaluation of the limiting value for the excitation energy can only be carried out on the basis of a strongly simplified nuclear model. By considering two extreme cases it will be shown that the limiting value of the excitation energy does not depend critically on the model used for its derivation. In this paper the method will be outlined for dipole transitions though, of course, a similar procedure may be applied to quadripole and higher transitions. The estimates obtained for quadripole transitions give a much higher limiting energy than in the dipole-case ($140A^{-2/3}$ MeV. as compared with $50A^{-2/3}$ MeV. for a dipole) and are therefore probably less useful.

The basic idea is to evaluate the sums

$$X = \sum_b |x_{ab}|^2 \quad . \quad . \quad . \quad . \quad . \quad . \quad . \quad . \quad . \quad (1)$$

and

$$H = \sum_b (E_b - E_a)|x_{ab}|^2, \quad . \quad . \quad . \quad . \quad . \quad (2)$$

by applying the completeness of the set of nuclear eigenfunctions, x_{ab} is the electric dipole moment (after the separation of the motion of the centre of gravity) of the transition $a \to b$ between the states a and b with energies E_a and E_b of a nucleus. If $a=0$ denotes the groundstate and $b=1$ the first excited state with $x_{01} \neq 0$, then all the $E_b - E_0$ are positive and one has

$$E_1 - E_0 < H/X. \quad . \quad . \quad . \quad . \quad . \quad . \quad . \quad . \quad . \quad (3)$$

In a one particle picture in which the nucleus consists of independent neutrons and protons the sums (1) and (2) can be readily evaluated :

$$X = \frac{R^2 Z}{5} \tfrac{1}{2}(1+I) \quad \text{and} \quad H = \frac{\hbar^2}{2M} Z \tfrac{1}{2}(1+I),$$

where $I = 1 - 2Z/A$ is the isotopic ratio, M is the nucleon mass and R the radius of the nucleus. The factor 1/5 corresponds to the assumption

that the nucleons are uniformly distributed over a sphere of radius R. The factor $\frac{1}{2}(1+I)$ takes account of the motion of the centre of gravity: it vanishes for a system consisting of particles of one and the same specific charge. Taking $RA^{-1/3}=1{\cdot}5\times10^{-13}$ cm. one obtains the estimate

$$E_1-E_0<\frac{50}{A^{2/3}}\ [\text{MeV.}], \quad . \quad . \quad . \quad . \quad . \quad . \quad . \quad (4)$$

for the position of the first dipole level of a nucleus.

It is well known that the independent particle model gives a poor description of the sum-over-cross-sections for nuclear photo effects and recent calculations by Levinger and Bethe (1950) on the yield of photo neutrons have shown a strong dependence of the results on the assumed exchange character of nuclear forces. This can readily be understood if one considers the tendency of group formation inherent in a force-picture with saturation properties. This group-formation will result in strong correlations between the coordinates of different particles (in particular between two neutrons and two protons forming an intranuclear α-particle), so that considerable changes may be expected in the values of H and X.

To see how the estimate (4) is affected by different assumptions about nuclear forces one can consider an independent particle model in which the nucleus is assumed to consist of αZ free protons, $\frac{1}{2}Z(1-\alpha)$ α-particles and $A-Z-Z(1-\alpha)$ free neutrons. The parameter α can then be interpreted as the degree of dissociation of the α-particles in the nucleus. A model of this type with a reasonable value of α (Wergelands (1941) results on Be^6 suggest a value $\alpha\sim0{\cdot}25$) should be expected to give a fair rendering of some of the effects of exchange forces: the formation of α-particles as relatively stable sub-units and the resultant correlations between the coordinates of the nucleons. In this model the sums (1) and (2) can again be evaluated in an elementary manner:

$$\left.\begin{aligned} X&=\frac{R^2Z}{10}\{I+\alpha+3I^2(1-\alpha)\}\\ H&=\frac{\hbar^2Z}{4M}\{I+\alpha\}\end{aligned}\right\} \quad . \quad . \quad . \quad . \quad . \quad . \quad (5)$$

In the case of complete dissociation of the α-particles this gives, of course, the result already obtained for the free neutron-proton model. The case $\alpha=0$ gives $X=0$ and $H=0$ if $A=2Z$. In this case all the particles must have the same specific charge so that both the cross-section and the average energy-loss of dipole transitions must vanish. From (5) one obtains the refined estimate for the position of the lowest dipole level:

$$E_1-E_0<\frac{5\hbar^2}{2MR^2}\,\frac{1}{1+3I^2(1-\alpha)/(I+\alpha)}, \quad . \quad . \quad . \quad . \quad . \quad (6)$$

and it is immediately obvious that for moderate isotopic ratios this expression is nearly independent of α. Even for very heavy nuclei the difference between the values of (6) for $\alpha=0$ and $\alpha=1$ respectively is not

more than 40 per cent. This small variation seems to indicate that the estimate of the position of the first dipole level is better than the theory from which it has been derived and suggests to try to determine a similar limit for quadripole levels by means of the free neutron-proton model. Again an elementary calculation similar to that leading to the inequality (4) gives

$$(E_1-E_0)_{E.Q}<\frac{140}{A^{2/3}}\,\text{MeV}. \quad . \quad . \quad . \quad . \quad . \quad . \quad (7)$$

This limit is not very useful for light nuclei since there it corresponds to an energy far in excess of the "ionization-energy" of a neutron. For $A>70$ it should fall into the discrete part (<8 MeV.) of the nuclear spectrum so that one concludes that every nucleus with $A>70$ should have at least one quadripole level in the discrete spectrum. The corresponding consideration for dipole levels gives a critical atomic number of $A\sim16$ above which every nucleus should have at least one discrete dipole level. Feenberg's calculations seem to indicate that the actual level usually occurs very near to its theoretical limit. O^{16} with a dipole level at 7 MeV. and a limiting energy of approximately 8 MeV. is an example for this behaviour.

References.

Feenberg, E., 1935, *Phys. Rev.*, **49**, 328.
Levinger, J. S., and Bethe, H. A., 1950, *Phys. Rev.*, **78**, 115.
Wergeland, H., 1941, *Norske Vid. Selsk. Skr.*, 1.

Examples on the Calculation of Energy States by the Uncertainty Relations.

By Hsin P. Soh,
National Chekiang University *.

[Received June 14, 1950.]

Although the Uncertainty Principle forms one of the most fundamental concepts in quantum mechanics, the possibility of making quantitative predictions based on this principle is little explored. In this letter we shall give some examples illustrating the possibilities in this direction.

I. *Hydrogen atom.*

The energy of the system satisfies the inequality

$$E\geqslant\frac{1}{2m}P_r^2-\frac{ze^2}{r},$$

since the contribution of angular motion is not included in the right side of the above expression. The minimum energy is given by the "spread" (mean square deviation) of P_r and that of r, *i. e.*

$$E_{min}=\frac{1}{2m}\Delta P_r^2-\frac{ze^2}{\Delta r},$$

---

* Communicated by Professor M. Born, F.R.S.

where ΔP_r is the minimum measurable momentum and Δr is the minimum measurable distance of the electron from any other particle, here the nucleus. The minimum of P_r is now postulated to be connected with that of r by the relation $\Delta P_r \Delta r \geqslant \hbar$ *. Hence

$$E_{min} = \frac{\hbar^2}{2m}\frac{1}{\Delta r^2} - \frac{ze^2}{\Delta r}.$$

The last expression can be minimized by finding a suitable value of Δr, which may be varied by changing, for instance, the wavelength of the light used in the measurement. Using this minimum value, $\Delta r = \hbar^2/ze^2m$, we get finally, $E \geqslant -z^2e^4m/2\hbar^2$.

II. *Relativistic hydrogen atom.*

For the relativistic hydrogen atom one has

$$E \geqslant [m_0^2c^4 + c^2P_r^2]^{\frac{1}{2}} - \frac{ze^2}{r} - m_0c^2.$$

The argument in the case of this problem is the same as in the last example, *i. e.*

$$E \geqslant [m_0^2c^4 + c^2\Delta P_r^2]^{\frac{1}{2}} - \frac{ze^2}{\Delta r} - m_0c^2 \geqslant \left[m_0^2c^4 + c^2\frac{\hbar^2}{(\Delta r)^2}\right]^{\frac{1}{2}} - \frac{ze^2}{\Delta r} - m_0c^2.$$

Varying Δr and substituting in this formula, we obtain

$$E \geqslant m_0c^2[(1-\alpha^2z^2)^{\frac{1}{2}} - 1], \qquad \alpha = \frac{e^2}{\hbar c}.$$

III. *Hydrogen atom including the motion of the nucleus.*

In this case

$$E \geqslant \frac{1}{2M}P_R^2 + \frac{1}{2m}P_r^2 - \frac{ze^2}{r_{12}}.$$

The minimum energy is given by the spread of P_R, P_r and r_{12}. But the minimum of r_{12}, the distance of the electron from the nucleus, cannot be smaller than either of the minimum measurable distance of the electron from any other particle, Δr, or of the minimum measurable distance of the nucleus from any other particle, ΔR. Hence if $\Delta r \geqslant \Delta R$, then

$$E \geqslant \frac{\hbar^2}{2M}\frac{1}{\Delta R^2} + \frac{\hbar^2}{2m}\frac{1}{\Delta r^2} - \frac{ze^2}{\Delta r}.$$

---

* In the case of two dimensional motion this expression can be rigorously derived from the wave property of the electron. We shall, however, treat it as a postulate. In dealing with more complicated atoms we shall also postulate $\Delta P_r \Delta r \geqslant nh$ for " higher quantum states ".

Now the first term is independent of the other terms and has its minimum value when ΔR has the greatest value, which by our assumption is at most equal to Δr. Hence

$$E \geqslant \frac{\hbar^2}{\Delta r^2}\left(\frac{1}{2M}+\frac{1}{2m}\right)-\frac{ze^2}{\Delta r},$$

and by simple variation, we get

$$E \geqslant -\frac{Mm}{M+m}\frac{z^2e_2}{2\hbar^2}.$$

The same lower limit is obtained if $\Delta r \leqslant \Delta R$ is assumed.

In the three examples given above the lower limit of energy obtained from uncertainty relation agrees in every case with that obtained by other methods.

IV. *Helium-like atoms.*

For helium-like atoms

$$E \geqslant \frac{1}{2m}(P_{r_1}^2+P_{r_2}^2)-ze^2\left(\frac{1}{r_1}+\frac{1}{r_2}\right)+\frac{e^2}{r_{12}}.$$

The minimum of the first four terms is given by the spread of P_{r_1}, P_{r_2}, r_1, and r_2. The minimum of the last term is given by the largest value of r_{12} which must be less than r_1+r_2. The last limit requires that the three particles should lie on a straight line which is hardly realizable. However, the inequality

$$E > \frac{\hbar^2}{2m}\left(\frac{1}{\Delta r_1^2}+\frac{1}{\Delta r_2^2}\right)-ze^2\left(\frac{1}{\Delta r_1}+\frac{1}{\Delta r_2}\right)+\frac{e^2}{\Delta r_1+\Delta r_2}$$

is certainly true. It sets a lower limit to the actual minimum. Minimizing the above expression by varying Δr_1 and Δr_2, we get

$$E > -2(z-\tfrac{1}{4})^2 Rh.$$

In the following Table the limits thus calculated are given together with the experimental minima for the first few atoms.

	H^-	He	Li	Be	B	C
E (cal.)	−1·125	−6·125	−15·12	−28·12	−45·12	−66·12
E (exp.)	−1·05	−5·807	−14·56	−27·56	−44·06	−64·8

The discrepancy between the theoretical and the experimental values is to be expected from the crudeness of our estimate. The significant point is that all the calculated values lie lower than the empirical ones. The agreement can be much improved by considering the uncertainty in the electronic distributions. Either by averaging over all directions, remembering that r_{12} must be greater than either Δ_{r_1} or Δ_{r_2}, or by assuming correlated normal distributions for the electrons, we obtain, practically in all cases, results in reasonably good agreement within 1/2 to 1/5 per cent, with the experimental values.

Other complicated systems, such as Li-like and Be-like atoms, have been treated in the same way with reasonably good results, by assuring Pauli's principle and using the relation $\Delta P_r \Delta r \geqslant 2\hbar$ for the third and fourth particles (see footnote). It is, however, needless to go into details until the physical ideas presented here, for instance, the argument in the third example, can be formulated on a mathematical basis capable of extension to many-body problems.

I wish to thank Mr. W. T. Soh for some of the earlier calculations on the Berylium system and Dr. T. M. Hu for much of the later calculations.

December 18, 1949.

LXXVII. *Notices of New Books and Periodicals received.*

Radiative Transfer. By S. Chandrasekhar. (Oxford : The Clarendon Press.) [Pp. 393.] Price 35*s*.

This book presents a systematic treatment of transfer in a plane parallel scattering medium, a subject which has been investigated principally by astrophysicists, but acquires new applications in the scattering of neutrons: indeed, other applications will assuredly be found in chemistry and applied physics for the quantitative results now available. The main line of attack consists in using certain principles of invariance (as that the diffuse scattering from a semi-infinite plane parallel atmosphere should be invariant to the addition of a layer of arbitrary optical thickness) to formulate integral equations : a method introduced by Ambarzumian in 1943 and greatly developed by Chandrasekhar himself. Astonishingly, the resulting non-linear inhomogeneous integral equations are then solved. Those who would recoil from the more difficult problems which are treated with success here, or who take no interest in radiative transfer, may nevertheless study with profit the application of Gaussian quadrature (and its generalization) to the approximate (and sometimes exact) solution of certain simpler integro-differential equations.

It is presumed that this will remain for long the standard text on its subject. But even should its techniques be superseded, the easy and illuminating style, and the continuous courtesy to the reader—in keeping him informed of where and how an argument is leading ; in converting the plain " list of references " at the end of each chapter into concise and instructive " bibliographical notes " ; in providing an index of definitions in addition to that of names and subjects—will allow it to stand as a model of the way in which a text in mathematical physics should be written. F. C. F.

Absorption Spectrophotometry. By G. F. Lothian, M.A., F. Inst.P. (A Hilger Publication.) Price 26*s*. net.

This book caters for the reader with a scientific background, commencing research in absorption spectrophotometry or requiring an informed survey of the practice and possibilities of the subject presented within reasonable compass. It succeeds admirably in these aims, and at the same time will be valued by experienced workers in the field as a balanced account of up-to-date practice.

The book is divided into three parts :—The first is introductory and assesses conditions affecting accuracy of measurement, and here, as throughout the book, the mathematics is an absolute minimum.

The second part, and perhaps the most valuable, presents a most interesting and varied collection of the types of problem arising in modern practice with appropriate methods of attack. Few readers will be familiar with the whole field surveyed, but specialists and non-specialists alike will profit by this comprehensiveness.

The third part discusses apparatus and techniques. The descriptions of apparatus are most effective, but those of actual techniques somewhat compressed.

The book is made up from good paper, is well illustrated with 70 figures and photographs, and also lists some 300 references, well indexed, and half of them within the 1944–48 period. This ample documentation mitigates those accounts which are necessarily brief in order to keep the book to its present length.

The reviewer finds a score of minor errors ; a more careful layout of the position of the figures with reference to the text and a greater consistency in lettering would not be amiss. However, this is a good work and pleasant to read.

Cosmic Rays. By L. JÁNOSSY. 2nd Edition. [Pp. 454, Plates 10.] (Oxford: Clarendon Press, 1950.) Price 40*s.* net.

THE first edition of this work was published only two years ago and was reviewed in this Journal (**39**, 826, 1948) as authoritatively written by an investigator who has himself made numerous contributions to the subject. The need for a new edition at so early a date brings with it difficulties for the author, because important contributions to the subject are continuing to appear in rapid succession through the application of the photographic emulsion technique. It was probably inevitable at this stage that the attempt to bring the work up to date had to be made by what one may term tinkering and repair rather than by re-writing. But when a third edition is planned, changes in construction and in emphasis will undoubtedly be imperative. A.M.T.

History of Physics. By MAX VON LAUE, translated by R. E. Oesper. [Pp. 150.] (Academic Press, New York.) Price $2.30.

IN a foreword to his book, Professor von Laue says that the first draft was a war product written in 1943. "Precisely because of this circumstance the thought of the culture that is the common property of all nations, and which was then being so despicably mistreated, was ever present throughout the period of composition". A very readable book by an eminent physicist.

Manual of Organic Chemistry for Advanced Students, Vol. I. By G. DYSON. [Pp. 984.] (Longmans Green.) Price 63*s.*

THIS is the first part of a three volume treatise and deals with the compounds of carbon, hydrogen, oxygen and the halogens. Its scope may be indicated by saying that it is more comprehensive than a text-book, without being a collection of specialized monographs. Compiled by one who has made very important contributions in the field of notation in organic chemistry it may be looked upon as authoritative. Readers of this journal should find the volume useful as a work of reference.

BOOKS RECEIVED

The Association of Research Institutes of Tohuku University Japan have started to issue a series of Science Reports consisting of collected papers on work carried out by them in Physics Chemistry and Metallurgy. Volume I. Numbers 1 and 2 (May and August 1949) have been received.

[*The Editors do not hold themselves responsible for the views expressed by their correspondents.*]